

ADSORPTION OF COPPER BY CRAB SHELL BIOCHAR

by

© David T Hopkins, B. Eng.

A Thesis Submitted to the School of Graduate Studies
in partial fulfillment of the requirements of the degree of

Master of Engineering

Process Engineering

Faculty of Engineering & Applied Science

Memorial University of Newfoundland

May 2021

St. John's, Newfoundland, Canada

Abstract

In Atlantic Canada, fisheries and seafood processing represent major industries and contribute heavily to the regional economy. By-products from seafood processing, such as shells and bones, make up a significant waste stream from this industry and are currently difficult to valorize. Pyrolysis, a thermochemical process involving biomass in the absence of oxygen, is a simple and effective means of valorizing biomass, producing three product streams: a biogas, a condensable bio-oil, and a solid residue called biochar. In this thesis, the properties of biochar produced from the snow crab (*Chionoecetes Opilio*) shell are studied, along with its capacity to remove copper (Cu^{2+}) and sulfate (SO_4^{2-}) from water. Chapter 2 of this thesis includes a review of the literature on the use of plant-based, or lignocellulosic biochar for the removal of metals from water and simulated Acid Mine Drainage (AMD), along with marine-based biochar. The findings indicate that while marine-shell biochar is a seldom studied field, these biochars have metal adsorption capacities that are generally well in excess of those from lignocellulosic feedstocks, owing largely to their minerality (primarily in the form of calcite (CaCO_3)) and their alkalinity. In Chapter 3, we synthesize a crab shell biochar (CSB) from snow crab shell and then characterize its properties using a range of techniques to analyze its surface morphology, proximate analysis, surface zeta potential, and surface chemistry. These results indicate that the CSB is highly alkaline (pH of 11.75) and porous, with a BET surface area of $20.71 \text{ m}^2/\text{g}$ and pore width ranging from 3-10 nm. Zeta potential analysis indicates that the CSB has a primarily negative charge in solution across the equilibrium pH values studied (pH values of 7-11.5). Spectroscopic analysis indicates the

biochar is mostly made of calcite, with some residual organic carbon groups, with some oxygenic and nitrogenic groups involved. Chapter 4 then analyzes the adsorptive performance of the CSB for Cu^{2+} and SO_4^{2-} , common constituents of AMD. This is performed through analysis of required dosage, effect of solution pH, adsorption kinetics, adsorption isotherms, and adsorption thermodynamics. The results indicate that the biochar can adsorb Cu^{2+} effectively at a dosage of 5 g/L, while adsorption of sulfate species is limited unless in the presence of Cu^{2+} , at this point individual studies on SO_4^{2-} are stopped. Cu^{2+} adsorption is further unaffected by acidity in solution under the initial pH values of 2-7, perhaps due to the alkalinity of the biochar. The adsorption capacity of the CSB is found to be 184.8 ± 10.2 mg/g for Cu^{2+} , with adsorption kinetics best fitting the Pseudo First Order Model. Thermodynamic analysis of Cu^{2+} adsorption demonstrates that adsorption capacity increases with increasing solution temperature, with adsorption from a 700 mg/L Cu^{2+} solution increasing from 52.2 ± 3.0 mg/g at 5 °C to 122.2 ± 2.0 mg/g at 30 °C. Mechanistic analysis demonstrated that the adsorption of Cu^{2+} was due to precipitation in the form of posnjakite ($\text{Cu}_4[(\text{OH})_6\text{SO}_4] \cdot \text{H}_2\text{O}$), as well as some influence from residual organic groups. Overall, this research demonstrates that biochar from crab shell is a highly effective adsorbent for Cu^{2+} , with a good potential for use in AMD owing to its alkalinity.

Acknowledgements

The research presented in this thesis could not have been performed without the funding provided by the Natural Sciences and Engineering Research Council of Canada (NSERC) and the Ocean Frontier Institute (OFI), the Memorial University of Newfoundland School of Graduate Studies, and the Memorial University of Newfoundland Faculty of Engineering & Applied Science.

I would like to thank, first and foremost, my supervisors for this project, Dr. Kelly Hawboldt and Dr. Stephanie MacQuarrie. Their continued support and guidance in this project was imperative in guiding the work of this thesis and helping me to become a better researcher, and for that, I have extreme gratitude towards them. Furthermore, I would like to thank Dr. Hawboldt for encouraging me to pursue research in this field, without her support I would certainly not have investigated this area.

I would also like to extend gratitude towards the many members of Memorial University's Core Research Equipment and Instrument Training (CREAIT) Network who helped to train me on various pieces of analytical equipment and performed certain tests as well where training was not possible, as well as Dr. Alain Adnot of Université Laval who performed X-Ray Photoelectron analysis. I extend sincere gratitude to Louisbourg Seafoods Limited for providing the crab shell used in the experiments as well. Other individuals who may be direct technical contributions to my research include students to whom I owe great thanks, including Women in Science & Engineering (WISE) student Julia Naterer, and work term students Zachary Kinsman and Saskia Selleng.

I would also like to thank my family for their continued support throughout this thesis. Their advice and moral support throughout this thesis was important in helping me complete this degree, and they have my sincere gratitude for this. I would also like to acknowledge the memory of my late grandfather, Dr. Robert Hopkins. Without his inspiration and love for researching and teaching chemical engineering, I would never have found my love for this field, and I am proud to be able to follow in his footsteps.

Table of Contents

Abstract	i
Acknowledgements	iii
List of Figures	vii
List of Tables	viii
List of Abbreviations	ix
Chapter 1 – Introduction & Overview	1
1.1 Scope & Objectives.....	4
1.2 Thesis Structure	5
1.3 Co-Authorship Statement.....	6
Bibliography:	7
Chapter 2 - Literature Review.....	10
Abstract	11
2.1 Introduction.....	12
2.2 Pyrolysis Feedstocks	13
2.2.1 Lignocellulosic Biomass	14
2.2.2 Marine Biomass	38
2.3 Conclusions.....	45
Bibliography:	47
Chapter 3 - Characterization of Crab Shell Biochar	58
Abstract	59
3.1 Introduction.....	60
3.2 Materials & Methodology.....	62
3.2.1 Biochar Production	62
3.2.2 Thermal Gravimetric Analysis.....	62
3.2.3 Surface Morphology	63
3.2.4 BET Surface Analysis.....	63
3.2.5 Elemental Analysis	64
3.2.6 X-Ray Diffraction Analysis	64
3.2.7 Fourier-Transform Infrared Spectroscopy	64

3.2.8	X-Ray Photoelectron Spectroscopy	65
3.2.9	Zeta Potential Analysis	65
3.2.10	Trace Element Analysis	66
3.3	Results and discussion	66
3.3.1	TGA	66
3.3.2	Scanning Electron Microscopy	68
3.3.3	Surface Area Analysis.....	69
3.3.4	Physicochemical Properties	70
3.3.5	X-Ray Diffraction Analysis	71
3.3.6	Fourier-Transform Infrared Spectroscopy	73
3.3.7	XPS	74
3.3.8	Zeta Potential Analysis	76
3.3.9	Trace Element Analysis	78
3.4	Conclusions.....	80
	Bibliography:	81
Chapter 4 – Removal of Copper and Sulfate from Solution using a Crab Shell Biochar..		86
	Abstract	87
4.1	Introduction.....	88
4.2	Materials & Methodology.....	90
4.2.1	Materials	90
4.2.2	Biochar Production	90
4.2.3	Adsorption Experiments	91
4.3	Results and discussion	96
4.3.1	Effect of Dosage.....	96
4.3.2	Effect of initial pH	99
4.3.3	Adsorption Isotherms.....	101
4.3.4	Adsorption Kinetics	103
4.3.5	Thermodynamic Parameters	106
4.3.6	Mechanistic Analysis	109
4.4	Conclusion	116
	Bibliography	118
Chapter 5 – Conclusions & Recommendations		124

Bibliography:	129
APPENDICES	130
APPENDIX A: XPS SPECTRA	131

List of Figures

Figure 2-1: pH_{IEP} of lignocellulosic biochar as observed from literature. Data obtained from [37], [54]–[65]	24
Figure 3-1: TGA Data for raw crab shell in the CSB	67
Figure 3-2: SEM images of the CSB, illustrating a complex pore network	69
Figure 3-3: Pore Size Distribution from N_2 -based NLDFT theory	71
Figure 3-4: XRD pattern for the CSB	72
Figure 3-5: FT-IR Spectra of the Crab Shell Biochar	74
Figure 3-6: Zeta Potential of the CSB	77
Figure 4-1: Percent Removal of Cu^{2+} and S from solution as a function of CSB dosage .	97
Figure 4-2: Effect of initial pH on adsorption of Cu^{2+} from solution	100
Figure 4-3: Langmuir isotherm fit to adsorption data for Cu^{2+}	101
Figure 4-4: Freundlich isotherm fit to adsorption data for Cu^{2+}	102
Figure 4-5: Fit of Experimental data to the PFO, PSO, and Elovich models for Cu^{2+} removal	104
Figure 4-6: Cu^{2+} adsorption capacity of the CSB as a function of temperature	107
Figure 4-7: Concentrations of Ca^{2+} and Mg^{2+} in solution at equilibrium as a function of temperature	108
Figure 4-8: XRD spectra of the CSB post-adsorption (pre-adsorption in insert)	110
Figure 4-9: Image of the CSB prior to adsorption, showing porous structure	113
Figure 4-10: SEM image of the CSB prior to pyrolysis	113
Figure 4-11: SEM Image of CSB post-adsorption illustrating widespread precipitation of Cu-based minerals across the biochar	114
Figure 4-12: SEM Image of CSB post-adsorption showing a close-up view of the Cu^{2+} precipitate, with some biochar pores still visible	114

Figure 4-13: Cu^{2+} precipitates, likely in the form of posnjakite, forming flaky, tightly packed crystals on the CSB surface.	115
---	-----

List of Tables

Table 2-1: Physicochemical properties of wood-based biochar	17
Table 2-2: Organic functional groups involved in metal adsorption	20
Table 2-3: Pyrolysis conditions and adsorption capacities of various woody biochars for metals	25
Table 2-4: Physicochemical Properties of Various Agricultural Biochars	34
Table 2-5: Equilibrium Adsorption Data for Various Biochars.....	36
Table 2-6: Characteristics of some fisheries waste biochars	40
Table 2-7: Adsorption capacities for various marine shell-derived biochars	42
Table 3-1: Proximate Analysis of Raw Crab and CSB.....	68
Table 3-2: Physicochemical properties of crustacean shell biochars.....	70
Table 3-3: XPS Results for the CSB.....	75
Table 3-4: Elemental Compositions of the CSB as determined by acid digest concentrations (mg/L).....	79
Table 4-1: Final concentrations of Ca^{2+} and Mg^{2+} in solution as a function of adsorbent dosage	98
Table 4-2: Adsorption isotherm fit statistics.....	102
Table 4-3: Adsorption kinetic model statistics for Cu^{2+}	105
Table 4-4: Thermodynamic parameters for the removal of Cu^{2+} from solution.....	106
Table 4-5: Cu^{2+} adsorption capacities from past studies.....	116

List of Abbreviations

AMD	Acid mine drainage
BET	Brunauer-Emmett-Teller
CEC	Cation exchange capacity
CHN	Carbon Hydrogen Nitrogen analysis
CSB	Crab shell biochar
EDX	Energy dispersive X-Ray spectroscopy
FT-IR	Fourier Transform-Infrared Spectroscopy
ICP-OES	Ion-coupled plasma optical emission spectroscopy
NLDFT	Non-local density functional theory
PDI	Potential determining ion
PFO	Pseudo-first order model
PSO	Pseudo-second order model
pH _{IEP}	Isoelectric pH
RMSE	Random mean square error
SEM	Scanning electron microscopy
SSA	Specific surface area
TG-MS	Thermal gravimetry-mass spectrometry
TGA	Thermal gravimetric analysis
XPS	X-Ray photoelectron spectroscopy
XRD	X-Ray diffraction

Chapter 1 – Introduction & Overview

The presence of heavy metals in industrial effluents poses a major hazard to both environmental and human health, making wastewater treatment an important process in many industries [1], [2]. In mines, metals and other harmful chemical species can enter the environment in the form of acid mine drainage (AMD), in which sulfide minerals from the mine react with water to produce acidic wastewater, which can then further leach other metals from surrounding rocks. This resultant AMD may contain high levels of heavy metals, including lead (Pb^{2+}), copper (Cu^{2+}), iron ($\text{Fe}^{2+/3+}$), and arsenic (As), as well as thiosalts, the latter of which leads to secondary environmental effects due to soil and microbial interactions [3]. Treatment of this wastewater is imperative prior to its disposal, and requires the removal of the toxic metals, thiosalts such as sulfate (SO_4^{2-}), and neutralization of the wastewater's pH in cases where the acidity of the water is not neutralized naturally [4], [5].

In mines where AMD is produced, passive methods for effluent treatment include limestone drains, wetlands, and reactive barriers [3], [6]. Other active techniques also exist for the removal of metals from aqueous solution, including chemical precipitation, ion exchange, membrane methods, electrochemical processes, and adsorption [7]. Of these, adsorption is highly attractive in many cases, as it is effective across a range of pollutant concentrations, does not produce secondary wastes such as sludges, and the adsorbents used can be generated from low-cost materials [3], [8]. In recent years, adsorbent research has focussed on the production of greener adsorbents, which are produced from more sustainable resources, with one very popular example being biochar [6]. Biochar is produced via pyrolysis, whereby biomass is heated under an oxygen-free atmosphere. This process yields biochar as a solid residue, along with a condensable

liquid bio-oil and gas stream which have other uses [9]. The bulk of the research in this field carried out to date has focussed on using plant-based, or lignocellulosic feedstocks in the pyrolysis process, such as agricultural residues [10] and forestry by-products [11]. Biochar has been commonly tested as an adsorbent for metals in past research [12]–[14]. Additionally, biochar can simultaneously reduce the acidity of AMD [15], making the prospect of using this material very valuable. Lignocellulosic biochars have demonstrated limited adsorption capacity for metals, however, which has created interest in the use of alternative feedstocks [15].

In coastal areas with large fisheries, by-products from fish and shellfish processing can contribute to large waste streams, which are often disposed of. By-products from the Canadian Crab fishery, primarily derived from the body of the snow crab, *Chionoecetes opilio*, make up roughly 30% of the catch weight [16]. With the Atlantic Canadian crab fishery landing over 67000 metric tonnes of crab in 2018 [17], at an estimated value of just under 750 million Canadian dollars [18], the by-product waste in this region represents an immense opportunity for by-product valorization in an industry that is critical to the area. The prevalence of this waste material has led to significant research efforts focussing on valorizing nutrients from waste crustacean shells [19]–[21]. However, the nutritional content of these shells is often very low, contributing less than 30% of the shell weight in crab [22].

In some recent studies, crustacean and mollusc shells have been applied as AMD treatments [23], [24], as their high CaCO_3 contents make them similar to limestone methods used in mining [3], [25], [26]. Despite this, these materials still contain relatively high levels of organic compounds, which can leach out and cause unpleasant

odors [27]. Pyrolyzing crab shell would present a simple method of biomass valorization and produce two useful product streams: a bio-oil, consisting of a variety of nitrogen-functionalized organic chemicals, and a biochar consisting primarily of calcium minerals and few residual organic groups [28]. Pyrolysis also serves to eliminate bacteria and viruses that could present in the feedstock and cause problems if used as a biosorbent. The use of this biochar stream has been studied in some past papers, though generally, research in this field is limited. Some papers have analyzed the use of crustacean-based biochar for the removal of organics [29], [30], and phosphates [31], with only one recent paper investigating its use for the removal of heavy metals from solution, despite its similarity with more common AMD treatments, and higher sustainability [32]. Further study on the characteristics of marine shell biochars, and their capacity and mechanisms for adsorbing metals from solution, is required to assess the effectiveness of this material as an AMD treatment.

1.1 Scope & Objectives

Research on the use of marine shells as a pyrolysis feedstock is already sparse, despite the prevalence of this material in many regions around the world. Furthermore, its use for the removal of metals from solution is rare and has only been studied a few times in the past. Given the widespread production of the feedstock in coastal areas, and its similarities to pre-existing AMD treatments, this thesis seeks to study the production and use of biochar made from snow crab (*Chionoecetes Opilio*) to remove Cu^{2+} and SO_4^{2-} from aqueous solution. The objectives of the thesis are listed below:

- Perform physicochemical characterizations on the crab shell biochar and relate these properties to the use of the material in metal adsorption.
- Determine the optimum dosage of this biochar for the removal of Cu^{2+} and SO_4^{2-} , and also study the effect of initial solution pH, concentration of solute, adsorption thermodynamics, and adsorption kinetics.
- Study the mechanisms in which the solutes are adsorbed by the biochar using additional physicochemical analyses.

1.2 Thesis Structure

Chapter 2 presents a literature review comparing biochar made from plant-based, lignocellulosic biochar, to marine-based biochar. The review begins by discussing the properties of lignocellulosic biochars, and how they relate to the adsorption capacity of these biochars for heavy metals. In turn, the properties of marine-based biochar in literature found to date is discussed in relation to that of the more commonly studied lignocellulosic biochar and further evaluated for its potential to remove metals from aqueous waste streams. This paper has been published in the Journal of Environmental Chemical Engineering.

Chapter 3 describes the synthesis of a Crab Shell Biochar (CSB) in a lab-scale apparatus and its properties are determined through intensive characterization. Here, the chemical and physical properties of the crab shell biochar are determined using a variety of tests, which are then placed in the context of using the CSB as a means of removing metals and

sulfates from solution. A modified version of this chapter will be submitted for publication.

Chapter 4 follows by using the CSB to remove Cu^{2+} and thiosalts from synthetic solutions. Analysis of the optimum dosage and pH is performed, followed by experiments aimed at determining the maximum adsorption capacity of the CSB for each chemical species, and the kinetics of adsorption. Thermodynamic parameters associated with adsorption are then studied by analyzing the effect of temperature on the extent of adsorption. Finally, mechanisms of adsorption are studied by analysis of the data in this chapter, as well as characterization of the biochar following adsorption. A modified version of this chapter will be submitted for publication.

Chapter 5 then provides a summary of the research performed in the preceding chapters and provides conclusions and recommendations for the future of the field of study.

1.3 Co-Authorship Statement

The principal author of this thesis, David Hopkins, acted as the primary author on all chapters included in this thesis and performed all experimental work and analysis except where otherwise noted. Dr. Kelly Hawboldt, who acted as the principal supervisor on this thesis, served to provide technical guidance, analytical support, and additional support in editing the thesis and is listed as a co-author on the manuscripts for chapters 2, 3, and 4. Dr. Stephanie MacQuarrie also provided technical guidance, analytical support, and editing for the work performed in chapters 3 and 4, and is listed as a co-author in these chapters.

Bibliography:

- [1] S. Chowdhury, M. A. J. Mazumder, O. Al-Attas, and T. Husain, "Heavy metals in drinking water: Occurrences, implications, and future needs in developing countries," *Sci. Total Environ.*, vol. 569–570, pp. 476–488, Nov. 2016.
- [2] E. Ferreira da Silva *et al.*, "Heavy metal pollution downstream the abandoned Coval da Mó mine (Portugal) and associated effects on epilithic diatom communities," *Sci. Total Environ.*, vol. 407, no. 21, pp. 5620–5636, Oct. 2009.
- [3] I. Moodley, C. M. Sheridan, U. Kappelmeyer, and A. Akcil, "Environmentally sustainable acid mine drainage remediation: Research developments with a focus on waste/by-products," *Miner. Eng.*, vol. 126, no. August 2017, pp. 207–220, 2018.
- [4] H. E. Ben Ali, C. M. Neculita, J. W. Molson, A. Maqsoud, and G. J. Zagury, "Performance of passive systems for mine drainage treatment at low temperature and high salinity: A review," *Miner. Eng.*, vol. 134, pp. 325–344, 2019.
- [5] P. L. Younger, "Mine water pollution in Scotland: nature, extent and preventative strategies," *Sci. Total Environ.*, vol. 265, no. 1–3, pp. 309–326, Jan. 2001.
- [6] E. Iakovleva and M. Sillanpää, "The use of low-cost adsorbents for wastewater purification in mining industries," *Environ. Sci. Pollut. Res.*, vol. 20, no. 11, pp. 7878–7899, 2013.
- [7] A. Azimi, A. Azari, M. Rezakazemi, and M. Ansarpour, "Removal of Heavy Metals from Industrial Wastewaters: A Review," *ChemBioEng Rev.*, vol. 4, no. 1, pp. 37–59, 2017.
- [8] M. A. Renu and K. Singh, "Heavy metal removal from wastewater using various adsorbents: a review," *J. Water Reuse Desalin.*, vol. 7, no. 4, pp. 387–419, 2017.
- [9] S. Papari and K. Hawboldt, "A review on the pyrolysis of woody biomass to bio-oil: Focus on kinetic models," *Renew. Sustain. Energy Rev.*, vol. 52, pp. 1580–1595, Dec. 2015.
- [10] R. Azargohar, S. Nanda, J. A. Kozinski, A. K. Dalai, and R. Sutarto, "Effects of temperature on the physicochemical characteristics of fast pyrolysis bio-chars derived from Canadian waste biomass," *Fuel*, vol. 125, pp. 90–100, 2014.
- [11] S. Papari, K. Hawboldt, and R. Helleur, "Pyrolysis: A Theoretical and Experimental Study on the Conversion of Softwood Sawmill Residues to Biooil," *Ind. Eng. Chem. Res.*, vol. 54, no. 2, pp. 605–611, Jan. 2015.
- [12] S. Mireles, J. Parsons, T. Trad, C. L. Cheng, and J. Kang, "Lead removal from

- aqueous solutions using biochars derived from corn stover, orange peel, and pistachio shell,” *Int. J. Environ. Sci. Technol.*, vol. 16, no. 10, pp. 5817–5826, 2019.
- [13] X. Tong, J. Li, J. Yuan, and R. Xu, “Adsorption of Cu(II) by biochars generated from three crop straws,” *Chem. Eng. J.*, vol. 172, no. 2–3, pp. 828–834, Aug. 2011.
- [14] X. Chen *et al.*, “Adsorption of copper and zinc by biochars produced from pyrolysis of hardwood and corn straw in aqueous solution,” *Bioresour. Technol.*, 2011.
- [15] K. K. Kefeni, T. A. M. Msagati, and B. B. Mamba, “Acid mine drainage: Prevention, treatment options, and resource recovery: A review,” *J. Clean. Prod.*, vol. 151, pp. 475–493, May 2017.
- [16] L. Beaulieu, J. Thibodeau, P. Bryl, and M. É. Carbonneau, “Characterization of enzymatic hydrolyzed snow crab (*Chionoecetes opilio*) by-product fractions: A source of high-valued biomolecules,” *Bioresour. Technol.*, vol. 100, no. 13, pp. 3332–3342, 2009.
- [17] Department of Fisheries and Oceans, “Seafisheries landed quantity by region, 2018,” 2018. [Online]. Available: <http://www.dfo-mpo.gc.ca/stats/commercial/land-debarq/sea-maritimes/s2018aq-eng.htm>. [Accessed: 29-Sep-2020].
- [18] Department of Fisheries and Oceans, “Seafisheries landed value by region, 2018,” 2018. [Online]. Available: <http://www.dfo-mpo.gc.ca/stats/commercial/land-debarq/sea-maritimes/s2018av-eng.htm>. [Accessed: 29-Sep-2020].
- [19] A. Ghaly, V. Ramakrishnan, M. Brooks, S. Budge, and D. Dave, “Fish Processing Wastes as a Potential Source of Proteins, Amino Acids and Oils: A Critical Review,” *J. Microb. Biochem. Technol.*, 2013.
- [20] R. Sowmya, T. M. Ravikumar, R. Vivek, K. Rathinaraj, and N. M. Sachindra, “Optimization of enzymatic hydrolysis of shrimp waste for recovery of antioxidant activity rich protein isolate,” *J. Food Sci. Technol.*, vol. 51, no. 11, pp. 3199–3207, Nov. 2014.
- [21] H. D. De Holanda and F. M. Netto, “Recovery of components from shrimp (*Xiphopenaeus kroyeri*) processing waste by enzymatic hydrolysis,” *J. Food Sci.*, 2006.
- [22] F. Boßelmann, P. Romano, H. Fabritius, D. Raabe, and M. Epple, “The composition of the exoskeleton of two crustacea: The American lobster *Homarus americanus* and the edible crab *Cancer pagurus*,” *Thermochim. Acta*, vol. 463, no.

1–2, pp. 65–68, 2007.

- [23] Z. A. DiLoreto, P. A. Weber, and C. G. Weisener, “Solid phase characterization and metal deportment in a mussel shell bioreactor for the treatment of AMD, Stockton Coal Mine, New Zealand,” *Appl. Geochemistry*, vol. 67, pp. 133–143, 2016.
- [24] M. Masukume, M. S. Onyango, and J. P. Maree, “Sea shell derived adsorbent and its potential for treating acid mine drainage,” *Int. J. Miner. Process.*, vol. 133, pp. 52–59, 2014.
- [25] A. M. Silva, R. M. F. Lima, and V. A. Leão, “Mine water treatment with limestone for sulfate removal,” *J. Hazard. Mater.*, vol. 221–222, pp. 45–55, 2012.
- [26] C. Zhou, X. Gong, J. Han, and R. Guo, “Removal of Pb(II) and Zn(II) from Aqueous Solutions by Raw Crab Shell: A Comparative Study,” *Water Environ. Res.*, vol. 88, no. 4, pp. 374–383, 2016.
- [27] K. Vijayaraghavan and R. Balasubramanian, “Is biosorption suitable for decontamination of metal-bearing wastewaters? A critical review on the state-of-the-art of biosorption processes and future directions,” *J. Environ. Manage.*, vol. 160, pp. 283–296, 2015.
- [28] Z. Sebestyén *et al.*, “Thermal degradation of crab shell biomass, a nitrogen-containing carbon precursor,” *J. Therm. Anal. Calorim.*, no. 0123456789, 2020.
- [29] L. Dai *et al.*, “Calcium-rich biochar from crab shell: An unexpected super adsorbent for dye removal,” *Bioresour. Technol.*, vol. 267, no. July, pp. 510–516, 2018.
- [30] Q. Xu, Q. Zhou, M. Pan, and L. Dai, “Interaction between chlortetracycline and calcium-rich biochar: Enhanced removal by adsorption coupled with flocculation,” *Chem. Eng. J.*, vol. 382, p. 122705, 2020.
- [31] L. Dai *et al.*, “Calcium-rich biochar from the pyrolysis of crab shell for phosphorus removal,” *J. Environ. Manage.*, 2017.
- [32] Y. Xiao, Y. Xue, F. Gao, and A. Mosa, “Sorption of heavy metal ions onto crayfish shell biochar: Effect of pyrolysis temperature, pH and ionic strength,” *J. Taiwan Inst. Chem. Eng.*, vol. 80, pp. 114–121, Nov. 2017.
- [33] A. Sdiri, T. Higashi, F. Jamoussi, and S. Bouaziz, “Effects of impurities on the removal of heavy metals by natural limestones in aqueous systems,” *J. Environ. Manage.*, vol. 93, no. 1, pp. 245–253, 2012.

Chapter 2 - Literature Review

This chapter has been published; D. Hopkins, K. Hawboldt. Biochar for the Removal of Metals from Solution: A Review of Lignocellulosic and Novel Marine Feedstocks. *Journal of Environmental Chemical Engineering* 8 (4).

Abstract

Biochar, derived from the pyrolysis of biomass, has received great attention in literature for many applications. Owing to its high specific surface area and surface chemistry, the use of biochar as an adsorbent for heavy metals from solution has become a promising environmental application of this material. While research has primarily focused on generating biochar from lignocellulosic feedstocks, emerging feedstocks, such as marine-shell-derived biochars have also shown promise as metal adsorbents with increased adsorptive capacity. In this paper, the mechanisms of metal adsorption from water are first analyzed from the perspective of the more commonly researched lignocellulosic biochar. Here, specific surface area, presence of organic functional groups, mineral content, and surface pH and charge are found to be controlling mechanisms for adsorption of metals, with the role of feedstock playing a primary role in determining these properties, along with pyrolysis conditions. This discussion leads to an analysis of the properties of marine-shell-based biochar as well as its adsorption capacity for a range of metals as found in recent literature. It is found that for many divalent cations, such as lead (Pb^{2+}), marine shell biochars have adsorption capacities that far exceed that of traditional lignocellulosic biochar owing to the high cation exchange capacity and moderate surface area of this material. As a result, pyrolysis of this material may present a simple method of valorizing a common waste product from the fisheries and transforming it into a potent adsorbent for wastewater treatment.

2.1 Introduction

Global heavy metal pollution has been particularly prominent in the last century, as global industrial demands increased [1]. These metals can be released into watersheds from municipal and industrial activities and are difficult to remove due to the high solubility of these contaminants in water posing a threat to global water resources [2]. Conventional removal methods can result in the generation of large amounts of toxic sludge and secondary pollutants and are often ineffective against lower, yet still hazardous concentrations of metals found in wastewaters [3].

Biosorbents sourced from waste biomass avoid many of the environmental and costs issues associated with other treatments [4]. In adsorption, a porous solid with a high surface area to volume/mass ratio and potentially various surface functional groups bind (through physisorption, chemisorption, or some combination) aqueous metals. The type of binding is a function of the metal species and functional group, specific surface area (SSA), and other adsorbent properties. Recent research has studied the use of chemically functionalized porous silicates for use as adsorbents and have been successful in adsorbing certain types of heavy metals [5]–[7]. However, these materials do have the drawback of being difficult to prepare and requiring high-cost equipment and reagents. Recently, research has turned to using biochar as an adsorbent. Biochar is a material produced during pyrolysis, in which biomass is heated at elevated temperatures in the absence of oxygen, producing gases, a liquid “oil”, or bio-oil, and solid biochar [8]. Pyrolysis temperatures are typically between 300-900°C and solid residence times between seconds (fast pyrolysis) and minutes/hours (slow pyrolysis) [9]. Numerous feedstocks can be used in the pyrolysis process, including woody biomass [10],

agricultural residues [10], [11], and sewage sludge [12]. In addition to these, fisheries by-products are now being analyzed as a pyrolysis feed in coastal environments [13], [14]. The application of biochars from fisheries by-products as adsorbents is a very new field, with few experimental or review papers existing on the topic.

In the current article, a review of the various classes of pyrolysis feedstocks used in metal adsorption from aqueous solutions is presented. This begins with the more well-known lignocellulosic and agriculturally derived biochars then moving to fisheries waste-derived biochars and comparing biochar properties. Biochar derived from municipal wastes has been omitted from this review due to the high potential for inconsistencies and impurities in these feedstocks. The potential of each feedstock to adsorb metals is then discussed with respect to physicochemical properties, and conclusions are drawn on the advantages and disadvantages of each.

2.2 Pyrolysis Feedstocks

Pyrolysis can be performed on a wide variety of organic feedstocks, predominantly biomass with high carbon content. This is a broad sweeping definition, as multiple types of feedstocks have been studied for adsorption of pollutants from aqueous streams. In the subsections to follow, the qualities and characteristics of the feedstocks, along with the quality of their subsequent biochars from the perspective of metal adsorption is detailed.

2.2.1 Lignocellulosic Biomass

Lignocellulosic biomass is one of the more traditional forms of biomass in use for pyrolysis today, with its major sources being from the forestry and agricultural sectors. The feedstock is dominated by several plant polymers, predominantly cellulose, lignin, and hemicellulose. The highly complex nature of these plant macromolecules is what enables the derivation of high-quality fuels and chemical products upon pyrolysis, leaving behind a solid char that can be used in adsorption [15]. The exact quantities of these components and the presence of other compounds in the plant polymer matrix are dependent upon the type of lignocellulosic biomass, however, the focus of this review is on “woody” and herbaceous/agricultural biomass (well-studied feedstocks) and marine biomass (an emerging feedstock).

2.2.1.1 Woody Biomass

Woody biomass is derived from wood materials from the pulp and paper and forestry industries. These materials are very rich in lignin, the complex 3D structure of which binds the other plant materials into tight fibres, accounting for the material’s high strength [16]. Pyrolysis of woody biomass not only provides a highly valuable bio-oil (yields of 45-75% depending on reactor type and feedstock) [8], but also the “by-product” solid biochar has physical and surface properties that lend to a number of different industrial applications as a biomaterial.

Woody biomass is rich in organic content which contributes to the formation of a complex pore network as it volatilizes during the pyrolysis process, primarily as

temperatures at and above 500 °C [17]. The result of the process is the volatilization of organic molecules from the wood surface, which chemically and physically alters the properties of the resultant biochar. The pyrolysis process in wood was investigated by Zhang et al. [18], who compared the pyrolysis of oak (a hardwood) and pine (softwood) across a temperature range of 350-900 °C. The group noted that as pyrolysis temperature increased at each interval, the pH of the resultant biochar increased as well. This was accompanied by an associated decrease in the presence of acidic functional groups on the biochar's Fourier Transform Infrared (FT-IR) spectra, indicating that higher pyrolysis temperatures lead to a loss of organic functional groups, such as carboxyl and alcohol groups, and enrichment of alkaline minerals in the biochar [18].

Other variables play a role in the results of pyrolysis as well and have been discussed in numerous past studies. Temperature is among the main factors influencing the SSA of biochar, with studies such as Ronsse et al. [19] illustrating a generally positive correlation between temperature and SSA of biochar. In this study, a positive correlation was observed between the SSA of a pine (softwood) biochar and temperature up to the temperature of 600 °C, at which point an increase in temperature lowered the SSA as measured by N₂ Brunauer-Emmett-Teller (BET) analysis [19]. Heating rate has also been implicated as an important factor in influencing SSA by Chen et al. [20], who pyrolyzed poplar, a hardwood, increasing surface area was observed in chars up to 600 °C at a heating rate of 30°C/min, the upper end of pyrolysis, and produced maximum SSA of 411.06 m²/g. A heating rate of 30 °C/min, versus 10 °C/min or 50 °C/min provided the highest SSA at each temperature studied. At the lowest heating rate volatilization of

organics from the surface of particles forms surface micropores, while at high heating rates, the pore walls are destroyed, eliminating micropores [20]. Kloss et al. noted similar results in a study comparing biochars from spruce, poplar, and wheat straw, with significant increases in SSA occurring from 460 °C to 525 °C, and little change at temperatures below 460 °C [21]. Much of this feedstock-based difference in SSA could be attributed to differences in feedstock compositions. Here, Carrier et al. [22] found a linear correlation between the hemicellulose content of a given feedstock and the SSA of its biochar, with lower hemicellulose contents resulting in higher SSA [22]. The SSA of various wood-based biochars is provided in Table 2-1 and indicates a large variation in the SSAs obtained in past papers, which may be attributed to partially to differences in feedstock species as reported above, or differences in the techniques used for SSA measurement, which can heavily impact surface area measurements [23]. Generally, however, it can be seen from this information that biochar SSA changes very little below 450 °C and increases dramatically above this level. Due to the variance in data available, however, correlations can only be made in individual studies and will be omitted here.

Table 2-1: Physicochemical properties of wood-based biochar

Feedstock	Pyrolysis Temperature (°C)	Pyrolysis Time (min)	SSA (m ² /g)	pH	C (wt%)	H (wt%)	N (wt%)	O (wt%)	Ash (wt%)	Ref.:
Hardwood	450	N/A (Fast)	0.43	5.57	53.41%	2.30%	0.07%	5.67%	39%	[10]
Hardwood (Acacia)	300-400	120	1.30	7.62	69.6%	4.3%	0.6%	22.0%	3.5%	[24]
Hardwood (Citrus)	300	N/A	0.8	7.76	60.37%	4.43%	1.43%	25.34%	8.43%	[25]
Hardwood (Citrus)	450	N/A	2.8	10.00	62.74%	3.35%	1.14%	23.21%	9.56%	[25]
Hardwood (Citrus)	600	N/A	182	9.48	73.84%	1.96%	1.21%	14.05%	8.94%	[25]
Hardwood (Eucalyptus)	300-400	120	1.60	5.91	69.4%	5.1%	0.4%	23.2%	1.9%	[24]
Hardwood (Jarrah)	700	30	309.29	9.43	86.0%	1.6%	0.2%	8.8%	3.3%	[26]
Softwood (Pine)	300	N/A	0.2	7.10	65.79%	4.70%	0.32%	23.91%	5.27%	[25]
Softwood (Pine)	450	N/A	0.1	7.61	77.69%	3.21%	0.30%	15.27%	3.54%	[25]

Softwood (Pine)	600	N/A	209	7.05	82.74%	2.06%	0.32%	11.01%	3.87%	[25]
Softwood (Pine)	700	120	29	6.6	68.65%	0.59%	0.09%	2.71%	27.97%	[27]
Softwood (Pine)	700	30	219.35	7.79	79.5%	3.0%	0.2%	15.1%	2.2%	[26]
Softwood (Not Specified)	500	N/A (Fast)	95.58	N/A	76.37%	2.36%	0.15%	N/A	N/A	[28]
Hardwood (Willow)	550	120	75.1	9.20	66.61%	2.64%	0.63%	7.72%	2.4%	[29]

While biochar SSA is implicated as an important factor in the adsorption of heavy metals [17], [30], it is not the only important factor from the standpoint of metal adsorption. The surface functional groups on the biochar surface play another vital role in adsorbing metals given their ability to chelate and otherwise adsorb metals from solution [31].

Woody biomass, as well as most other lignocellulosic biomass, is rich in organic functional groups that can present in the final biochar, and in turn interact with aqueous metals through chelation, ion exchange, electrostatic interaction, and other adsorptive interactions [32]. Wang et al. investigated the chemical structure of several lignocellulosic biochars and noted the presence of hydroxyl (-O-H), aliphatic carbon (-C-H), carbonyl (-C=O), some amine groups (-N-H), and various aromatic carbon bonds (-C=C, -C-H). The group also notes the transformation of these groups as temperature is increased from 500 °C to 700 °C with hydroxyl and aliphatic groups being removed from the biochar, the loss of most amine groups, as well as the near-complete loss of C=O groups associated with esters, ketones, and carboxyl groups [33]. Fourier Transform Infrared (FT-IR) analysis or X-Ray Photoelectron Spectroscopy (XPS) [34] can be used to evaluate the changes in the electronic structure of functional groups in the biochar. A summary of functional group analyses is outlined in

Table 2-2, illustrating functional groups involved in adsorbing specific metals. This phenomenon presents a trade-off in the biochar production process, whereas higher temperatures correspond to higher SSAs, but also fewer organic functional groups [35].

Table 2-2: Organic functional groups involved in metal adsorption

Functional Group	Metal Interaction(s)	Ref.:
C-H	As(III)	[36]
COOH	As(III)	[36]
OH	As(III)	[36]
C-H	As(V)	[36]
COOH	As(V)	[36]
O-H	As(V)	[36]
C-H (aromatic)	Cd ²⁺	[37]
C ⁺ - π	Cd ²⁺	[37]
C ⁺ - π	Cd ²⁺	[38]
C=O	Cd ²⁺	[38]
COOH	Cd ²⁺	[37]
COOH	Cd ²⁺	[39]
OH	Cd ²⁺	[37]
C-O	Cu ²⁺	[32]
C=O	Cu ²⁺	[32]
COOH	Cu ²⁺	[31]
COOH	Cu ²⁺	[39]
COOH	Cu ²⁺	[40]
OH	Cu ²⁺	[40]
R-NH ₂	Cu ²⁺	[32]
COOH	Ni ²⁺	[31]
COOH	Ni ²⁺	[40]
OH	Ni ²⁺	[40]
C ⁺ - π	Pb ²⁺	[34]
COOH	Pb ²⁺	[41]
OH	Pb ²⁺	[41]
COOH	Zn ²⁺	[31]

COOH	Zn ²⁺	[39]
------	------------------	------

Harvey et al. [38] noted that the adsorption of cadmium (Cd²⁺) onto biochar was heavily controlled by the fact that the Cd²⁺ ion, being a soft lewis acid, favors soft bases for interaction. Therefore, while Cd²⁺ will interact with deprotonated carboxylic groups (perhaps mainly by electrostatic force), it prefers π electron interactions with the biochar surface [38]. Carrier et al. [31] studied an activated carbon using XPS to analyze mechanisms of metal adsorption. Carboxylate chelation is proposed to drive for copper (Cu²⁺), nickel (Ni²⁺), and (Zn²⁺) removal from solution, physisorption for Cd²⁺, manganese (Mn²⁺), and Zn²⁺, and hydrolysis to an oxide form for Cu²⁺, Mn²⁺, Ni²⁺, and lead (Pb²⁺) [31].

Woody biomass, though primarily constituted of an organic structure, also contains low quantities inorganic minerals that can contribute to the adsorption of heavy metals. The inorganic content of plant matter varies between classes and species of plant, woods generally having a very low mineral content (2.7% average by weight), and agricultural grasses and straws having a slightly higher content (7.8% average by weight) [42]. In pyrolysis, inorganics concentrate in the biochar as the organic volatilize [21]. In turn, the biochar mineral contents can become significant and can contribute to the adsorptive capacity of the char towards metals. Characterizations of this mineral fraction of biochar have been performed by Cruz Ceballos et al. [43], who found quantities of up to 0.26% by weight of halite salts in softwood biochar, along with a variety of other silicate, aluminum, and calcium-based minerals. Minerals were also found to be in higher quantities in the softwood bark biochar studied, with an overall mineral content of 4.45

weight percent for a char produced at 325 °C [43]. This mineral content can in turn contribute to the adsorption of metals through mechanisms such as ion exchange and co-precipitation [30]. However, in the case of woody biochar, Shen et al. [44] noted that whereas woody biochar has such a low mineral content, its contribution to ion exchange and co-precipitation mechanisms might be insignificant, though the role of alkaline minerals in determining biochar pH is likely still substantial [44].

The pH and electric charge of the biochar surface are also key parameters in determining adsorption capacity. The pH and surface charge depend on the feedstock and pyrolysis conditions used, leading to different adsorption characteristics [45]. In terms of pyrolysis conditions, increases in pyrolysis temperature (particularly above 400 °C) increase surface pH as a result of the increased loss of acidic functional groups on the biochar surface, and subsequent enrichment of alkaline minerals in the char [18], [46]. The change in pH occurs over a very narrow treatment temperature range, for example, the pH of biochar produced from corncob and miscanthus grass increased dramatically over the range of 400-450 °C, after which further temperature increases had little effect [47]. It was also observed by Budai et al. that pH could be directly correlated with the volatile matter of the feedstock material. The correlation found was that pH increased with decreasing amounts of volatile matter, which the group attributed to the fact that acidic functional groups contribute strongly to the composition of volatile matter in biochar [47]. From this information, biochar pH is primarily a function of temperature, though it is noted by Zhao et al. [48] that the heterogeneity of minerals in different feedstocks can also play a role [48]. Metals adsorption capacities have been demonstrated to be a function of zeta potential in past studies [49]. This effect is significant in the case of the

nitrate (NO_3^-) ion [50], arsenate (AsO_4^{3-}) and phosphate (PO_4^{3-}) [49], and Cd^{2+} [45], though it likely plays some role in the adsorption of all ions.

The impact of pH on metal adsorption is complex and is dependent on solution conditions. Generally, pH, in this case, relates to the mobility of the hydrogen ions in the acidic functional groups of the biochar and the associated charges they produce. For example, at very low pH, metal adsorption on the surface of biochar tends to be low, as acidic functional groups do not easily deprotonate to allow for chelation or ion exchange [51], [52]. This change in charge relates to the zeta potential of the biochar, which is a measure of the surface charge on the biochar [53]. Hong et al. demonstrated that the zeta potential of biochar tends to increase (while remaining negative across all studied solution pH) with increasing pyrolysis temperature due to loss of organic functional groups [45], while Fang et al. saw that the zeta potential of their softwood biochar only became positive for biochars produced over 500 °C and at solution $\text{pH} < 4$ [54]. Figure 2-1 demonstrates this trend for a variety of feedstocks through the measure of the isoelectric point (pH_{IEP}) of the biochar or the pH at which the surface charge of the biochar is zero.

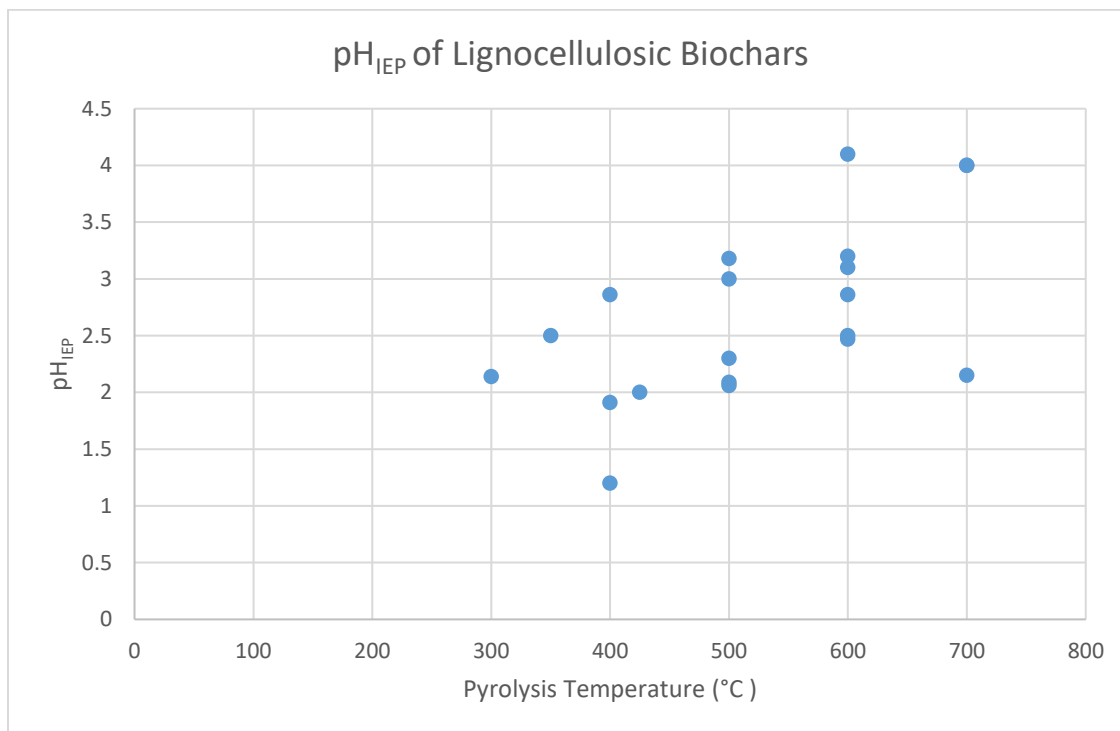


Figure 2-1: pH_{IEP} of lignocellulosic biochar as observed from literature. Data obtained from [37], [54]–[65]

The interplay between these factors and the pyrolysis conditions leads to complex behavior for metal adsorption on woody biochar. As a result, the optimum metal adsorption capacity for biochar from a certain source must be determined through extensive experimentation to determine the best balance of all properties. Table 2-3 demonstrates the results of some past metal adsorption studies using wood-based biochars as an adsorbent. From this table, the complexity of metal-adsorbent interactions is displayed, with biochars demonstrating varying adsorption capacities for different metals. As such, it is best to approach a review on this topic on a case-by-case basis.

Table 2-3: Pyrolysis conditions and adsorption capacities of various woody biochars for metals

Pyrolysis Feed	Pyrolysis Type	Pyrolysis Temperature (°C)	Pyrolysis Time (min)	Metal Tested	Q _{max} (mg/g)	Ref.:
Softwood (Pine)	Slow	-	120	Pb ²⁺	35.4	[66]
Softwood (Pine)	Slow	300	Not Provided	Pb ²⁺	2.847	[25]
Softwood (Pine)	Slow	450	Not Provided	Pb ²⁺	2.867	[25]
Softwood (Pine)	Slow	600	Not Provided	Pb ²⁺	1.685	[25]
Softwood (Pine)	Slow	-	120	Mg ²⁺	10.3	[66]
Softwood (Pine)	Slow	-	120	Cr(VI)	35.4	[66]
Softwood (Pine)	Slow	-	120	Ca ²⁺	4.81	[66]
Softwood (Pine)	Slow	300	Not Provided	As(V)	0.225	[25]
Softwood (Pine)	Slow	450	Not Provided	As(V)	0.229	[25]
Softwood (Pine)	Slow	600	Not Provided	As(V)	0.152	[25]
Softwood (Pine)	Slow	700	120	Cu ²⁺	2.73	[27]

Hardwood (Japanese Oak)	Slow	500	Not Provided	As(V)	3.89	[36]
Hardwood (Japanese Oak)	Slow	500	Not Provided	As(III)	3.06	[36]
Hardwood (Hickory)	Slow	600	60	Pb ²⁺	71.43	[67]
Hardwood (Hickory)	Slow	600	60	Cu ²⁺	12.3	[67]
Hardwood (Hickory)	Slow	600	60	Cd ²⁺	4.75	[67]
Hardwood (Eucalyptus)	Slow	300-400	120	Cu ²⁺	3.48	[24]
Hardwood (Citrus)	Slow	300	Not Provided	Pb ²⁺	7.153	[25]
Hardwood (Citrus)	Slow	450	Not Provided	Pb ²⁺	7.129	[25]
Hardwood (Citrus)	Slow	600	Not Provided	Pb ²⁺	7.729	[25]
Hardwood (Citrus)	Slow	300	Not Provided	As(V)	0.124	[25]
Hardwood (Citrus)	Slow	450	Not Provided	As(V)	0.115	[25]
Hardwood (Citrus)	Slow	600	Not Provided	As(V)	0.116	[25]
Hardwood (Acacia)	Slow	300-400	120	Cu ²⁺	9.70	[24]
Hardwood	Fast	450	5 s	Zn ²⁺	4.98	[10]

Hardwood	Slow	600	N/A	Zn ²⁺	6.4	[51]
Hardwood	Slow	600	N/A	Pb ²⁺	47.66	[51]
Hardwood	Slow	600	N/A	Ni ²⁺	6.16	[51]
Hardwood	Fast	450	5 s	Cu ²⁺	3.71	[10]
Hardwood	Slow	600	N/A	Cu ²⁺	6.42	[51]
Hardwood	Slow	350	240	Pb ²⁺	2.500	[34]
Hardwood	Slow	450	240	Pb ²⁺	2.499	[34]
Hardwood	Slow	550	240	Pb ²⁺	2.600	[34]
Hardwood	Slow	650	240	Pb ²⁺	2.050	[34]
Hardwood (Willow)	Slow	550	120	Cu ²⁺	13.0	[29]
Hardwood (Willow)	Slow	550	120	Ni ²⁺	11.7	[29]
Hardwood (Willow)	Slow	550	120	Cd ²⁺	76.4	[29]

In the case of Pb²⁺, the adsorption capacity varies considerably (1.685 mg/g to 71.43 mg/g) as the pyrolysis temperature, residence time, and feedstock change. Mohan et al. [68] found that lead sorption by woody biochars depended heavily on the amount of minerals present as evidenced by the release of native metals from the four biochars they tested, which were all produced at 400-450 °C. In this case, biochar from oak bark was found to have the second-highest mineral content of biochars studied, while also having the highest SSA, which likely leads to it having the highest adsorption capacity for Pb²⁺ from the chars studied here. The presence of functional groups and formation of hydroxides did account for some of the adsorption, highlighting the importance of functional groups in the adsorption process [68]. Zama et al. [34] also looked at the

adsorption of Pb^{2+} on a hardwood (mulberry) from biochars produced between 350 °C and 650 °C. Here, the adsorption capacity of chars produced at 350 °C, 450 °C, and 550 °C all produced similar adsorption capacities (2.5, 2.499, and 2.600 mg/g respectively) while at 650 °C there was a drop in adsorption capacity to 2.050 mg/g. This drop may be due to the drop in SSA for this biochar compared to others produced in the paper and could also be due to the loss of functional groups that Zama et al. found to be heavily involved in adsorbing lead [34]. Results such as this demonstrate that adsorption capacities can have variability based on numerous factors and should therefore always be carefully evaluated from case to case due to the complexity of the evolution of biochar properties.

On comparing results, it can be seen that certain metals are also selective towards certain biochars due to apparent feedstock and pyrolysis produced properties. Most biochars produced from woody feedstocks have ash contents that rarely exceed 10% by weight, however, in the studies by Abdel-Fattah et al. [66] and Shen et al. [51], ash quantities are notably high. Abdel-Fattah et al. found an ash quantity of 18.31% for a pinewood biochar (temperature not specified), where calcium oxide (CaO) dominated the inorganic contents at 27.7%, leading to a large Cation Exchange Capacity (CEC) of 33.048 cmol/kg [66]. Whereas one of the largest contributing mechanisms to lead adsorption is cation exchange with other divalent metals [30], it is therefore highly likely that this was a major contributing factor to the atypically high adsorption capacity of this biochar. Biochar in the study by Shen et al. [51] was produced at 600 °C from Salisbury wood (a hardwood), had 1.35wt% CaO and CEC between 5.62 and 7.20 cmol/kg (depending on particle size), and was mildly acidic pH [51]. The lower CEC is not nearly as high as

Abdel-Fattah's biochar however the adsorption capacity was slightly higher, likely due to different feedstocks and process conditions which would result in differences in SSA and functional groups.

Precipitation and ion exchange reactions with calcium (Ca) have been noted as possible mechanisms for Cu^{2+} and Zn^{2+} adsorption. Feng and Guo [69] used modified orange peels in the adsorption of aqueous solutions of Pb^{2+} , Cu^{2+} , and Zn^{2+} . Surface complexation was also proposed as a possible mechanism of adsorption for these metals [69]. Sheng et al. [70], proposed Cu^{2+} formed complexes with ethers, carboxylates, and hydroxyl groups on the surface of dried algae. Zn^{2+} adsorbed through ionic bonds to the carboxylate groups of the algae, while Ni^{2+} formed complexes similar to Cu^{2+} , though its adsorption was lower due to the greater chelating capacity of Ni^{2+} . Pb^{2+} was adsorbed primarily through carboxylate groups [70]. Similar results adsorption capacities for divalent heavy metal cations have been found elsewhere in literature [71].

The adsorption of arsenic (As) and chromium (Cr) from solution involve mechanisms that are more complex due to the fact these metals can be present as oxyanions in solution. The most common form of As in aqueous solutions is as an oxyanion, arsenite (AsO_3^{3-}), or arsenate (AsO_4^{3-}). Cr, meanwhile, can be present as either a lone cation, oxyanion, or a hydroxide, depending on the electrochemical conditions of the environment [30]. Electrostatic interactions between the metal complex and adsorbent surface are more complex, with As generally showing low adsorption capacities [25], [36] for woody biomass-based chars due to the overall negative charges on the surface of these materials under neutral or basic solution conditions. Recent studies have investigated modifying biochars with various cationic functional groups to improve the

adsorption of As and Cr under neutral and basic conditions. Agrafioti et al. [72] modified rice husk and solid waste biochar with Ca, atomic iron, and Fe(III) for adsorption of Cr and As. Both adsorption via electrostatic interactions and precipitation were increased in the doped biochars. Bismuth doped wheat biochar showed similar electrostatic interactions for As(V) oxyanions (arsenate), while As(III) (arsenite) adsorbed via ligand exchange, as reported by Zhu et al. [73]. The weakness of arsenic adsorption in unmodified biochars is due to weakly repulsive electrostatic charges between the anionic arsenic and negatively charged biochar surface [34]. Therefore, under neutral or basic conditions biochar requires modification for the adsorption of metal anions such as arsenic or chromium.

2.2.1.2 Herbaceous and Agricultural Biomass

Herbaceous and agricultural biomass sources are much more diverse than woody biomass. Blends of different herbaceous and agricultural feedstocks can be co-pyrolyzed resulting in a “tunable” biochar. This biomass is made up of “waste” discards from processing of agricultural resources, with examples including straw [10], [11], [74], grasses [25], [48], [75], seeds and husks [25], [72], and other residues of crops and processing by-products [76], [77]. Being lignocellulosic in chemistry, these feedstocks share many commonalities with woody biomass, but also have some differences owing to changes in their chemistry. Primarily, the organic functionality of biochar made from crop straws and husks, one of the most common agricultural residues, is very similar in functional group content to wood-based biochar. FT-IR spectra produced by Zama et al.

[34] found similar functionalities in mulberry wood biochar and peanut straw biochar [34].

It is mainly through other biochar properties in which the distinction between biochar feedstocks becomes apparent. Wang et al. [33] compared these differences in a study using two hardwoods, as well as rice straw, wheat straw, maize straw, rice husks, and coconut shell to produce biochar at either 500 °C or 700 °C under slow pyrolysis. Here, it was found that agricultural feedstocks produced higher biochar yields with higher pH and mineral content than their wood-based counterparts. SSA was found to be lower for agricultural feedstocks when pyrolyzing at 500 °C, however, at 700 °C all feedstocks were of comparable SSAs [33]. A similar result was found by Mukherjee et al. [35] who pyrolyzed feedstocks at 650 °C and found that the grass they pyrolyzed had an SSA of 77 m²/g, in comparison to 225 m²/g and 285 m²/g for oak and pine, respectively [35]. The solid residence time is another factor impacting SSA of biochars in slow pyrolysis. Zhao et al. [78] noted that when pyrolyzing rapeseed stems at 500 °C, increasing residence time from 10 minutes to 60 minutes had a positive effect (98.4 m²/g), however, a further increase to 100 minutes led to a drop in SSA to 91.4 m²/g [78]. Other studies have shown mixed results indicating increasing SSA with increasing residence times at lower temperatures, but lower SSA at longer residence time and higher temperatures [19]. These findings may result from the higher hemicellulose content of many agricultural residues in comparison to wood-based feedstocks [22], as it was reported by Vassilev et al. [79] that the hemicellulose content of agricultural straws and husks was 31.5% and 27.4% by weight, respectively, whereas for wood it was 23.4% by weight [79].

Agricultural residues often contain higher levels of minerals than wood [42], which is in turn reflected in biochar ionic content. Maiti et al. [80] characterized char from pyrolysis of rice husks at different temperatures for use as a fuel. The char had an appreciable ionic composition, with Ca, Fe, potassium (K), and silicon (Si), all of which could contribute to increased adsorptive effects through ionic exchange [80]. Y. Wang et al. [33] characterized the several agricultural biochars in comparison with wood biochar and found that the CEC was much higher in agricultural biochar in comparison to woody biochar (1.3-3.0 cmol/kg in wood-based char in comparison to 11.7-34.8 cmol/kg in agricultural char) [33]. This high quantity of soluble cations in native agricultural feedstocks has been demonstrated to play a significant role in the adsorption of metals in literature. A study by Park et al. [81] using rice straw biochar, 62.3% of Cu^{2+} adsorption and 42.5% of Zn^{2+} adsorption was a result of ion exchange of native cations with the pollutant cations [81]. Furthermore, Liu and Fan [82] studied the adsorption of Cd^{2+} on a rice straw biochar, where magnesium (Mg) and Ca in the char were found to play a major role in adsorption. The results indicated that this occurred primarily through ion exchange, in which the minerals containing Mg^{2+} and Ca^{2+} exchanged these cations for Cd^{2+} , which in turn formed a precipitate within the biochar structure [82].

More intensive studies on the mineral fraction of biochar have also taken place. Yuan et al. [83] studied the composition of the inorganic fraction in canola, corn, soybean, and peanut straw. Here, the biochar was enriched primarily in alkali minerals including KCl, $\text{CaMg}(\text{CO}_3)$, $\text{Ca}(\text{CO}_3)$, and SiO_2 , leading to higher biochar pH and zeta potential [83]. Wang et al. [33] noted that the biochars they produced from crop straws had higher pH than those from hardwood and softwood biochar produced at the same temperature,

further confirming the above observation [33]. The zeta potential of agricultural straws has been studied in relation to adsorption. Tong et al. [84] found that their biochar samples, made from peanut, soybean, and canola straw, all remained negatively charged in solution down to a pH of 3.5, which they suspect played some role in the adsorption of Cu^{2+} [84].

Due to the diverse feedstocks, the biochar from agricultural feedstock varies widely in SSA, elemental, porosity, and pH. Table 2-4 outlines the properties of various agriculturally derived biochars as a function of production conditions.

Table 2-4: Physicochemical Properties of Various Agricultural Biochars

Feedstock	Pyrolysis Temperature (°C)	Time (min)	SSA (m ² /g)	pH	C (wt%)	H (wt%)	N (wt%)	O (wt%)	Ash (wt%)	Ref.:
Rice Straw	600	240	162.6	9.89	68.7%	2.3%	3.0%	25.9%	NM	[81]
Rice Straw	600	180	156.2	7.3	78.50%	NM	0.7%	13.39%	10.65%	[85]
Rice Husk	300	120	2.57	7.47	52%	3.85%	1.65%	42.32%	32.49%	[86]
Rice Husk	500	120	18.41	10.47	57%	1.98%	1.39%	39.80%	44.38%	[86]
Rice Husk	750	120	53.08	10.51	64%	1.28%	0.96%	43.55%	49.93%	[86]
Cornstraw	600	180	70.0	8.5	72.0%	NM	1.09%	18.3%	3.19%	[85]
Wheatstraw	600	300	26.3	9.9	54%	2%	0.9%	2.3%	41.1%	[11]
Wheatstraw	600	180	183.3	7.2	72.9%	NM	0.81%	17.2%	8.11%	[85]
Wheatstraw	400	300	4.8	9.1	65.7%	4.05%	1.05%	NM	9.7%	[21]
Wheatstraw	460	300	2.8	8.7	72.4%	3.15%	1.07%	NM	12.0%	[21]
Wheatstraw	525	300	14.2	9.2	74.4%	2.83%	1.04%	NM	12.7%	[85]
Switchgrass	300	N/A (Fast)	1.2	8.21	59.32%	4.64%	2.34%	31.68%	NM	[25]
Switchgrass	450	N/A (Fast)	10	9.74	64.02%	2.87%	2.23%	28.27%	NM	[25]
Switchgrass	600	N/A (Fast)	15	9.84	68.15%	2.21%	1.90%	24.99%	NM	[25]

Alfafa	300	N/A (Fast)	0.6	8.38	64.72%	5.26%	3.10%	24.24%	NM	[25]
Alfafa	450	N/A (Fast)	0.7	9.17	69.66%	3.01%	2.42%	22.13%	NM	[25]
Alfafa	600	N/A (Fast)	0.2	10.35	73.25%	1.91%	2.22%	19.43%	NM	[25]
Cottonstraw	600	180	49.4	8.4	74.8%	NM	0.69%	17.64%	2.90	[85]
Corn Stalk	400	N/A (Fast)	NM	8.47	50.60%	2.38%	1.28%	19.33%	25.73%	[41]
Corn Stalk	450	N/A (Fast)	NM	9.82	53.07%	2.19%	1.28%	15.36%	27.49%	[41]
Corn Stalk	500	N/A (Fast)	NM	10.3	54.68%	2.09%	1.12%	12.38%	29.2%	[41]
Corn Stalk	550	N/A (Fast)	NM	10.64	55.47%	1.99%	1.30%	9.75%	31.02%	[41]
Corn Stalk	600	N/A (Fast)	NM	10.99	57.13%	1.85%	1.01%	6.21%	33.43%	[41]
Canna Indica	400	120	5.81	10.12	48.29%	2.85%	2.40%	17.31%	29.17%	[61]
Canna Indica	500	120	7.73	10.32	51.69%	1.43%	0.93%	13.69%	32.27%	[61]
Canna Indica	600	120	10.40	10.47	52.61%	1.31%	1.54%	9.79%	34.76%	[61]

* NM – Not measured

Most of the biochars show only moderate SSA until reaching advanced temperatures above 500 °C. This is similar to what was observed in the case of woody biochar in Table 2-1. The sorption capacities of various agricultural chars for metals are outlined in Table 2-5.

Table 2-5: Equilibrium Adsorption Data for Various Biochars

Feedstock	Pyrolysis Type	Pyrolysis Temperature (°C)	Pyrolysis Time (min)	Pollutants Tested:	Qmax (mg/g)	Ref.:
Cornstraw	Slow	600	120	Cu ²⁺	11.8	[10]
Cornstraw	Slow	600	120	Zn ²⁺	7.48	[10]
Wheat Straw	Slow	600	300	Cd ²⁺	17.92	[11]
Wheat Straw	Slow	600	300	Ni ²⁺	16.26	[11]
Wheat Straw	Slow	300	120	Pb ²⁺	56.0	[46]
Wheat Straw	Slow	500	120	Pb ²⁺	76.9	[46]
Wheat Straw	Slow	700	120	Pb ²⁺	100.0	[46]
Alfalfa	Slow	300	Not Provided	Pb ²⁺	7.517	[25]
Alfalfa	Slow	300	Not Provided	As(V)	0.153	[25]
Alfalfa	Slow	450	Not Provided	Pb ²⁺	7.355	[25]
Alfalfa	Slow	450	Not Provided	As(V)	0.276	[25]
Alfalfa	Slow	600	Not Provided	Pb ²⁺	7.587	[25]
Alfalfa	Slow	600	Not Provided	As(V)	0.146	[25]
Rice Straw	Slow	600	240	Cu ²⁺	56.5	[81]

Rice Straw	Slow	600	240	Zn ²⁺	38.6	[81]
Rice Straw	Slow	400	240	Cd ²⁺	38.5	[87]
Rice Straw	Slow	700	240	Cd ²⁺	62.3	[87]
Rice Straw	Slow	400	240	Ni ²⁺	25.7	[87]
Rice Straw	Slow	700	240	Ni ²⁺	57.4	[87]
Rice Straw	Slow	300	240	Cd ²⁺	18.94	[37]
Rice Straw	Slow	500	240	Cd ²⁺	14.65	[37]
Rice Straw	Slow	700	240	Cd ²⁺	18.12	[37]
Wheat Straw	Slow	300	120	Cd ²⁺	38.4	[82]
Wheat Straw	Slow	500	120	Cd ²⁺	52.1	[82]
Wheat Straw	Slow	700	120	Cd ²⁺	69.8	[82]

Table 2-5 illustrates that many crop residues have a significant adsorption capacity for heavy metals relative to woody biochar, with the major exception being the case of As(V). The low adsorption capacity for arsenic observed here may be attributed to the fact that As adsorption is primarily electrostatically controlled [25].

In contrast, divalent metals have been shown to have high adsorption capacities on agriculture-based biochars. Deng et al. [87] observed that a very important factor involved in the adsorption of Ni²⁺ and Cd²⁺ was ion exchange with native cations, demonstrating the importance that the high mineral content of these chars has a large impact on metal adsorption [87]. Liu and Fan [82] studied the adsorption of Cd²⁺ on a rice straw biochar, where Mg and Ca in the char were found to play a major role in adsorption. The results indicated that this occurred primarily through ion exchange, in which the minerals containing Mg and Ca exchanged these cations for Cd²⁺, which in turn formed a precipitate within the biochar structure. In addition to this, coordination with organic functionalities on the biochar and cation- π interactions, particularly in the

300 °C biochar as minerals were not as concentrated in this sample [82]. Gao et al. [37] produced rice straw biochar between 300 and 700 °C, where adsorption of Cd by the biochar was dominated by ion exchange with carbonates, hydroxides, and phosphates, and complexation with silicon compounds [37]. Silica (SiO₂) shows an adsorption mechanism not comparable to other minerals listed here. Being poorly soluble, ion exchange has not been stated in literature as a common adsorption mechanism for the mineral. Its impact has been assessed by Xu and Chen [88], who attributed the adsorption of Cd²⁺ partially to electrostatic interactions with the SiO₂ as the mineral's oxygen atoms became negatively charged under its isoelectric pH of 3.0 [88]. Further study on this topic is highly warranted to better understand the impact that mineral groups in biochar have on the adsorption of heavy metals. Zama et al. [34] studied biochar derived from buckwheat husk, corn cobs, mulberry wood, and peanut shells as an adsorbent for Pb²⁺ and observed the formation of a number of lead carbonates, phosphates, and hydroxides. This was attributed to ion exchange with the native biochar minerals [34].

2.2.2 Marine Biomass

While biochar from terrestrial-based waste biomass has been studied extensively, there have been very few publications studying biochar derived from fish harvesting/processing by-products. Fish and marine crustacean discards represent a major source of waste in the fisheries and aquaculture sectors, with much of this waste being disposed of at sea. Up to 30% of the total catch weight of snow crab in Canada ends up

as discards, while discards of certain shrimp species can range from 35-45% of the biomass weight [89]. In general, the “by-product” from fish harvesting/processing varies by species, season, and location and be as low as 20 wt% (mass by-product/mass of landed material) to as high as 80 wt% [90]. The environmental impact of disposal of these discards to the ocean (the most common disposal method) includes nutrient imbalances, decreased marine oxygen levels, increased turbidity, and many other effects that could potentially harm aquatic life [90]. Current research on recovering value from these by-products is predominantly focused on the isolation of different nutrient streams from the waste [89]–[92]. However, this ignores the less nutrient-rich material or badly degraded material, which has various other potential applications as feedstocks for polyurethanes [93], epoxy composites [94], other polymers [95], biocomposites [96], and biosorbents [97]–[99], among others.

Pyrolysis of fish and seafood processing wastes presents a simple method for valorizing these low-nutritive by-products. Crab and shrimp shell discards are two of the most prominent seafood processing wastes in Atlantic Canada and contain minerals and other functional groups that could enhance the adsorption of aqueous contaminants. Namely, crustacean waste is rich in the mineral calcium carbonate (CaCO_3), along with other impurity metal carbonates [100] and in some cases apatite [101], along with chitin, a glucosamine-based biopolymer, and other organics [102]. CaCO_3 itself is capable of engaging in adsorption, through mechanisms such as ion exchange, co-precipitation, and electrostatic interactions [103], giving it similar properties to the mineral fraction of lignocellulosic biochar. Crustacean shells are high in chitin, a major biopolymer consisting of glucosamine ($\text{C}_6\text{H}_{13}\text{NO}_5$) monomers [104]. In its virgin form, chitin has

already seen numerous applications in wastewater treatment due to complexation with various functional groups (particularly the amide), precipitation on the chitin surface, and in some cases electrostatic effects [105]–[107]. Furthermore, chitin has been shown to form highly aromatic structures with good SSA upon pyrolysis, leading to good performance as an adsorbent for organics [108], [109]. The characteristics of marine-based biochar are summarized in Table 2-6.

Table 2-6: Characteristics of some fisheries waste biochars

Feedstock	Pyrolysis Temperature (°C)	S.A. (m ² /g)	C (wt%)	H (wt%)	N (wt%)	Ca (wt%)	Ref.:
Crayfish Shells	300	32.67	23.45%	0.92%	1.85%	20.47%	[110]
Crayfish Shells	450	25.46	20.63%	0.31%	1.28%	22.56%	[110]
Crayfish Shells	600	63.79	21.17%	0.22%	1.26%	16.08%	[110]
Crab Shell	300	3.52	25.21%	2.21%	3.26%	22.91%	[14]
Crab Shell	600	52.13	19.20%	0.28%	2.01%	27.38%	[14]
Crab Shell	900	48.44	9.08%	0.89%	1.00%	36.14%	[14]
Shrimp Shell	500	13.3	52.1%	NM	NM	21.03%	[48]
Fish Frames	200	10.7	20.13%	NM	6.25%	17.68%	[13]
Fish Frames	600	85.0	11.63%	NM	2.53%	23.82%	[13]
Fish Frames	900	81.9	10.73%	NM	1.48%	24.91%	[13]
Pure Chitin	600	410	84.9%	2.0%	6.5%	N/A	[111]

Only a few papers have studied the adsorptive performance of marine-based feedstocks in solution and have shown very promising results, which are summarized in Table 2-7. Dai

et al. [14] studied the pyrolysis of crab shell from an unspecified species in China and subsequently analyzed its adsorption capacity for phosphorous in the form of phosphates. They report a complete removal of phosphorous from solution at a concentration of 80 mg/L of PO_4^{3-} for biochar produced at 800°C. The group attributes this exceptionally high performance due to the formation of lime as the pyrolysis temperature exceeded 700°C [14]. Studies on the adsorption affinities of lime for phosphates have been proven in past studies where the adsorption is proposed to occur either through surface complexation or precipitation [112], [113]. Xiao et al. [110] pyrolyzed crayfish shells at three temperatures (300, 450, and 600 °C) for 2 hours and tested the produced biochar for Pb^{2+} adsorption. These chars had high calcium content. Adsorption was performed at an initial pH of 7, and char produced at 600 °C had the highest adsorption capacity at 190.7 mg Pb/g. These chars also exhibited good SSAs, reaching up to 63.79 m^2/g as shown in Table 2-6, along with the other properties of the biochar [110].

Biochars from fish bones are also highly mineral-rich. Carbonate apatite ($\text{Ca}_{10}(\text{PO}_4)_6(\text{CO}_3)$) is the dominant mineral over pyrolysis temperatures below 800 °C and degrading to primarily oxyapatite ($\text{Ca}_{10}(\text{PO}_4)_6\text{O}$) at higher temperatures [13]. Wang et al. [114] used elemental analysis to show the simultaneous loss of calcium and gain of both Pb^{2+} and PO_4^{3-} mass in fish bone biochar, indicating a likely ion exchange between Ca^{2+} and Pb^{2+} followed by chemisorption of the Pb^{2+} (properties shown in Table 2-6). Chemisorption of Pb^{2+} was verified by XPS, showing the formation of a bond between the PO_4^{3-} and Pb^{2+} . Precipitation due to reaction of lead with dissolved carbonates from calcium carbonate may have also contributed to this effect, as shown by the loss of the carbonate band intensities in the char's FT-IR spectra before and after adsorption [114].

A similar mechanism for lead sorption was proposed in a study by Piccirillo et al. [13]. Biochar produced from cod bones adsorbed Pb^{2+} at a pH slightly under 6, primarily through the mechanism of ion exchange, achieving an adsorption capacity of 714.24 mg/g [13].

Table 2-7: Adsorption capacities for various marine shell-derived biochars

Feedstock	Pyrolysis Temperature (°C)	Pyrolysis Time (min)	Pollutant(s) Tested:	q_{max} (mg/g)	Ref.:
Crayfish Shells	350	120	Pb^{2+}	176.7	[110]
Crayfish Shells	450	120	Pb^{2+}	157.3	[110]
Crayfish Shells	600	120	Pb^{2+}	190.7	[110]
Crayfish Shells ^a	600	120	$Pb^{2+}/Cu^{2+}/As(III)$	7.5/3.6/2.0	[110]
Crab shell	300	120	PO_4^{3-}	64	[14]
Crab shell	400	120	PO_4^{3-}	53.6	[14]
Crab shell	500	120	PO_4^{3-}	52	[14]
Crab shell	600	120	PO_4^{3-}	20.8	[14]
Crab shell	700	120	PO_4^{3-}	59.2	[14]
Crab shell	800	120	PO_4^{3-}	80	[14]
Crab shell	900	120	PO_4^{3-}	80	[14]
Grass Carp Bones	400	60	Pb^{2+}	341.931	[114]
Grass Carp Bones	500	60	Pb^{2+}	688.523	[114]

Grass Carp Bones	600	60	Pb ²⁺	404.28	[114]
Fish Bones	400	60	Pb ²⁺	638.72	[13]
Fish Bones	600	60	Pb ²⁺	409.40	[13]
Fish Bones	900	60	Pb ²⁺	293.07	[13]

^a This experiment was performed on a ternary solution of Pb²⁺, Cu²⁺, and As(III)

The pyrolysis of chitin to produce pyrolysis oils and biochar has been studied. Qiao et al. [115] used Thermal Gravimetry-Mass Spectrometry (TG-MS) from ambient temperature to 900 °C, and XPS to analyze the gaseous and solid products from the pyrolysis of pure chitin. The gas and vapour fraction consisted mainly of very light hydrocarbon gases, ammonia, water, and formic acid and heavily aromatized biochars with some functional groups remaining from the virgin material [115]. Magnacca et al. [104] found similar results for pyrolyzed chitin at lower temperatures which resulted in higher nitrogen content which formed ring structures such as pyrazines, pyridines, and pyrroles in the char and vapour phase [104], as had previously been observed by Corazarri et al. [116]. The nitrogen functionalized aromatic rings produced by pyrolysis of chitinous biomass are perhaps the most important features of this char. White et al. [117] used shrimp shells as a feedstock for hydrothermal treatment, followed by slow pyrolysis peaking at 750°C. The char was treated with acetic acid to remove minerals. Pyrrolic and pyridinic nitrogen compounds were formed as well as quaternary nitrogen all bound within the graphitic phase [117]. Ilnicka et al. [111] characterized phosphoric acid-activated chitin-based biochar and found additional evidence for the presence of nitrogen in the carbon ring structures of the char [111].

Less common are studies on the adsorptive properties of chitinous biochars with respect to heavy metals, but some studies on nitrogen-doped carbonaceous adsorbents do somewhat bridge the gap. Shin et al. [118] fabricated carbon nanoparticles using pyrroles, finding that following carbonization, a high number of pyridinic and pyrrolic nitrogen atoms could be detected using XPS, which contain unpaired electrons due to the sp^2 hybridization on the nitrogen atom of these rings. Adsorption tests on silver (Ag^+), Cr^{3+} , Pb^{2+} , Ni^{2+} , Zn^{2+} , and mercury (Hg^{2+}) in solution demonstrated that these components participated in adsorption of hard metals (Cr^{3+} , Zn^{2+} , and Ni^{2+} in this case) [118]. Veselá and Slovák [119] produced a nitrogen-doped adsorbent from pyrolysis of a xerogel in ammonia showed an increased adsorption capacity for Cu^{2+} and Pb^{2+} , which in this case was attributed to complexation with pyridine and pyrrole components of the pyrolyzed xerogel [119].

Biochars with both high mineral content and high nitrogen content have potential for use as effective metal adsorbents. Other than the studies noted above, the study of pyrolysis of chitinous biomass and the resulting chemical alterations to the chars throughout pyrolysis is limited, and therefore tailoring pyrolysis conditions to produce chars appropriate to adsorption application is required. A deeper analysis on this feedstock could also benefit seafood producers by providing a simpler method of processing this waste that could be readily performed on or nearby the main processing plant, cutting many of the current costs which are currently leading to the immediate disposal of the majority of shellfish processing wastes.

2.3 Conclusions

Biochar is a highly versatile material, with adsorption capacity that can be readily tuned towards adsorbing the contaminant of interest by altering either the feedstock material or pyrolysis conditions, or both, in other cases. This capability, combined with its low cost of production and environmental sustainability, makes biochar a highly attractive candidate for a metal adsorbent. The use of lignocellulosic feedstocks for biochar production has been studied thoroughly, though much of this research has focused on slow pyrolysis. While this can produce biochars of very high quality, it is noted that the production of bio-oils and biogas from slow pyrolysis is limited, therefore restricting the profitability of this process to the biochar produced. Further research focusing on fast pyrolysis biochars could enable better process optimization for designing a biochar that serves as a competitive metal adsorbent, while also yielding high-value chemicals from the bio-oil and gas streams and could make the process more feasible on a commercial scale. In addition to this, other feedstocks, such as fisheries residues, have not been heavily studied, even though their biochars have presented good adsorbent properties in the few literature results that exist on them. These biochars could serve as potent adsorbents for wastewaters containing heavy metals, while also providing a simple valorization route for a waste product that currently serves little to no purpose in many rural communities.

Future research will aim to correlate the properties of both slow and fast lignocellulosic biochars, as well as study their adsorptive capacity to observe underlying patterns and to determine whether fast pyrolysis char can perform similarly in adsorptive performance to the slow pyrolysis chars studied in this review. Furthermore, the adsorptive performance

of marine-derived biochars will be studied in-depth to understand its feasibility as an adsorbent, and how this performance compares with other more common adsorbents. Further study in this field could facilitate the future expanded commercialization and optimization of biochar as a metal adsorbent and provide benefits across numerous industries.

Acknowledgements:

The authors would like to acknowledge the support of NSERC and the Ocean Frontier Institute (OFI) for their contributions in funding this project.

Bibliography:

- [1] J. O. Nriagu, "A History of Global Metal Pollution," *Science* (80-), 1996.
- [2] D. S. Malik, C. K. Jain, and A. K. Yadav, "Removal of heavy metals from emerging cellulosic low-cost adsorbents: a review," *Appl. Water Sci.*, 2016.
- [3] A. Azimi, A. Azari, M. Rezakazemi, and M. Ansarpour, "Removal of Heavy Metals from Industrial Wastewaters: A Review," *ChemBioEng Rev.*, vol. 4, no. 1, pp. 37–59, 2017.
- [4] M. A. Renu and K. Singh, "Heavy metal removal from wastewater using various adsorbents: a review," *J. Water Reuse Desalin.*, vol. 7, no. 4, pp. 387–419, 2017.
- [5] J. Aguado, J. M. Arsuaga, A. Arencibia, M. Lindo, and V. Gascón, "Aqueous heavy metals removal by adsorption on amine-functionalized mesoporous silica," *J. Hazard. Mater.*, 2009.
- [6] A. Benhamou, M. Baudu, Z. Derriche, and J. P. Basly, "Aqueous heavy metals removal on amine-functionalized Si-MCM-41 and Si-MCM-48," *J. Hazard. Mater.*, 2009.
- [7] S. Babel and T. A. Kurniawan, "Low-cost adsorbents for heavy metals uptake from contaminated water: A review," *Journal of Hazardous Materials*. 2003.
- [8] S. Papari and K. Hawboldt, "A review on the pyrolysis of woody biomass to bio-oil: Focus on kinetic models," *Renew. Sustain. Energy Rev.*, vol. 52, pp. 1580–1595, Dec. 2015.
- [9] S. Papari, K. Hawboldt, and R. Helleur, "Pyrolysis: A Theoretical and Experimental Study on the Conversion of Softwood Sawmill Residues to Biooil," *Ind. Eng. Chem. Res.*, vol. 54, no. 2, pp. 605–611, Jan. 2015.
- [10] X. Chen *et al.*, "Adsorption of copper and zinc by biochars produced from pyrolysis of hardwood and corn straw in aqueous solution," *Bioresour. Technol.*, 2011.
- [11] A. Bogusz, K. Nowak, M. Stefaniuk, R. Dobrowolski, and P. Oleszczuk, "Synthesis of biochar from residues after biogas production with respect to cadmium and nickel removal from wastewater," *J. Environ. Manage.*, vol. 201, pp. 268–276, Oct. 2017.
- [12] H. Lu, W. Zhang, Y. Yang, X. Huang, S. Wang, and R. Qiu, "Relative distribution of Pb²⁺ sorption mechanisms by sludge-derived biochar," *Water Res.*, 2012.
- [13] C. Piccirillo, I. S. Moreira, R. M. Novais, A. J. S. Fernandes, R. C. Pullar, and P.

- M. L. Castro, "Biphasic apatite-carbon materials derived from pyrolysed fish bones for effective adsorption of persistent pollutants and heavy metals," *J. Environ. Chem. Eng.*, 2017.
- [14] L. Dai *et al.*, "Calcium-rich biochar from the pyrolysis of crab shell for phosphorus removal," *J. Environ. Manage.*, 2017.
- [15] S. Vaz, "An analytical chemist's view of lignocellulosic biomass," *BioResources*, 2015.
- [16] P. McKendry, "Energy production from biomass (part 1): Overview of biomass," *Bioresource Technology*. 2002.
- [17] M. F. Aller, "Biochar properties: Transport, fate, and impact," *Crit. Rev. Environ. Sci. Technol.*, vol. 46, no. 14–15, pp. 1183–1296, 2016.
- [18] H. Zhang, C. Chen, E. M. Gray, and S. E. Boyd, "Effect of feedstock and pyrolysis temperature on properties of biochar governing end use efficacy," *Biomass and Bioenergy*, vol. 105, pp. 136–146, Oct. 2017.
- [19] F. Ronsse, S. van Hecke, D. Dickinson, and W. Prins, "Production and characterization of slow pyrolysis biochar: Influence of feedstock type and pyrolysis conditions," *GCB Bioenergy*, vol. 5, no. 2, pp. 104–115, 2013.
- [20] D. Chen, Y. Li, K. Cen, M. Luo, H. Li, and B. Lu, "Pyrolysis polygeneration of poplar wood: Effect of heating rate and pyrolysis temperature," *Bioresour. Technol.*, vol. 218, pp. 780–788, 2016.
- [21] S. Kloss *et al.*, "Characterization of Slow Pyrolysis Biochars: Effects of Feedstocks and Pyrolysis Temperature on Biochar Properties," *J. Environ. Qual.*, vol. 41, no. 4, p. 990, 2012.
- [22] M. Carrier, J.-E. Joubert, S. Danje, T. Hugo, J. Görgens, and J. (Hansie) Knoetze, "Impact of the lignocellulosic material on fast pyrolysis yields and product quality," *Bioresour. Technol.*, vol. 150, pp. 129–138, Dec. 2013.
- [23] G. Sigmund, T. Hüffer, T. Hofmann, and M. Kah, "Biochar total surface area and total pore volume determined by N₂ and CO₂ physisorption are strongly influenced by degassing temperature," *Sci. Total Environ.*, vol. 580, pp. 770–775, Feb. 2017.
- [24] D. Arán, J. Antelo, S. Fiol, and F. Macías, "Influence of feedstock on the copper removal capacity of waste-derived biochars," *Bioresour. Technol.*, 2016.
- [25] S. Wang *et al.*, "Physicochemical and sorptive properties of biochars derived from woody and herbaceous biomass," *Chemosphere*, 2015.

- [26] S. Jiang, L. Huang, T. A. H. Nguyen, V. Rudolph, H. Yang, and D. Zhang, "Copper and zinc adsorption by softwood and hardwood biochars under elevated sulphate-induced salinity and acidic pH conditions," *Chemosphere*, vol. 142, pp. 64–71, Jan. 2016.
- [27] Z. Liu, F. S. Zhang, and J. Wu, "Characterization and application of chars produced from pinewood pyrolysis and hydrothermal treatment," *Fuel*, vol. 89, no. 2, pp. 510–514, Feb. 2010.
- [28] H. Bamdad, K. Hawboldt, and S. Macquarrie, "Nitrogen Functionalized Biochar as a Renewable Adsorbent for Efficient CO₂ Removal," *Energy and Fuels*, vol. 32, no. 11, pp. 11742–11748, 2018.
- [29] S. Wang, J.-H. Kwak, M. S. Islam, M. A. Naeth, M. Gamal El-Din, and S. X. Chang, "Biochar surface complexation and Ni(II), Cu(II), and Cd(II) adsorption in aqueous solutions depend on feedstock type," *Sci. Total Environ.*, vol. 712, p. 136538, Apr. 2020.
- [30] H. Li, X. Dong, E. B. da Silva, L. M. de Oliveira, Y. Chen, and L. Q. Ma, "Mechanisms of metal sorption by biochars: Biochar characteristics and modifications," *Chemosphere*, vol. 178, pp. 466–478, 2017.
- [31] A. J. Carrier, I. Abdullahi, K. A. Hawboldt, B. Fiolek, and S. L. MacQuarrie, "Probing Surface Functionality on Amorphous Carbons Using X-ray Photoelectron Spectroscopy of Bound Metal Ions," *J. Phys. Chem. C*, vol. 121, no. 47, pp. 26300–26307, 2017.
- [32] R. Xie, Y. Jin, Y. Chen, and W. Jiang, "The importance of surface functional groups in the adsorption of copper onto walnut shell derived activated carbon," *Water Sci. Technol.*, vol. 76, no. 11–12, pp. 3022–3034, 2017.
- [33] Y. Wang, Y. Hu, X. Zhao, S. Wang, and G. Xing, "Comparisons of biochar properties from wood material and crop residues at different temperatures and residence times," *Energy and Fuels*, vol. 27, no. 10, pp. 5890–5899, 2013.
- [34] E. F. Zama, Y. G. Zhu, B. J. Reid, and G. X. Sun, "The role of biochar properties in influencing the sorption and desorption of Pb(II), Cd(II) and As(III) in aqueous solution," *J. Clean. Prod.*, 2017.
- [35] A. Mukherjee, A. R. Zimmerman, and W. Harris, "Surface chemistry variations among a series of laboratory-produced biochars," *Geoderma*, vol. 163, no. 3–4, pp. 247–255, Jul. 2011.
- [36] N. K. Niazi *et al.*, "Arsenic removal by Japanese oak wood biochar in aqueous solutions and well water: Investigating arsenic fate using integrated spectroscopic and microscopic techniques," *Sci. Total Environ.*, vol. 621, pp. 1642–1651, Apr.

2018.

- [37] L.-Y. Gao *et al.*, “Relative distribution of Cd²⁺ adsorption mechanisms on biochars derived from rice straw and sewage sludge,” *Bioresour. Technol.*, vol. 272, pp. 114–122, Jan. 2019.
- [38] O. R. Harvey, B. E. Herbert, R. D. Rhue, and L. J. Kuo, “Metal interactions at the biochar-water interface: Energetics and structure-sorption relationships elucidated by flow adsorption microcalorimetry,” *Environ. Sci. Technol.*, vol. 45, no. 13, pp. 5550–5556, 2011.
- [39] C. Wang and H. Wang, “Carboxyl functionalized Cinnamomum camphora for removal of heavy metals from synthetic wastewater-contribution to sustainability in agroforestry,” *J. Clean. Prod.*, vol. 184, pp. 921–928, May 2018.
- [40] Z. Mahdi, Q. J. Yu, and A. El Hanandeh, “Investigation of the kinetics and mechanisms of nickel and copper ions adsorption from aqueous solutions by date seed derived biochar,” *J. Environ. Chem. Eng.*, vol. 6, no. 1, pp. 1171–1181, Feb. 2018.
- [41] L. Liu *et al.*, “Adsorption characteristics and mechanism of Pb(II) by agricultural waste-derived biochars produced from a pilot-scale pyrolysis system,” *Waste Manag.*, vol. 100, pp. 287–295, 2019.
- [42] S. V. Vassilev, D. Baxter, L. K. Andersen, and C. G. Vassileva, “An overview of the chemical composition of biomass,” *Fuel*. 2010.
- [43] D. C. Cruz Ceballos, K. Hawboldt, and R. Hellleur, “Effect of production conditions on self-heating propensity of torrefied sawmill residues,” *Fuel*, vol. 160, pp. 227–237, 2015.
- [44] Z. Shen, Y. Zhang, F. Jin, O. McMillan, and A. Al-Tabbaa, “Qualitative and quantitative characterisation of adsorption mechanisms of lead on four biochars,” *Sci. Total Environ.*, vol. 609, pp. 1401–1410, 2017.
- [45] M. Hong, L. Zhang, Z. Tan, and Q. Huang, “Effect mechanism of biochar’s zeta potential on farmland soil’s cadmium immobilization,” *Environ. Sci. Pollut. Res.*, vol. 26, no. 19, pp. 19738–19748, 2019.
- [46] J.-H. Kwak *et al.*, “Biochar properties and lead(II) adsorption capacity depend on feedstock type, pyrolysis temperature, and steam activation,” *Chemosphere*, vol. 231, pp. 393–404, Sep. 2019.
- [47] A. Budai *et al.*, “Surface properties and chemical composition of corncob and miscanthus biochars: Effects of production temperature and method,” *J. Agric. Food Chem.*, 2014.

- [48] L. Zhao, X. Cao, O. Mašek, and A. Zimmerman, "Heterogeneity of biochar properties as a function of feedstock sources and production temperatures," *J. Hazard. Mater.*, vol. 256–257, pp. 1–9, Jul. 2013.
- [49] A. Dieguez-Alonso *et al.*, "Designing biochar properties through the blending of biomass feedstock with metals: Impact on oxyanions adsorption behavior," *Chemosphere*, vol. 214, pp. 743–753, 2019.
- [50] L. Long, Y. Xue, X. Hu, and Y. Zhu, "Study on the influence of surface potential on the nitrate adsorption capacity of metal modified biochar," *Environ. Sci. Pollut. Res.*, vol. 26, no. 3, pp. 3065–3074, 2019.
- [51] Z. Shen, F. Jin, F. Wang, O. McMillan, and A. Al-Tabbaa, "Sorption of lead by Salisbury biochar produced from British broadleaf hardwood," *Bioresour. Technol.*, vol. 193, pp. 553–556, Oct. 2015.
- [52] M. S. Alam *et al.*, "Thermodynamic Analysis of Nickel (II) and Zinc (II) Adsorption to Biochar," *Environ. Sci. Technol.*, vol. 52, no. ii, pp. 6246–6255, 2018.
- [53] H. N. Tran, S. J. You, A. Hosseini-Bandegharai, and H. P. Chao, "Mistakes and inconsistencies regarding adsorption of contaminants from aqueous solutions: A critical review," *Water Res.*, vol. 120, pp. 88–116, 2017.
- [54] Q. Fang, B. Chen, Y. Lin, and Y. Guan, "Aromatic and hydrophobic surfaces of wood-derived biochar enhance perchlorate adsorption via hydrogen bonding to oxygen-containing organic groups," *Environ. Sci. Technol.*, vol. 48, no. 1, pp. 279–288, 2014.
- [55] M. Essandoh, B. Kunwar, C. U. Pittman, D. Mohan, and T. Mlsna, "Sorptive removal of salicylic acid and ibuprofen from aqueous solutions using pine wood fast pyrolysis biochar," *Chem. Eng. J.*, vol. 265, pp. 219–227, Apr. 2015.
- [56] B. Choudhary, D. Paul, A. Singh, and T. Gupta, "Removal of hexavalent chromium upon interaction with biochar under acidic conditions: mechanistic insights and application," *Environ. Sci. Pollut. Res.*, vol. 24, no. 20, pp. 16786–16797, 2017.
- [57] M. Teixidó, J. J. Pignatello, J. L. Beltrán, M. Granados, and J. Peccia, "Speciation of the ionizable antibiotic sulfamethazine on black carbon (Biochar)," *Environ. Sci. Technol.*, vol. 45, no. 23, pp. 10020–10027, 2011.
- [58] J. Yang, T. Ma, X. Li, J. Tu, Z. Dang, and C. Yang, "Removal of Heavy Metals and Metalloids by Amino-Modified Biochar Supporting Nanoscale Zero-Valent Iron," *J. Environ. Qual.*, vol. 47, pp. 1196–1204, 2018.

- [59] X. Guo *et al.*, “Application of goethite modified biochar for tylosin removal from aqueous solution,” *Colloids Surfaces A Physicochem. Eng. Asp.*, vol. 502, pp. 81–88, Aug. 2016.
- [60] L. Han, L. Qian, R. Liu, M. Chen, J. Yan, and Q. Hu, “Lead adsorption by biochar under the elevated competition of cadmium and aluminum,” *Sci. Rep.*, vol. 7, no. 1, p. 2264, 2017.
- [61] M. E. González *et al.*, “Effects of pyrolysis conditions on physicochemical properties of oat hull derived biochar,” *BioResources*, vol. 12, no. 1, pp. 2040–2057, 2017.
- [62] L. Qian, M. Chen, and B. Chen, “Competitive adsorption of cadmium and aluminum onto fresh and oxidized biochars during aging processes,” *J. Soils Sediments*, vol. 15, no. 5, pp. 1130–1138, 2015.
- [63] L. Qian and B. Chen, “Dual role of biochars as adsorbents for aluminum: The effects of oxygen-containing organic components and the scattering of silicate particles,” *Environ. Sci. Technol.*, vol. 47, no. 15, pp. 8759–8768, 2013.
- [64] X. Cui *et al.*, “Potential mechanisms of cadmium removal from aqueous solution by *Canna indica* derived biochar,” *Sci. Total Environ.*, vol. 562, pp. 517–525, Aug. 2016.
- [65] J. Kim and S. Hyun, “Sorption of ionic and nonionic organic solutes onto giant *Miscanthus*-derived biochar from methanol-water mixtures,” *Sci. Total Environ.*, vol. 615, pp. 805–813, Feb. 2018.
- [66] T. M. Abdel-Fattah, M. E. Mahmoud, S. B. Ahmed, M. D. Huff, J. W. Lee, and S. Kumar, “Biochar from woody biomass for removing metal contaminants and carbon sequestration,” *J. Ind. Eng. Chem.*, vol. 22, pp. 103–109, Feb. 2015.
- [67] H. Wang, B. Gao, S. Wang, J. Fang, Y. Xue, and K. Yang, “Removal of Pb(II), Cu(II), and Cd(II) from aqueous solutions by biochar derived from KMnO₄ treated hickory wood,” *Bioresour. Technol.*, vol. 197, pp. 356–362, Dec. 2015.
- [68] D. Mohan *et al.*, “Sorption of arsenic, cadmium, and lead by chars produced from fast pyrolysis of wood and bark during bio-oil production,” *J. Colloid Interface Sci.*, vol. 310, no. 1, pp. 57–73, Jun. 2007.
- [69] N. Feng and X. Guo, “Characterization of adsorptive capacity and mechanisms on adsorption of copper, lead and zinc by modified orange peel,” *Trans. Nonferrous Met. Soc. China*, vol. 22, no. 5, pp. 1224–1231, May 2012.
- [70] P. X. Sheng, Y.-P. Ting, J. P. Chen, and L. Hong, “Sorption of lead, copper, cadmium, zinc, and nickel by marine algal biomass: characterization of biosorptive

- capacity and investigation of mechanisms,” *J. Colloid Interface Sci.*, vol. 275, no. 1, pp. 131–141, Jul. 2004.
- [71] X. Li, D. Zhang, F. Sheng, and H. Qing, “Adsorption characteristics of Copper (II), Zinc (II) and Mercury (II) by four kinds of immobilized fungi residues,” *Ecotoxicol. Environ. Saf.*, vol. 147, pp. 357–366, Jan. 2018.
- [72] E. Agrafioti, D. Kalderis, and E. Diamadopoulos, “Ca and Fe modified biochars as adsorbents of arsenic and chromium in aqueous solutions,” *J. Environ. Manage.*, vol. 146, pp. 444–450, 2014.
- [73] N. Zhu, T. Yan, J. Qiao, and H. Cao, “Adsorption of arsenic, phosphorus and chromium by bismuth impregnated biochar: Adsorption mechanism and depleted adsorbent utilization,” *Chemosphere*, 2016.
- [74] R. Azargohar, S. Nanda, J. A. Kozinski, A. K. Dalai, and R. Sutarto, “Effects of temperature on the physicochemical characteristics of fast pyrolysis bio-chars derived from Canadian waste biomass,” *Fuel*, vol. 125, pp. 90–100, 2014.
- [75] Y. Han, A. A. Boateng, P. X. Qi, I. M. Lima, and J. Chang, “Heavy metal and phenol adsorptive properties of biochars from pyrolyzed switchgrass and woody biomass in correlation with surface properties,” *J. Environ. Manage.*, 2013.
- [76] Y. Yao, B. Gao, F. Wu, C. Zhang, and L. Yang, “Engineered biochar from biofuel residue: Characterization and its silver removal potential,” *ACS Appl. Mater. Interfaces*, 2015.
- [77] X. Dong, L. Q. Ma, and Y. Li, “Characteristics and mechanisms of hexavalent chromium removal by biochar from sugar beet tailing,” *J. Hazard. Mater.*, 2011.
- [78] B. Zhao *et al.*, “Effect of pyrolysis temperature, heating rate, and residence time on rapeseed stem derived biochar,” *J. Clean. Prod.*, vol. 174, pp. 977–987, 2018.
- [79] S. V. Vassilev, D. Baxter, L. K. Andersen, C. G. Vassileva, and T. J. Morgan, “An overview of the organic and inorganic phase composition of biomass,” *Fuel*, vol. 94, pp. 1–33, Apr. 2012.
- [80] S. Maiti, S. Dey, S. Purakayastha, and B. Ghosh, “Physical and thermochemical characterization of rice husk char as a potential biomass energy source,” *Bioresour. Technol.*, 2006.
- [81] J. H. Park *et al.*, “Recycling of rice straw through pyrolysis and its adsorption behaviors for Cu and Zn ions in aqueous solution,” *Colloids Surfaces A Physicochem. Eng. Asp.*, 2017.
- [82] L. Liu and S. Fan, “Removal of cadmium in aqueous solution using wheat straw

- biochar: effect of minerals and mechanism,” *Environ. Sci. Pollut. Res.*, vol. 25, no. 9, pp. 8688–8700, 2018.
- [83] J.-H. Yuan, R.-K. Xu, and H. Zhang, “The forms of alkalis in the biochar produced from crop residues at different temperatures,” *Bioresour. Technol.*, vol. 102, no. 3, pp. 3488–3497, Feb. 2011.
- [84] X. Tong, J. Li, J. Yuan, and R. Xu, “Adsorption of Cu(II) by biochars generated from three crop straws,” *Chem. Eng. J.*, vol. 172, no. 2–3, pp. 828–834, Aug. 2011.
- [85] J. Sun, F. Lian, Z. Liu, L. Zhu, and Z. Song, “Biochars derived from various crop straws: Characterization and Cd(II) removal potential,” *Ecotoxicol. Environ. Saf.*, 2014.
- [86] L. Wei *et al.*, “Biochar characteristics produced from rice husks and their sorption properties for the acetanilide herbicide metolachlor,” *Environ. Sci. Pollut. Res.*, 2017.
- [87] Y. Deng, S. Huang, D. A. Laird, X. Wang, and Z. Meng, “Adsorption behaviour and mechanisms of cadmium and nickel on rice straw biochars in single- and binary-metal systems,” *Chemosphere*, vol. 218, pp. 308–318, Mar. 2019.
- [88] Y. Xu and B. Chen, “Organic carbon and inorganic silicon speciation in rice-bran-derived biochars affect its capacity to adsorb cadmium in solution,” *J. Soils Sediments*, vol. 15, no. 1, pp. 60–70, 2014.
- [89] R. Sowmya, T. M. Ravikumar, R. Vivek, K. Rathinaraj, and N. M. Sachindra, “Optimization of enzymatic hydrolysis of shrimp waste for recovery of antioxidant activity rich protein isolate,” *J. Food Sci. Technol.*, vol. 51, no. 11, pp. 3199–3207, Nov. 2014.
- [90] A. Ghaly, V. Ramakrishnan, M. Brooks, S. Budge, and D. Dave, “Fish Processing Wastes as a Potential Source of Proteins, Amino Acids and Oils: A Critical Review,” *J. Microb. Biochem. Technol.*, 2013.
- [91] H. D. De Holanda and F. M. Netto, “Recovery of components from shrimp (*Xiphopenaeus kroyeri*) processing waste by enzymatic hydrolysis,” *J. Food Sci.*, 2006.
- [92] K. Zhang, B. Zhang, B. Chen, L. Jing, Z. Zhu, and K. Kazemi, “Modeling and optimization of Newfoundland shrimp waste hydrolysis for microbial growth using response surface methodology and artificial neural networks,” *Mar. Pollut. Bull.*, 2016.
- [93] K. M. Zia, M. Barikani, M. Zuber, I. A. Bhatti, and M. A. Sheikh, “Molecular

- engineering of chitin based polyurethane elastomers,” *Carbohydr. Polym.*, vol. 74, no. 2, pp. 149–158, Oct. 2008.
- [94] M. A. El-Fattah, A. M. El Saeed, A. M. Azzam, A.-R. M. Abdul-Raheim, and H. H. Hefni, “Improvement of corrosion resistance, antimicrobial activity, mechanical and chemical properties of epoxy coating by loading chitosan as a natural renewable resource,” *Prog. Org. Coatings*, vol. 101, pp. 288–296, Dec. 2016.
- [95] F. Li and R. C. Larock, “Novel polymeric materials from biological oils,” *J. Polym. Environ.*, vol. 10, no. 1–2, pp. 59–67, 2002.
- [96] H. Ge, B. Zhao, Y. Lai, X. Hu, D. Zhang, and K. Hu, “From crabshell to chitosan-hydroxyapatite composite material via a biomorphic mineralization synthesis method,” *J. Mater. Sci. Mater. Med.*, vol. 21, no. 6, pp. 1781–1787, 2010.
- [97] K. Vijayaraghavan, H. Y. N. Winnie, and R. Balasubramanian, “Biosorption characteristics of crab shell particles for the removal of manganese(II) and zinc(II) from aqueous solutions,” *Desalination*, vol. 266, no. 1–3, pp. 195–200, Jan. 2011.
- [98] R. J. R. Monteiro, C. B. Lopes, L. S. Rocha, J. P. Coelho, A. C. Duarte, and E. Pereira, “Sustainable approach for recycling seafood wastes for the removal of priority hazardous substances (Hg and Cd) from water,” *J. Environ. Chem. Eng.*, vol. 4, no. 1, pp. 1199–1208, 2016.
- [99] C. Jeon, “Adsorption behavior of silver ions from industrial wastewater onto immobilized crab shell beads,” *J. Ind. Eng. Chem.*, vol. 32, pp. 195–200, Dec. 2015.
- [100] R. H. Rødde, A. Einbu, and K. M. Vårum, “A seasonal study of the chemical composition and chitin quality of shrimp shells obtained from northern shrimp (*Pandalus borealis*),” *Carbohydr. Polym.*, vol. 71, no. 3, pp. 388–393, Feb. 2008.
- [101] J. G. Kunkel, W. Nagel, and M. J. Jercinovic, “Mineral Fine Structure of the American Lobster Cuticle,” *J. Shellfish Res.*, 2012.
- [102] C. Londono-Zuluaga, H. Jameel, R. W. Gonzalez, and L. Lucia, “Crustacean shell-based biosorption water remediation platforms: Status and perspectives,” *J. Environ. Manage.*, vol. 231, pp. 757–762, Feb. 2019.
- [103] R. Zhang, J. J. Richardson, A. F. Masters, G. Yun, K. Liang, and T. Maschmeyer, “Effective Removal of Toxic Heavy Metal Ions from Aqueous Solution by CaCO₃ Microparticles,” *Water, Air, Soil Pollut.*, vol. 229, no. 4, p. 136, Apr. 2018.
- [104] G. Magnacca, F. Guerretta, A. Vizintin, P. Benzi, M. C. Valsania, and R. Nisticò, “Preparation, characterization and environmental/electrochemical energy storage

- testing of low-cost biochar from natural chitin obtained via pyrolysis at mild conditions,” *Appl. Surf. Sci.*, 2018.
- [105] G. L. Dotto, M. L. G. Vieira, and L. A. A. Pinto, “Kinetics and mechanism of tartrazine adsorption onto chitin and chitosan,” *Ind. Eng. Chem. Res.*, 2012.
- [106] D. Zhou, L. Zhang, and S. Guo, “Mechanisms of lead biosorption on cellulose/chitin beads,” *Water Res.*, 2005.
- [107] Y. Sağ and Y. Aktay, “Kinetic studies on sorption of Cr(VI) and Cu(II) ions by chitin, chitosan and *Rhizopus arrhizus*,” *Biochem. Eng. J.*, 2002.
- [108] M. Zhang *et al.*, “Characterization of nitrogen-rich biomaterial-derived biochars and their sorption for aromatic compounds,” *Environ. Pollut.*, vol. 195, pp. 84–90, 2014.
- [109] M. A. Zazycki *et al.*, “Chitin derived biochar as an alternative adsorbent to treat colored effluents containing methyl violet dye,” *Adv. Powder Technol.*, vol. 30, no. 8, pp. 1494–1503, 2019.
- [110] Y. Xiao, Y. Xue, F. Gao, and A. Mosa, “Sorption of heavy metal ions onto crayfish shell biochar: Effect of pyrolysis temperature, pH and ionic strength,” *J. Taiwan Inst. Chem. Eng.*, vol. 80, pp. 114–121, Nov. 2017.
- [111] A. Ilnicka, P. A. Gauden, A. P. Terzyk, and J. P. Lukaszewicz, “Nano-Structured Carbon Matrixes Obtained from Chitin and Chitosan by a Novel Method,” *J. Nanosci. Nanotechnol.*, 2016.
- [112] K. C. Bal Krishna, M. R. Niaz, D. C. Sarker, and T. Jansen, “Phosphorous removal from aqueous solution can be enhanced through the calcination of lime sludge,” *J. Environ. Manage.*, 2017.
- [113] Y. Li *et al.*, “Phosphate removal from aqueous solutions using raw and activated red mud and fly ash,” *J. Hazard. Mater.*, 2006.
- [114] W. Wang, Y. Liu, S. Song, and W. Cai, “Facile pyrolysis of fishbone charcoal with remarkable adsorption performance towards aqueous Pb (II),” *J. Environ. Chem. Eng.*, 2017.
- [115] Y. Qiao *et al.*, “Pyrolysis of chitin biomass: TG–MS analysis and solid char residue characterization,” *Carbohydr. Polym.*, vol. 133, pp. 163–170, Nov. 2015.
- [116] I. Corazzari *et al.*, “Advanced physico-chemical characterization of chitosan by means of TGA coupled on-line with FTIR and GCMS: Thermal degradation and water adsorption capacity,” *Polym. Degrad. Stab.*, 2015.

- [117] R. J. White, M. Antonietti, and M. M. Titirici, "Naturally inspired nitrogen doped porous carbon," *J. Mater. Chem.*, 2009.
- [118] K.-Y. Shin, J.-Y. Hong, and J. Jang, "Heavy metal ion adsorption behavior in nitrogen-doped magnetic carbon nanoparticles: Isotherms and kinetic study," *J. Hazard. Mater.*, 2011.
- [119] P. Veselá and V. Slovák, "N-doped carbon xerogels prepared by ammonia assisted pyrolysis: Surface characterisation, thermal properties and adsorption ability for heavy metal ions," *J. Anal. Appl. Pyrolysis*, 2014.

Chapter 3 - Characterization of Crab Shell Biochar

A modified version of this chapter will be submitted for publication. It has been proofread and revised by Dr. Kelly Hawboldt and Dr. Stephanie MacQuarrie

Abstract

Crab shell is produced in large quantities in Atlantic Canada as a by-product from seafood processing. Currently, this waste stream has limited use and is often landfilled. Pyrolysis of this material to form a biochar could form a valuable material. In this paper, a biochar from snow crab (*Chionoecetes opilio*) shell is produced and characterized for its use as a heavy metal adsorbent for acid mine drainage (AMD). Thermal Gravimetric Analysis indicated that the biochar was primarily mineral-rich with an ash content of 57.32%. Scanning Electron Microscopy demonstrated that the biochar was a slightly porous material, as confirmed by N₂-BET surface area analysis which demonstrated a specific surface area of 20.71 m²/g and pore sizes between 3-10 nm. The pH of the biochar was 11.75, with this alkalinity being derived from the presence of calcite (CaCO₃) as found from X-Ray Diffraction and Fourier Transform Infrared spectroscopy. X-Ray Photoelectron Spectroscopy further confirmed the presence of CaCO₃ via the Ca2p spectra, while also demonstrating the presence of some residual organic carbon and nitrogen groups in the biochar. The biochar zeta potential was found to be largely negative at each value of equilibrium pH owing to the presence of CaCO₃. Trace element analysis demonstrated that the biochar was primarily calcium-rich, along with some residual sodium, potassium, phosphorous, and magnesium. The characterizations performed here to illustrate that the crab shell biochar has high potential to be useful as a metal adsorbent from AMD and require further investigation into its use as an adsorbent.

3.1 Introduction

The crab fishery is a vital industry in much of eastern Canada, with landings of the snow crab (*Chionoecetes Opilio*), also known as the Queen crab, being valued at over \$700 million in 2018, with over 67000 tonnes caught [1], [2]. The processing of this crab, however, generates by-products, primarily in the form of shells. For snow crab, by-product amounts can be upwards of 30% of the total catchweight, this by-product contains value-added chemicals that if recovered would not only reduce costs associated with waste disposal but also provide an economic benefit to the industry as a whole [3]. Much of the research in this field to date has focussed on the extraction of nutrients [3]–[6] and the biomaterial chitin [7], [8], as well as advanced composites [9] and polymers [10]. While these techniques are promising, they often require a great degree of processing and/or quality assurance/control measures, which could pose challenges for some crab processors.

Alternatively, pyrolysis of this material is a simple process and could offer an inexpensive and readily accessible method for valorizing this waste. Further, since the process temperature is in excess of 450 °C, any concerns regarding viral or bacterial contamination from the feedstock are eliminated. In pyrolysis, materials are heated to high temperatures in the absence of oxygen, leading to a thermal decomposition. This decomposition yields three products; a condensable vapour (bio-oil), a non-condensable biogas, and solid biochar [11]. Common pyrolysis feedstocks include lignocellulosic materials, such as wood [12], [13], and agricultural by-products [14]–[16]. Biochar from these materials has high porosity and varied organic surface functionality.

Notably, biochar has been the subject of frequent study as an adsorbent for aqueous metals [13], [17]. The functionality of biochar plays a role in the adsorption of metals, while the surface area enhances the removal extent through the provision of additional adsorption sites [18]. The low cost of biochar and the simplicity of its production makes it an attractive solution for acid mine drainage (AMD), a common effluent stream from mine sites that often contain high levels of metals, and thus requires treatment before disposal [19].

In contrast, the production of biochar from crustacean shells is limited, with only a few papers on the topic in the past few years [20]–[23]. In this work, we will characterize a crab shell derived from snow crab (*Chionoecetes opilio*) with respect to properties relevant to adsorption. Herein, we will test the proximate composition of the biochar, to determine mineral content in comparison with the initial adsorbent, which has relevance in adsorptive mechanisms. Specific surface area (SSA) is analyzed, which is relevant in terms of the number of accessible surface sites for adsorption [24], as well as analyzing surface morphology to view porosity of the surface. Elemental analysis is used to determine the amounts of carbon, nitrogen, and hydrogen in the biochar, which is then backed by Fourier Transform-Infrared (FT-IR) analysis, X-Ray Diffraction (XRD), and X-Ray Photoelectron Spectroscopy (XPS) to determine the surface chemistry of the biochar. Zeta potential analysis is then performed to determine the charge of the double layer surrounding the biochar, which could have an impact on adsorption due to electrostatic effects [25]. Lastly, acid digestion is carried out on the biochar to determine the trace elements present, to determine ions relevant to ion exchange in the shell, and to analyze for the presence of any potentially hazardous elements.

3.2 Materials & Methodology

3.2.1 Biochar Production

Snow crab (*Chionoecetes opilio*) shells were obtained from processing by-products from Louisbourg Seafoods Limited, of Louisbourg, Nova Scotia, Canada. The raw shell was then ground to a particle size of less than 2.0 mm using a rotary grinder. Prior to pyrolysis, the ground crab shell dried in an oven at 70 °C overnight. For pyrolysis, samples were loaded in 5 g batches into a horizontal tube furnace, which was flushed using ultrapure (99.999%) N₂. Pyrolysis was carried out at 500 °C on the basis of previous experiments on this system. The fast pyrolysis was carried out by first loading the sample boat containing the crab shell into the center of the furnace, and then removing it once pyrolysis vapors stopped entering the condensing flask, a process which takes approximately 5 minutes. Upon completion, the biochar was removed from the furnace and covered to prevent it from oxidizing until cool, at which point it was stored in a refrigerated room until ready for further use.

3.2.2 Thermal Gravimetric Analysis

Thermal Gravimetric Analysis (TGA) was carried out using a TA Instruments Q500. Samples were prepared by first grinding them in a mortar and pestle to reduce mass and heat transfer resistances. The TGA started under a flow of N₂ at 50 mL/min, while the temperature increased at a rate of 15 °C/min until reaching 750 °C. At this point, the gas flow was switched from N₂ to air, and held at 750 °C for 15 minutes to allow full oxidation of the sample. The sample moisture content was determined as the mass

percent lost from room temperature to 105 °C, the volatile matter was determined as the mass percent lost from 105 °C to 600 °C, the ash percentage was measured as the total mass remaining following full oxidation, and the mass lost due to decarboxylation of CaCO₃ was determined according to the equation:

$$\text{Decarboxylation (wt\%)} = 100\% - (\%moisture + \%volatiles + \%ash) \quad (3 - 1)$$

3.2.3 Surface Morphology

Surface Morphology was analyzed using Scanning Electron Microscopy (SEM) and was performed in Memorial University of Newfoundland's Micro Analysis Facility using an FEI MLA 650 FEG instrument. SEM was used to analyze the microscopic structure of the CSB, while Energy Dispersive X-Ray (EDX) spectroscopy coupled to the device.

3.2.4 BET Surface Analysis

Brunauer-Emmett-Teller (BET) analysis was conducted using a Micromeritics Tristar II Plus to determine the biochar surface area. A sample of 0.1 grams of Crab Shell Biochar (CSB) was first weighed into a sample tube, which was then degassed under a flow of nitrogen at 120 °C overnight prior to analysis. Following degassing, the sample was installed into the analyzer, where N₂ was used as an adsorbate at a temperature of 77 K (-196 °C), which was maintained using a liquid nitrogen bath. The data obtained from this procedure was then analyzed according to the BET theory [26].

N₂ BET data was also used to calculate the biochar's pore size distribution, according to the Non-Local Density Functional Theory (NLDFT) [27].

enabled the elucidation of the chemical structure of crystalline phases in the biochar structure.

3.2.5 Elemental Analysis

Elemental analysis involving the elements carbon, hydrogen, and nitrogen (CHN analysis) was conducted at the Aquatic Research Cluster (ARC) of Memorial University of Newfoundland using a Perkin-Elmer 2400 Series II CHN analyzer.

Biochar surface pH was measured according to Chen et al. (2011) [13]. Briefly, this involved mixing biochar in water at a ratio of 1:10 (w/v) and mixing the suspension using a shaking table. The biochar pH was measured after 30 minutes of mixing using a Fischer Scientific AB200 pH meter, which was calibrated prior to use.

3.2.6 X-Ray Diffraction Analysis

X-Ray Diffraction (XRD) spectra were obtained using a Rigaku Ultima IV diffractometer with a Cu X-Ray source at MUN's TERRA Facility. The diffractometer was operated at a voltage of 40 kV and amperage of 44 mA at a step size of 0.02° step change. The range analyzed was between 5° and 100° at a rate of 2θ/minute. Diffractogram peaks were then matched to existing databases using Materials Data Incorporated (MDI) JADE software [28].

3.2.7 Fourier-Transform Infrared Spectroscopy

Fourier-Transform Infrared Spectroscopy (FT-IR) was performed using a Bruker Alpha FT-IR spectrometer with Alpha-P single bounce diamond ATR. Samples were ground to

a fine powder prior to use. The range of wavelengths studied was between 4000 cm^{-1} to 400 cm^{-1} , with a resolution of 4 cm^{-1} and 24 scans.

3.2.8 X-Ray Photoelectron Spectroscopy

X-Ray Photoelectron Spectroscopy (XPS) was performed at Université Laval using an AXIS-ULTRA instrument by KRATOS (UK) in order to analyze the surface chemistry of the biochar. For this study, C1s, O1s, N1s, and Ca2p peaks were analyzed to probe relevant functional groups. Spectral analysis was performed using CasaXPS software [30].

3.2.9 Zeta Potential Analysis

Zeta potential was performed according to a modification of methodology by Derkani et al. [29]. First, the CSB was ground to a fine powder to ensure proper measurement. A sample of 0.1 g of the CSB was then mixed in 100mL of deionized water. Adjustment of pH was performed using 0.1M HCl and 0.1M NaOH solutions, and the samples were then mixed for 24 hours to achieve equilibrium of the solution. The pH of each sample was measured again prior to use before the zeta potential was measure using a Malvern Zetasizer Nano ZS. Plots of Zeta potential against pH were then created to determine the charge of the biochar colloids.

3.2.10 Trace Element Analysis

Acid Digestion of the CSB was utilized to obtain the total metal concentration of the biochar. A mass of 0.1 grams was first measured and added to a plastic digestion vial with 1 mL of 68% HNO₃ and 1.0 mL of 30% H₂O₂ and left to flux on a hot plate at 75 °C. This process took place for 48 hours, after which the mixture was dried down. The procedure was then repeated until no effervescence occurred when adding the acid and hydrogen peroxide, and the solution was clear. After this, the solution was evaporated and 6M HCl was added to the remaining solids. When the solution appeared clear and did not effervesce, the solution was dried and 5 mL of 6M HCl was added to the remaining solid, after which the sample was left to flux at 100 °C for 24 hours. The solution was again dried, and diluted nitric acid was added to transform the metals back to nitrate form. The final solution was then analyzed using a Perkin-Elmer 5300 DV Inductively Coupled Plasma Optical Emission Spectroscopy (ICP-OES) device at Memorial University's Micro-Analysis Facility for a suite of trace elements.

3.3 Results and discussion

3.3.1 TGA

TGA results for raw crab shell and the CSB are presented in Figure 3-1, with proximate analysis based on this graph in Table 3-1. Raw crab shell unsurprisingly contains more moisture than the biochar and significantly more volatiles. The crab shell loses much of the moisture and some volatiles during pyrolysis. Volatile compounds made up a large fraction of the mass lost by the crab shell between 100 °C and 500 °C, primarily due to

the decomposition of chitin [31], [32]. As a result of the fact that the CSB had already lost much of its volatile content, the material had a higher ash content in comparison to the raw shell material.

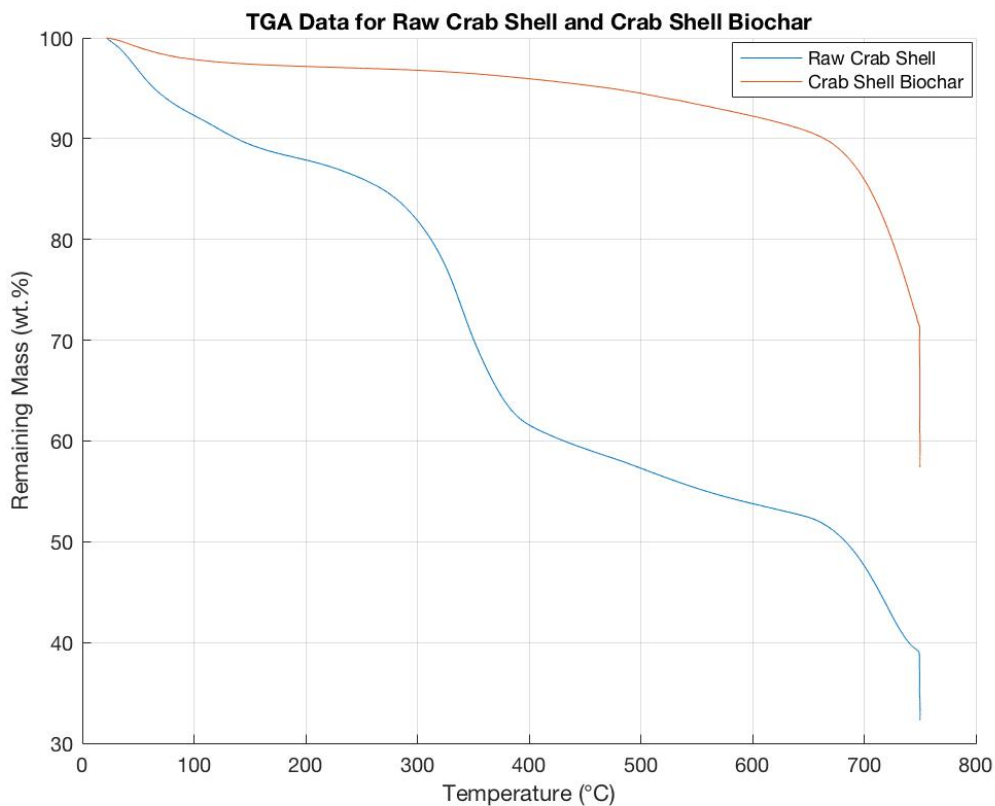


Figure 3-1: TGA Data for raw crab shell in the CSB

An additional loss of mass occurring in both samples at approximately 600 °C can be attributed to the start of calcination (CaCO_3 decomposing to CaO) [20], [33]. There is an additional possibility that some of this lost material may be due to the remaining organic carbon either devolatilizing or burning away once the gas was switched to air at 750 °C [34], [35]. From this information, it is likely that the calcium in the CSB still exists in the form of CaCO_3 .

Table 3-1: Proximate Analysis of Raw Crab and CSB

Material	% Moisture	% Volatiles	% Ash	% Decarboxylation
Raw Crab Shell	7.99%	37.00%	32.28%	22.73%
CSB	2.21%	6.69%	57.32%	33.77%

3.3.2 Scanning Electron Microscopy

Pore networks are demonstrated in all biochar samples through SEM in Figure 3-2. These pores are likely related to the virgin structure of crab shell and contain nanostructures of chitin and protein in small canals throughout the crab shell [36], which have been demonstrated to remain stable after treatment at 500 °C [35]. The organic chitin and protein are pyrolyzed leaving behind some remaining biochar, while the CaCO₃ surrounding the shells, being stable at the temperatures used here [33] would be left in place to form these pore structures.

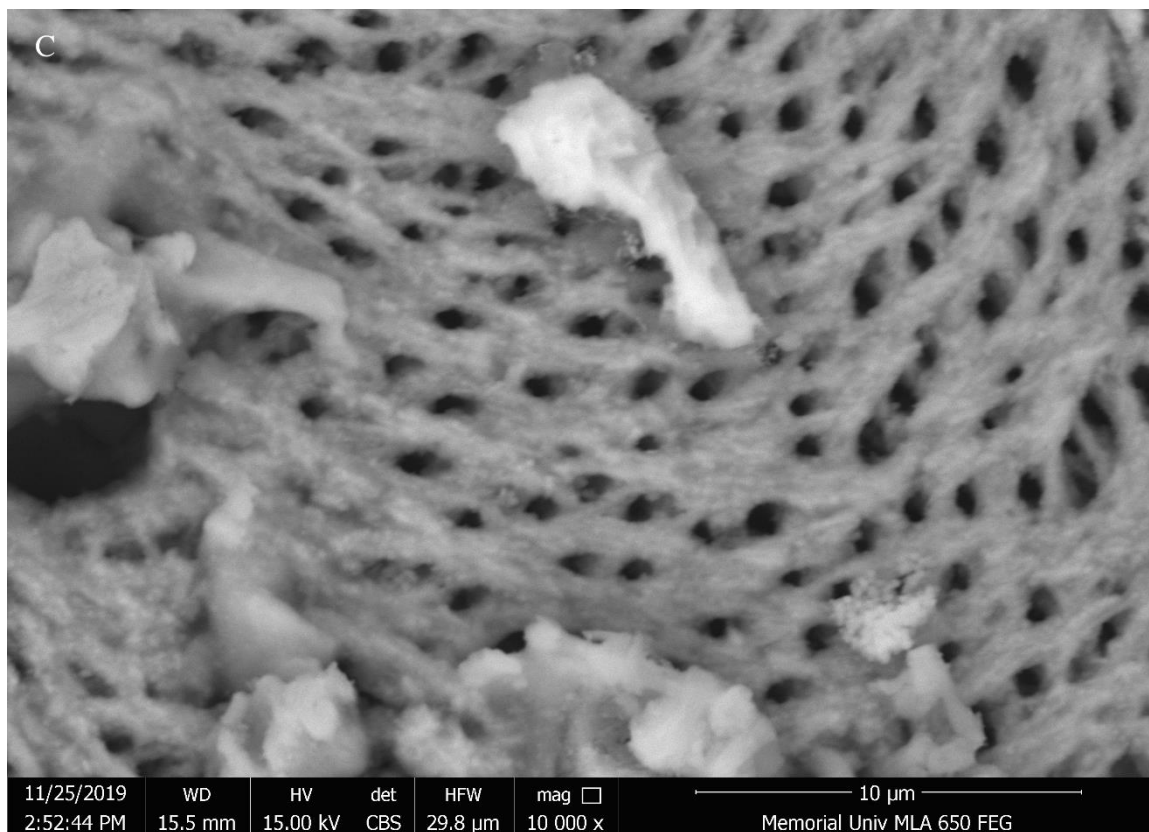


Figure 3-2: SEM images of the CSB, illustrating a complex pore network

3.3.3 Surface Area Analysis

The BET surface area for the CSB was found to be $20.71 \text{ m}^2/\text{g}$, a result which is in line with that of similar materials reported by the literature as seen in Table 3-2. These pores are possibly related to the natural structure of crab shell and contain tube-like structures of chitin and protein in small canals throughout the crab shell [36]. The organic chitin and protein are volatilized, while the stable CaCO_3 surrounding the shells would be left in place to form these pore structures.

3.3.4 Physicochemical Properties

The values of physicochemical properties, including elemental analysis, BET SSA, and pH for CSB and other marine shell biochars are shown in Table 3-2. The pH for this biochar was 11.75, in line with other marine shell biochars [23].

Table 3-2: Physicochemical properties of crustacean shell biochars

Feedstock	Production Temperature (°C)	BET SSA (m ² /g)	C (wt%)	H (wt%)	N (wt%)	pH	Ref.
Crab Shell	500	20.71	20.158	0.401	2.27	11.75	This work
Crayfish Shell	450	25.46	20.63	0.31	1.28	N/A	[37]
Crab Shell	300	3.52	25.21	2.21	3.26	11.25	[20]
Crab Shell	500	14.90	20.68	0.97	2.38	N/A	[20]
Shrimp Shell	500	13.3	N/A	N/A	N/A	10.3	[23]

Porosity data from NLDFT theory indicates that the pore size distribution in the CSB is distributed across a range of micropores as shown in Figure 3-3. This figure demonstrates that a large portion of the pore volume exists in the 3-10 nm range, with most being approximately 5 nm in size. These results show some similarities with those of a previous study that found pores approximately 3 nm in size in a shrimp shell biochar, though it is important to note that the composition of this feedstock is slightly different from that in crab, and thus porosity results may differ [38]. Similarly, Liu et al. found an average pore diameter of 7.4177 nm in their shrimp shell biochar, with a range between 2 and 50 nm [39].

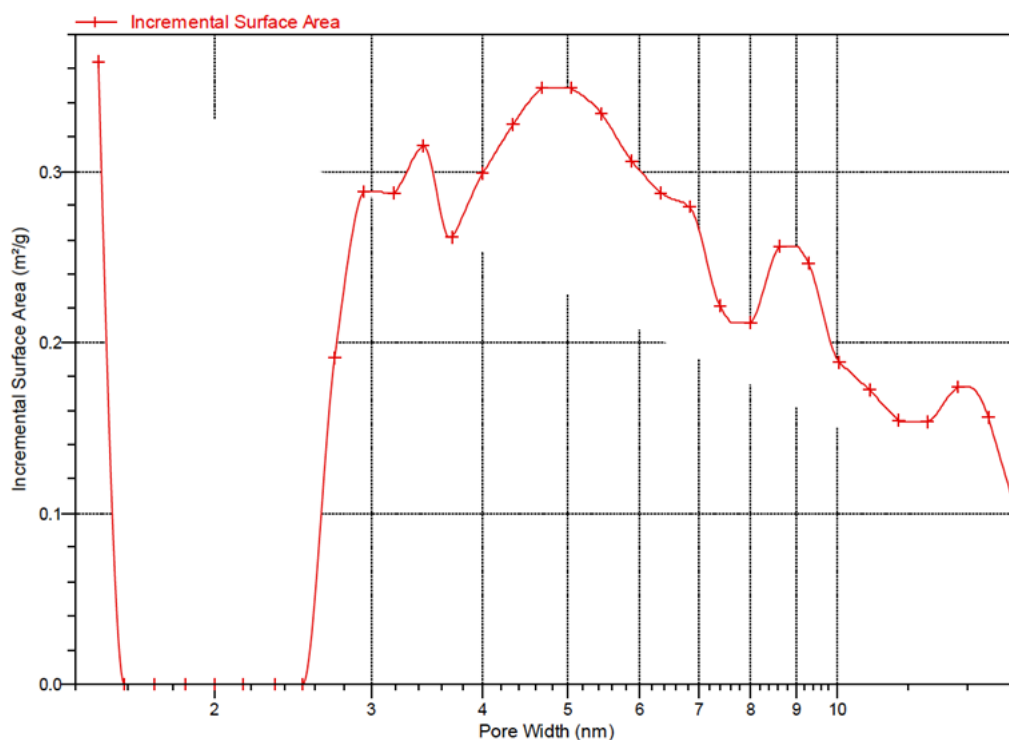


Figure 3-3: Pore Size Distribution from N_2 -based NLDFT theory

3.3.5 X-Ray Diffraction Analysis

The x-ray diffractogram for the CSB is pictured in Figure 3-4. The diffractogram of this biochar demonstrates that the shell's mineral structure is primarily composed of calcite, a mineral-based on $CaCO_3$ [40]. In addition, some hydroxyapatite ($Ca_5(PO_4)_3OH$) is observed, though this is likely in small traces owing to its lower intensity. The presence of this latter mineral has been indicated in past studies, which also state that the mineral is present in small traces [31]. Calcination of the calcite in the CSB to form CaO was not observed from the XRD pattern, which is understandable as the pyrolysis was conducted at 500 °C, below the threshold where calcination begins to occur and was conducted at a low residence time.

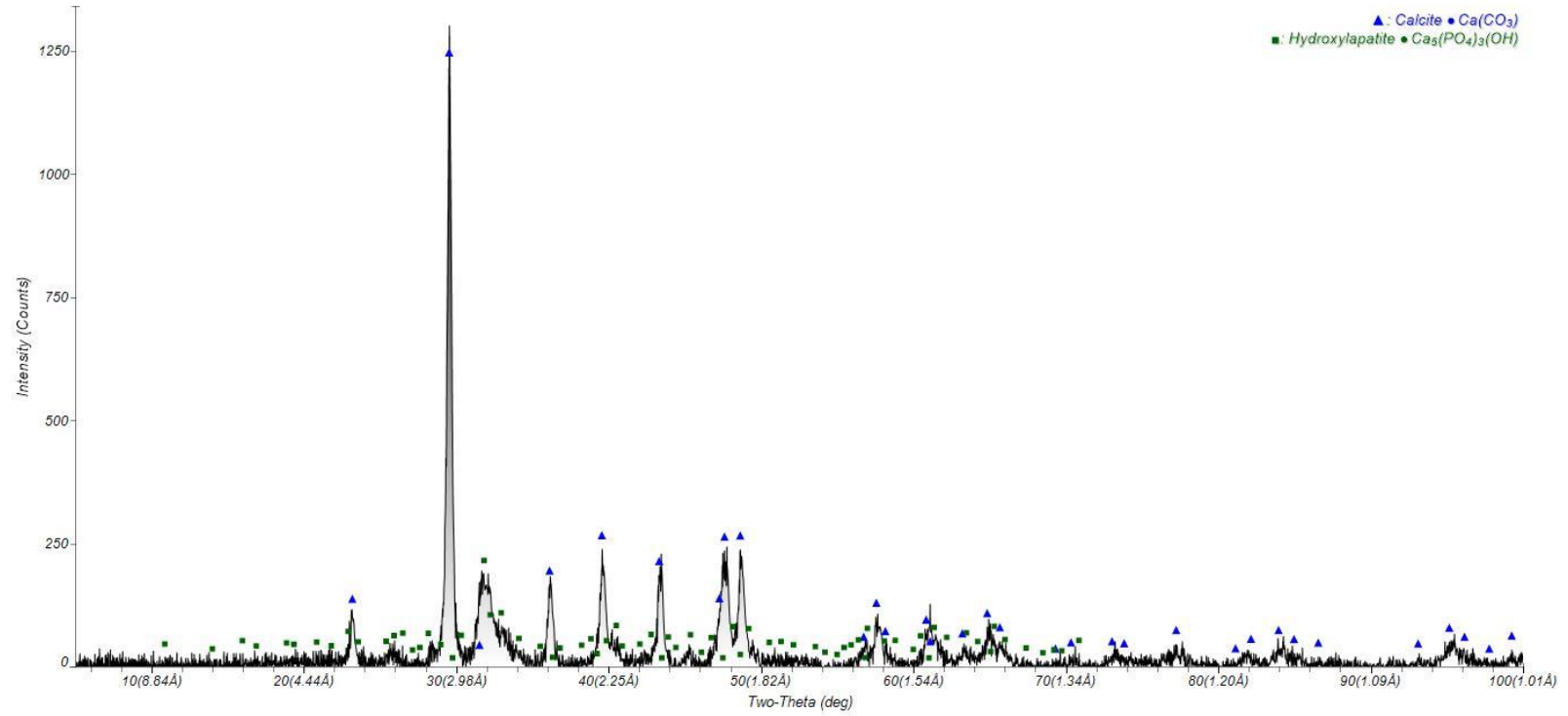


Figure 3-4: XRD pattern for the CSB

3.3.6 Fourier-Transform Infrared Spectroscopy

FT-IR data of the CSB is illustrated in Figure 3-5. This spectrum is indicative of material rich in CaCO_3 , with a small peak at 871 cm^{-1} likely relating to asymmetric C-O bending mode, and a larger, broad band near 1410 cm^{-1} attributed to asymmetric C-O stretching [29]. A slight peak at 710 cm^{-1} is attributed to the presence of calcite as well through C-O bending [21], [29]. Smaller peaks throughout the spectra may be assigned to remaining organics in the CSB. Some C-H stretching is noted at a small peak at 2950 cm^{-1} [41]. A broad peak at approximately 1080 cm^{-1} can also be attributed to asymmetric stretching of CO_3^{2-} [42], or possibly from an organic group such as C-O-C [43]. These potential organic functionalities are not strong in comparison to those of carbonates, explained by the low quantity of organics relative to minerals, as evidenced by TGA data. The spectra for CaCO_3 also contain a broad peak between 3400 and 3600 cm^{-1} that is not present in that of the CSB. This peak is commonly associated with the stretching of hydroxyl (-O-H) groups. This may be due to the presence of moisture absorbed by the CaCO_3 , which has been shown to occur owing to the hygroscopicity of the CaCO_3 surface [42], [44].

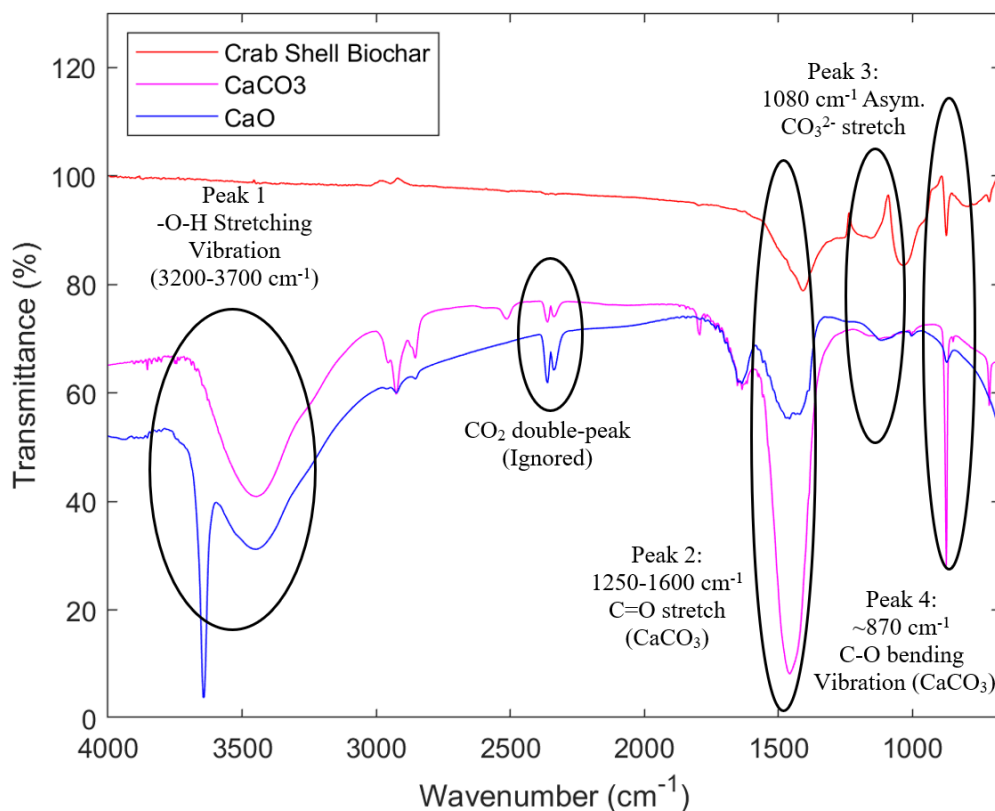


Figure 3-5: FT-IR Spectra of the Crab Shell Biochar

3.3.7 XPS

XPS results are summarized in Table 3-3, illustrating the dominant peaks found on each atom selected and the percent area taken up by each peak. Full spectra of each atom are presented in appendix A. XPS data for the CSB, in the C1s and O1s spectra, indicated further that the material was highly dominated by carbonates, with some additional functionalities. Some carbon on the C1s spectra was visible in terms of C-C and C-H groups located at 285.0 eV (C1), aromatic C-O at 286.2 eV (C2), C=O at 287.23 eV (C3), carboxylic acids at 288.73 eV (C4), and CO₃ groups at 290.24 (C5) [45]. The O1s spectrum for the CSB has its main peak at 531.64 eV, which is attributed to the carbonate

of CaCO_3 [46]. The smaller peak at 532.66 eV is attributed to the presence of C-O, which may come from the residual organic matter in the biochar [31].

Table 3-3: XPS Results for the CSB

Atom/peak	Binding Energy (eV)	Area %
C1s		
C1	285	65.84%
C2	286.04	12.92%
C3	287.23	4.17%
C4	288.73	4.43%
C5	290.24	6.05%
O1s		
O1	531.64	83.39%
O2	532.66	16.61%
Ca2p		
Ca2p3/2	347.73	59.56%
Ca2p1/2	351.29	40.44%
N1s		
N1	398.86	53.92%
N2	400.57	46.08%

The N1s spectrum of the CSB shows two primary peaks, one at 398.86 eV, and another at 400.57 eV. This could be attributed to pyridinic and pyrrolic nitrogen, respectively, as was observed in a paper by Chen et al. on a crab shell-derived activated carbon [47], and

Yu et al. on a shrimp shell derived biochar [38]. The $\text{Ca}2p_{3/2}$ spectrum provides additional confirmation to the presence of CaCO_3 in the biochar, with a binding energy of 347.73 eV [46]. While this energy does overlap slightly with Ca(OH)_2 and CaO , there is no evidence for these compounds in the XRD. Additionally, the C1s energy at 290.19 eV provides further evidence for the presence of this mineral in the biochar [46].

3.3.8 Zeta Potential Analysis

Zeta potential values are plotted as a function of equilibrium pH in Figure 3-6. It is important to note here that the alkalinity of the biochar leads to a drift in solution pH from initial conditions, and therefore it is difficult to give a true estimate of the zeta potential of CaCO_3 -rich materials under acidic conditions. The method is still useful for understanding the zeta potential of the biochar under equilibrium conditions, which are necessary for accurate zeta potential methods.

The values shown in the figure indicate that the surface of the CSB is largely negative in the equilibrium pH ranges studied, with an isoelectric point, or pH_{IEC} , of approximately 7.1. This value is similar to that observed by Dai et al. (2018) in their crab shell biochar [22], indicating that the surface is largely occupied by negatively charged species in this pH range [48]. This finding is in line with the XRD observations presented in this section which illustrate that the CSB is primarily composed of CaCO_3 ,

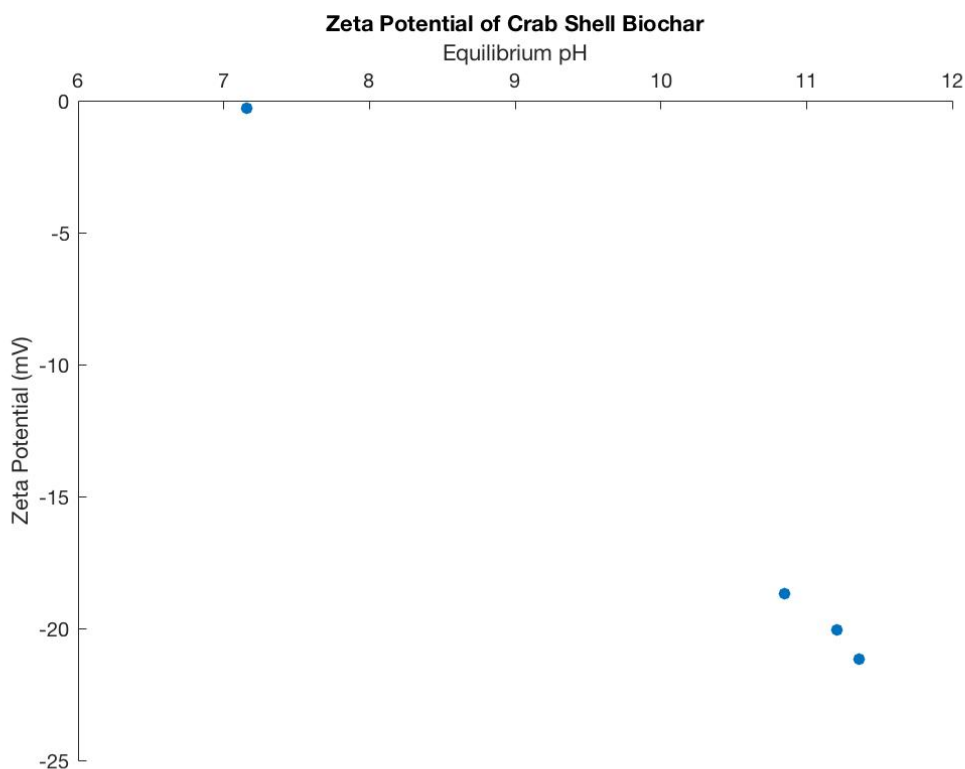


Figure 3-6: Zeta Potential of the CSB

In addition to this, studies on other CaCO_3 based surfaces have been carried out. Moulin & Roques (2003) performed a detailed analysis of the surface charge of calcite (CaCO_3) particles. Here, they importantly note that the Potential Determining Ions (PDIs) related to the determination of zeta potential may include $\text{Ca}^{2+}_{(\text{aq})}$ and $\text{CO}_3^{2-}_{(\text{aq})}$ in addition to $\text{H}^{+}_{(\text{aq})}$ and $\text{OH}^{-}_{(\text{aq})}$ due to dissolution of calcite in solution [49]. These ions can in turn populate the shear plane of the biochar particles and influence the charge of the particles. Competition of these ions or ion exchange may then play a role in determining the adsorption capacity of this material. For example, the negative surroundings of the biochar particles may lead to electrostatic effects in adsorption, whereby negatively

charged molecules would be repelled and positively charged species would be attracted [50].

3.3.9 Trace Element Analysis

Results from acid digestion of the CSB are shown in Table 3-4. The analysis demonstrates that CSB has high concentrations of Ca, magnesium (Mg), potassium (K), and sodium (Na), which are important in cationic ion exchange, and may be useful in the removal of metals such as copper from solution [51]. In addition, appreciable phosphorous levels were found in solution, which could take the form of phosphates in calcium minerals as has been demonstrated in past research on crustacean shells [31], [33], [52]. Smaller amounts of iron (Fe), aluminum (Al), zinc (Zn), copper (Cu), strontium (Sr), and tin (Sn) were also present in solution, which could be leached from solution during adsorption. It is important to note, though, that the acid digestion process took place in an acidic solution at elevated temperatures and so the extent to which this might occur in real applications may be lower. This is still an aspect that should be studied in future to ensure that adsorption of metals using this material does not lead to secondary pollution of wastewaters. Concentrations of vanadium (V), nickel (Ni), chromium (Cr), arsenic (As), lead (Pb), boron (B), cobalt (Co), molybdenum (Mo), rubidium (Rb), antimony (Sb), lanthanum (La), cerium (Ce), and titanium (Ti) were below detection limits, and so are not reported in the table below.

Table 3-4: Elemental Compositions of the CSB as determined by acid digest concentrations (mg/L)

Element	Concentration (mg/L)
Fe	138.14
Al	75.35
Mg	18806.32
Ca	281774.60
Na	20909.86
Zn	48.35
Cu	18.20
Mn	25.11
K	7974.63
P	41254.60
Ba	25.74
Sr	4489.65
Li	3.13
Sn	113.02
Si	31.39

3.4 Conclusions

In this chapter, the characteristics of a crab shell-derived biochar are evaluated using a variety of physicochemical techniques and compared with those of other biochar. The CSB was found to be primarily mineral-rich, with a significantly lower amount of organic volatiles in comparison to the feedstock owing to loss of these groups during pyrolysis. Meanwhile, textural analysis using SEM revealed that the structure of the newly formed biochar contained some new porosity, as was further demonstrated by its BET SSA. Spectroscopic analysis of the biochar determined that it consisted primarily of CaCO_3 , along with a few organic functional groups, including carboxyl groups, ketones, pyridines, and pyrroles which could only be determined through XPS analysis. These functionalities could aid in adsorption if they are accessible to solution metals. Zeta potential of the char was highly negative, while trace element analysis demonstrated that the biochar contained few elements of concern for secondary pollution. As a result, the CSB made in this study has favorable properties for use in removing heavy metals from solution, with strong similarities to calcite used in current AMD application. Furthermore, the preparation of this material is simple, and it can be sourced from an existing industrial waste product. Further consideration of this material as a pyrolysis feedstock should be considered to encourage scale-up and commercial consideration.

Bibliography:

- [1] Department of Fisheries and Oceans, “Seafisheries landed value by region, 2018,” 2018. [Online]. Available: <http://www.dfo-mpo.gc.ca/stats/commercial/land-debarq/sea-maritimes/s2018av-eng.htm>. [Accessed: 29-Sep-2020].
- [2] Department of Fisheries and Oceans, “Seafisheries landed quantity by region, 2018,” 2018. [Online]. Available: <http://www.dfo-mpo.gc.ca/stats/commercial/land-debarq/sea-maritimes/s2018aq-eng.htm>. [Accessed: 29-Sep-2020].
- [3] L. Beaulieu, J. Thibodeau, P. Bryl, and M. É. Carbonneau, “Characterization of enzymatic hydrolyzed snow crab (*Chionoecetes opilio*) by-product fractions: A source of high-valued biomolecules,” *Bioresour. Technol.*, vol. 100, no. 13, pp. 3332–3342, 2009.
- [4] M. Hamdi, R. Nasri, N. Dridi, S. Li, and M. Nasri, “Development of novel high-selective extraction approach of carotenoproteins from blue crab (*Portunus segnis*) shells, contribution to the qualitative analysis of bioactive compounds by HR-ESI-MS,” *Food Chem.*, vol. 302, p. 125334, 2020.
- [5] H. D. De Holanda and F. M. Netto, “Recovery of components from shrimp (*Xiphopenaeus kroyeri*) processing waste by enzymatic hydrolysis,” *J. Food Sci.*, 2006.
- [6] F. Shahidi and J. Synowiecki, “Isolation and Characterization of Nutrients and Value-Added Products from Snow Crab (*Chionoecetes Opilio*) and Shrimp (*Pandalus Borealis*) Processing Discards,” *J. Agric. Food Chem.*, vol. 39, no. 8, pp. 1527–1532, 1991.
- [7] S. Ifuku, “Chitin and chitosan nanofibers: Preparation and chemical modifications,” *Molecules*, vol. 19, no. 11, pp. 18367–18380, 2014.
- [8] R. Castro, I. Guerrero-Legarreta, and R. Bórquez, “Chitin extraction from *Allopetrolisthes punctatus* crab using lactic fermentation,” *Biotechnol. Reports*, vol. 20, p. e00287, 2018.
- [9] H. Ge, B. Zhao, Y. Lai, X. Hu, D. Zhang, and K. Hu, “From crabshell to chitosan-hydroxyapatite composite material via a biomorphic mineralization synthesis method,” *J. Mater. Sci. Mater. Med.*, vol. 21, no. 6, pp. 1781–1787, 2010.
- [10] F. Li and R. C. Larock, “Novel polymeric materials from biological oils,” *J. Polym. Environ.*, vol. 10, no. 1–2, pp. 59–67, 2002.
- [11] S. Papari, K. Hawboldt, and R. Helleur, “Pyrolysis: A Theoretical and Experimental Study on the Conversion of Softwood Sawmill Residues to Biooil,”

- Ind. Eng. Chem. Res.*, vol. 54, no. 2, pp. 605–611, Jan. 2015.
- [12] T. M. Huggins, A. Haeger, J. C. Biffinger, and Z. J. Ren, “Granular biochar compared with activated carbon for wastewater treatment and resource recovery,” *Water Res.*, vol. 94, pp. 225–232, May 2016.
- [13] X. Chen *et al.*, “Adsorption of copper and zinc by biochars produced from pyrolysis of hardwood and corn straw in aqueous solution,” *Bioresour. Technol.*, 2011.
- [14] M. E. González *et al.*, “Effects of pyrolysis conditions on physicochemical properties of oat hull derived biochar,” *BioResources*, vol. 12, no. 1, pp. 2040–2057, 2017.
- [15] R. Azargohar, S. Nanda, J. A. Kozinski, A. K. Dalai, and R. Sutarto, “Effects of temperature on the physicochemical characteristics of fast pyrolysis bio-chars derived from Canadian waste biomass,” *Fuel*, vol. 125, pp. 90–100, 2014.
- [16] S. Mireles, J. Parsons, T. Trad, C. L. Cheng, and J. Kang, “Lead removal from aqueous solutions using biochars derived from corn stover, orange peel, and pistachio shell,” *Int. J. Environ. Sci. Technol.*, vol. 16, no. 10, pp. 5817–5826, 2019.
- [17] X. Tong, J. Li, J. Yuan, and R. Xu, “Adsorption of Cu(II) by biochars generated from three crop straws,” *Chem. Eng. J.*, vol. 172, no. 2–3, pp. 828–834, Aug. 2011.
- [18] M. F. Aller, “Biochar properties: Transport, fate, and impact,” *Crit. Rev. Environ. Sci. Technol.*, vol. 46, no. 14–15, pp. 1183–1296, 2016.
- [19] H. E. Ben Ali, C. M. Neculita, J. W. Molson, A. Maqsoud, and G. J. Zagury, “Performance of passive systems for mine drainage treatment at low temperature and high salinity: A review,” *Miner. Eng.*, vol. 134, pp. 325–344, 2019.
- [20] L. Dai *et al.*, “Calcium-rich biochar from the pyrolysis of crab shell for phosphorus removal,” *J. Environ. Manage.*, 2017.
- [21] Q. Xu, Q. Zhou, M. Pan, and L. Dai, “Interaction between chlortetracycline and calcium-rich biochar: Enhanced removal by adsorption coupled with flocculation,” *Chem. Eng. J.*, vol. 382, p. 122705, 2020.
- [22] L. Dai *et al.*, “Calcium-rich biochar from crab shell: An unexpected super adsorbent for dye removal,” *Bioresour. Technol.*, vol. 267, no. July, pp. 510–516, 2018.
- [23] L. Zhao, X. Cao, O. Mašek, and A. Zimmerman, “Heterogeneity of biochar

- properties as a function of feedstock sources and production temperatures,” *J. Hazard. Mater.*, vol. 256–257, pp. 1–9, Jul. 2013.
- [24] H. Li, X. Dong, E. B. da Silva, L. M. de Oliveira, Y. Chen, and L. Q. Ma, “Mechanisms of metal sorption by biochars: Biochar characteristics and modifications,” *Chemosphere*, vol. 178, pp. 466–478, 2017.
- [25] M. Hong, L. Zhang, Z. Tan, and Q. Huang, “Effect mechanism of biochar’s zeta potential on farmland soil’s cadmium immobilization,” *Environ. Sci. Pollut. Res.*, vol. 26, no. 19, pp. 19738–19748, 2019.
- [26] S. Brunauer, P. H. Emmett, and E. Teller, “Adsorption of Gases in Multimolecular Layers,” *J. Am. Chem. Soc.*, vol. 60, no. 2, pp. 309–319, 1938.
- [27] N. A. Seaton, J. P. R. B. Walton, and N. Quirke, “A new analysis method for the determination of the pore size distribution of porous carbons from nitrogen adsorption measurements,” *Carbon N. Y.*, vol. 27, no. 6, pp. 853–861, 1989.
- [28] MDI, “MDI Jade.” Materials Data, Inc., Livermore California, 2019.
- [29] M. H. Derkani *et al.*, “Mechanisms of Surface Charge Modification of Carbonates in Aqueous Electrolyte Solutions,” *Colloids and Interfaces*, vol. 3, no. 4, p. 62, 2019.
- [30] N. Fairley, “CasaXPS version 2.3.15.” 2002.
- [31] Z. Sebestyén *et al.*, “Thermal degradation of crab shell biomass, a nitrogen-containing carbon precursor,” *J. Therm. Anal. Calorim.*, no. 0123456789, 2020.
- [32] Y. Qiao *et al.*, “Pyrolysis of chitin biomass: TG–MS analysis and solid char residue characterization,” *Carbohydr. Polym.*, vol. 133, pp. 163–170, Nov. 2015.
- [33] F. Boßelmann, P. Romano, H. Fabritius, D. Raabe, and M. Epple, “The composition of the exoskeleton of two crustacea: The American lobster *Homarus americanus* and the edible crab *Cancer pagurus*,” *Thermochim. Acta*, vol. 463, no. 1–2, pp. 65–68, 2007.
- [34] A. Krutof, “Enhancement of Fast Pyrolysis Oil Fuel Properties Through Co-Pyrolysis and Improved Analysis,” Memorial University of Newfoundland, 2019.
- [35] F. Nekvapil *et al.*, “From Blue Bioeconomy toward Circular Economy through High-Sensitivity Analytical Research on Waste Blue Crab Shells,” *ACS Sustain. Chem. Eng.*, vol. 7, no. 19, pp. 16820–16827, 2019.
- [36] P.-Y. Chen, A. Y.-M. Lin, J. McKittrick, and M. A. Meyers, “Structure and mechanical properties of crab exoskeletons,” *Acta Biomater.*, vol. 4, no. 3, pp.

587–596, 2008.

- [37] Y. Xiao, Y. Xue, F. Gao, and A. Mosa, “Sorption of heavy metal ions onto crayfish shell biochar: Effect of pyrolysis temperature, pH and ionic strength,” *J. Taiwan Inst. Chem. Eng.*, vol. 80, pp. 114–121, Nov. 2017.
- [38] J. Yu *et al.*, “Hierarchical porous biochar from shrimp shell for persulfate activation: A two-electron transfer path and key impact factors,” *Appl. Catal. B Environ.*, vol. 260, no. September 2019, p. 118160, 2020.
- [39] J. Liu, X. Yang, H. Liu, W. Cheng, and Y. Bao, “Modification of calcium-rich biochar by loading Si/Mn binary oxide after NaOH activation and its adsorption mechanisms for removal of Cu(II) from aqueous solution,” *Colloids Surfaces A Physicochem. Eng. Asp.*, vol. 601, no. April, p. 124960, 2020.
- [40] C. Zhou, X. Gong, J. Han, and R. Guo, “Removal of Pb(II) and Zn(II) from Aqueous Solutions by Raw Crab Shell: A Comparative Study,” *Water Environ. Res.*, vol. 88, no. 4, pp. 374–383, 2016.
- [41] A. Krutof and K. A. Hawboldt, “Co-pyrolysis of softwood with waste mussel shells: Biochar analysis,” *Fuel*, vol. 282, p. 118792, 2020.
- [42] H. A. Al-Hosney and V. H. Grassian, “Water, sulfur dioxide and nitric acid adsorption on calcium carbonate: A transmission and ATR-FTIR study,” *Phys. Chem. Chem. Phys.*, vol. 7, no. 6, pp. 1266–1276, 2005.
- [43] K. B. Cantrell, P. G. Hunt, M. Uchimiya, J. M. Novak, and K. S. Ro, “Impact of pyrolysis temperature and manure source on physicochemical characteristics of biochar,” *Bioresour. Technol.*, vol. 107, pp. 419–428, Mar. 2012.
- [44] C. Santschi and M. J. Rossi, “Uptake of CO₂, SO₂, HNO₃ and HCl on calcite (CaCO₃) at 300 K: Mechanism and the role of adsorbed water,” *J. Phys. Chem. A*, vol. 110, no. 21, pp. 6789–6802, 2006.
- [45] B. W. Muir, S. L. McArthur, H. Thissen, G. P. Simon, H. J. Griesser, and D. G. Castner, “Effects of oxygen plasma treatment on the surface of bisphenol A polycarbonate: a study using SIMS, principal component analysis, ellipsometry, XPS and AFM nanoindentation,” *Surf. Interface Anal.*, vol. 38, pp. 1186–1197, 2006.
- [46] B. Demri and D. Muster, “XPS study of some calcium compounds,” *J. Mater. Process. Tech.*, vol. 55, no. 3–4, pp. 311–314, 1995.
- [47] T. Chen, S. Deng, B. Wang, J. Huang, Y. Wang, and G. Yu, “CO₂ adsorption on crab shell derived activated carbons: Contribution of micropores and nitrogen-containing groups,” *RSC Adv.*, vol. 5, no. 60, pp. 48323–48330, 2015.

- [48] H. N. Tran, S. J. You, A. Hosseini-Bandegharai, and H. P. Chao, “Mistakes and inconsistencies regarding adsorption of contaminants from aqueous solutions: A critical review,” *Water Res.*, vol. 120, pp. 88–116, 2017.
- [49] P. Moulin and H. Roques, “Zeta potential measurement of calcium carbonate,” *J. Colloid Interface Sci.*, vol. 261, no. 1, pp. 115–126, 2003.
- [50] S. Budyanto, Y. L. Kuo, and J. C. Liu, “Adsorption and precipitation of fluoride on calcite nanoparticles: A spectroscopic study,” *Sep. Purif. Technol.*, vol. 150, pp. 325–331, 2015.
- [51] Y. Deng, S. Huang, D. A. Laird, X. Wang, and Z. Meng, “Adsorption behaviour and mechanisms of cadmium and nickel on rice straw biochars in single- and binary-metal systems,” *Chemosphere*, vol. 218, pp. 308–318, Mar. 2019.
- [52] J. G. Kunkel, W. Nagel, and M. J. Jercinovic, “Mineral Fine Structure of the American Lobster Cuticle,” *J. Shellfish Res.*, 2012.

Chapter 4 – Removal of Copper and Sulfate from Solution using a Crab Shell Biochar

A modified version of this chapter will be submitted for publication. It has been proofread and revised by Dr. Kelly Hawboldt and Dr. Stephanie MacQuarrie

Abstract

Biochar is a material produced from the pyrolysis of biomass with the potential to remove metals from water and treat the acidity of acid mine drainage (AMD). Feedstocks from plant-based sources are the most commonly studied feedstocks to date, however, other important biomass sources are also of interest. This chapter focuses on the use of a crab shell-based biochar for the adsorption of copper (Cu^{2+}) and sulfate from solution, two aqueous contaminants common to AMD. The crab shell is a by-product of crab processing. The study conditions were pH from 2-7, initial Cu concentrations of 100-2500 mg/L, biochar dosages of 1-20 g/L, temperatures of 5-30 °C, and sulfate concentrations from 50-1500 mg/L (equivalent S mg/L). The Cu^{2+} adsorbed varied from 88.1%-99.8% for biochar loadings of 1-20 g/L and maximum adsorption occurred in under two hours. Sulfate was removed to a much lesser extent, and removal was due to the formation of posnjakite ($\text{Cu}_4[(\text{OH})_6\text{SO}_4]\cdot\text{H}_2\text{O}$), a copper basic salt. Initial solution pH did not affect the removal of Cu^{2+} from solution in the pH range of 2-7 but prevented any adsorption of S, likely due to competition from the chloride (Cl^-) ion which was introduced through the acid. The maximum adsorption capacity was 184.8 ± 10.2 mg/g for Cu^{2+} . As temperature increased from 5 to 30 °C, Cu^{2+} adsorption increased from 52.2 ± 3.0 mg/g to 122.2 ± 2.0 mg/g. Overall, the research demonstrates that the crab shell biochar is a feasible adsorbent for Cu^{2+} with limited or no inhibition from the presence of sulfate.

4.1 Introduction

Acid Mine Drainage (AMD) produces large amounts of wastewater containing hazardous levels of heavy metals and sulfates [1]. To avoid damage to the environment and health and safety, these contaminants must be removed from the AMD prior to disposal. A wide variety of techniques have been investigated for this treatment, including chemical and electrochemical techniques, ion exchange, membrane technologies, and adsorption [2]. Of these, adsorption has the benefit of being a simple process that can work over a wide range of pollutant concentrations, is simple to operate, and does not generate toxic sludges, among other benefits [2], [3]. Biochar, a material derived from the pyrolysis of organic materials, has been investigated as a metal adsorbent [4], [5]. Common feedstocks for pyrolysis include forestry by-products such as sawdust and wood bark [5], [6], and agricultural by-products [7]–[9], among other materials. The use of by-products as a feedstock for the pyrolysis process enables a low cost of production, and also valorizes waste streams from other industries.

In addition to the lignocellulosic feedstocks mentioned above, new feedstocks from sources such as fisheries waste are also being considered. The fisheries sector produces by-products in the form of fish frames and shells, the bulk of which is disposed of at sea or landfill. In the case of the Canadian snow crab fishery, as much as 30% of the total catch weight ends up as a by-product, which is often disposed of at sea or in landfills [10]. The by-products from processing of crustaceans such as crab are rich in calcium carbonate (CaCO_3), along with proteins and the biopolymer chitin [10]. These materials have been studied as biosorbents, demonstrating high percent removal for a variety of metals in solution [11]. Richards et al. used dried crab shell as an adsorbent for copper

(Cu^{2+}) and zinc (Zn^{2+}) from water, demonstrating that the crab shell outperformed a commercial activated carbon and biochar for Cu^{2+} and Zn^{2+} , particularly at high concentrations [12]. Zhou et al. studied the use of crab shell for removal of lead (Pb^{2+}) and Zn^{2+} from water, finding that it had a very high percent removal for both metals (709 mg/g and 117 mg/g, respectively), that was in large part due to the high quantity of CaCO_3 in the shell, which dissolved into the water and led to microprecipitation of the heavy metal ions [13]. CaCO_3 as an adsorbent in AMD treatment shows high adsorption capacities for a wide range of transition metals [14]–[19] and moderate capacity for sulfates [20].

Pyrolysis of crustacean processing by-product to generate biochar has been studied in recent studies [21], [22], and the resultant biochar has been studied as an adsorbent for aqueous phosphate [23], dyes [24], antibiotics [22], and a metal solution containing Pb^{2+} , Cu^{2+} , and arsenic III (As(III)) [25]. Biochars made from marine shells have high mineral content, alkalinity, and surface area making them particularly applicable to AMD treatment in terms of both removing metals from solution and neutralizing the pH of the AMD [26, 27]. Research in this field is limited, however, and demands further study to realize the full capability of this class of biochar.

In this study, we investigate the use of biochar based on crab shell to remove contaminants from water in batch experiments. This biochar, having been characterized in a previous chapter, is studied for the removal of aqueous sulfate, (SO_4^{2-}) and Cu^{2+} . Sulfate is of interest as it is the driver for acidity in AMD and could potentially interfere with adsorption of toxic metals (here represented as Cu^{2+}) [17], [27], [28]. Neither of these compounds have been studied in existing literature on adsorption using marine by-

product-based biochars, thus representing a novel opportunity in this work. This work involves a detailed study of the removal of each solute by studying the effects of biochar dose, effect initial solution pH, adsorption kinetics, effect of solute concentration, and finally the effect of temperature on equilibrium adsorption capacity. The properties of the biochar following adsorption are then studied to provide information on the potential mechanisms involved in the adsorption process.

4.2 Materials & Methodology

4.2.1 Materials

Snow crab (*Chionoecetes opilio*) shells were obtained from processing by-products from Louisbourg Seafoods Limited, of Louisbourg, Nova Scotia, Canada. $\text{CuSO}_4 \cdot 5\text{H}_2\text{O}$ and $\text{Na}_2\text{SO}_4 \cdot 10\text{H}_2\text{O}$ were obtained from Fisher Chemicals. 0.1 M HCl solution was obtained from Sigma-Aldrich Canada, while NaOH pellets were obtained from ACP Chemicals Inc. The H_2O_2 used in digestion was purchased from ACP Chemicals Inc., and 16 M HNO_3 was purchased from Caledon Laboratories Ltd.

4.2.2 Biochar Production

The raw shell was ground to a particle size of less than 2.0 mm using a rotary grinder. Prior to pyrolysis, the ground crab shell dried in an oven at 70 °C overnight. For pyrolysis, samples were loaded in 5 g batches into a horizontal tube furnace, which was flushed using ultrapure (99.999%) N_2 . Pyrolysis was carried out at 500 °C. The fast pyrolysis was carried out by first loading the sample boat containing the crab shell into the center of the furnace, and then removing it once pyrolysis vapors stopped entering the

condensing flask, a process which took approximately 5 minutes. Upon completion, the biochar was removed from the furnace and covered to prevent it from oxidizing until cool and was then stored in a refrigerator.

4.2.3 Adsorption Experiments

The adsorptive performance of the CSB for Cu^{2+} and SO_4^{2-} was evaluated through batch adsorption experiments, using $\text{CuSO}_4 \cdot 5\text{H}_2\text{O}$ to represent Cu^{2+} in solution and anhydrous Na_2SO_4 to represent SO_4^{2-} . The concentration of these compounds in solution following adsorption was determined by ICP-OES using a Perkin-Elmer 5300 DV at Memorial University's Micro-Analysis Facility (MAF). Other elements were also analyzed based on their concentrations in the CSB and potential roles in ion exchange (Ca^{2+} and Mg^{2+}). Whereas sulfate is known to speciate in solution [29], sulfate removal was measured in terms of total sulfur removed rather than the amount of sulfate removed. Following analysis, the adsorptive performance of the CSB was evaluated by calculating the percent removal or adsorptive capacity by formulas 4-1 and 4-2, respectively, which are listed as follows:

$$\% \text{ Removal} = \frac{C_i - C_f}{C_i} * 100 \quad (4 - 1)$$

$$q_e = \frac{(C_i - C_f) * V}{m} \quad (4 - 2)$$

Where q_e is the equilibrium adsorption capacity at a given concentration in mg/g, C_i is the initial concentration of either Cu^{2+} or S in mg/L, C_f is the final concentration of the

respective pollutant in mg/L, V is the solution volume in liters, and m is the mass of adsorbent added to the solution in grams.

4.2.4.1 Dosage Experiments

First, experiments were carried out to determine the appropriate dosage of CSB in solution for each sample. Solutions containing 251 mg/L of Cu^{2+} and 1500 mg/L of SO_4^{2-} (500.7 mg/L of S equivalent) were prepared in distilled water (18.2 M Ω). 100 mL of either solution was then added to an Erlenmeyer flask, after which CSB was added according to dosages of 1 g/L, 5 g/L, 10 g/L, and 20 g/L. These solutions were allowed to mix on a shaker table for 24 hours, after which the solutions were filtered using Whatman No. 41 ashless filter paper.

4.2.4.2 Effect of pH on adsorption

The effects of solution pH on adsorptive performance were evaluated by altering the pH of the $\text{CuSO}_4/\text{Na}_2\text{SO}_4$ solutions to values of 2, 4, 5, or 7 using either 0.1 M HCl or 0.1 M NaOH. After each solution was created, the CSB was added, and the solutions were left on a shaker for 24 hours, after which the pH of the solution was measured again, and the samples were sent for analysis via ICP-OES.

4.2.4.3 Adsorption Isotherm Experiments

Adsorption isotherm experiments were carried out by varying the concentration of each chemical species in solution. For Cu^{2+} , concentrations used were 100mg/L, 400mg/L, 700mg/L, 1500mg/L, and 2500mg/L. Adsorption took place over the place of 24 hours.

The results of these experiments were then fit to the Langmuir and Freundlich isotherms using non-linear regression. The Langmuir isotherm, which assumes monolayer adsorption to the material surface, is represented by the following equation:

$$q_e = \frac{q_{max}K_L C_e}{1 + K_L C_e} \quad (4 - 3)$$

Where q_e is the equilibrium adsorption capacity in mg/g, q_{max} is the maximum adsorption capacity in mg/g, K_L is the adsorption constant in L/mg, and C_e is the concentration of metal in solution in mg/L [30]. The Langmuir isotherm also leads to the definition of R_L , which is defined as a dimensionless Langmuir parameter or equilibrium parameter [29], and is defined as follows in equation 3-4:

$$R_L = \frac{1}{1 + K_L C_0} \quad (4 - 4)$$

Where K_L is the Langmuir adsorption constant as stated above in L/mg, and C_0 is the initial concentration of adsorbate in the adsorption process in mg/L. Whereas a range of C_0 values exist when performing isotherm analysis, a range of R_L values must also be presented at each C_0 value used. The R_L values can in turn be interpreted as indications of the favourability of adsorption, where $R_L > 1$ indicates unfavorable adsorption, R_L between 0 and 1 indicates favorable adsorption, and $R_L = 0$ indicates irreversible adsorption [31].

The Freundlich isotherm [32] describes the relationship of the amount of adsorbed solute to the equilibrium concentration of solute in solution using an exponential equation, which is described as follows:

$$q_e = K_F C_e^n \quad (4 - 5)$$

Where q_e is the adsorption capacity of the adsorbent in mg/g, K_F is the Freundlich constant in $(\text{mg/g})/(\text{mg/L})^n$, and n is a dimensionless Freundlich intensity parameter. The intensity parameter can be further analyzed as an indicator of the favourability of the adsorption process, with $n > 1$ indicating unfavourable adsorption, an n value between 0 and 1 indicating favourable adsorption, and $n = 0$ indicating irreversible adsorption [31].

4.2.4.4 Adsorption Kinetics

Adsorption kinetics were determined by studying Cu^{2+} adsorption over time. Here, solutions were separated after 10, 30, 60, and 120 minutes and analyzed to determine the extent of adsorption from solution at each point in time. Data was then analyzed to determine the “best” fit to models. Models analyzed included pseudo-first-order (PFO), pseudo-second-order (PSO), and Elovich kinetic models. The PFO model is as follows [33]:

$$q_t = q_{max}(1 - e^{-k_1 t}) \quad (4 - 6)$$

The PSO model is [34]:

$$q_t = \frac{q_{max}^2 k_2 t}{1 + q_{max} k_2 t} \quad (4 - 7)$$

Finally, the Elovich model, developed as a model for adsorption from heterogeneous surfaces, is [33]:

$$q_t = \frac{1}{\beta} \ln(\alpha\beta + 1) \quad (4 - 8)$$

Where q_t is the adsorption capacity of the biochar at a given point of time t in mg/g, q_{max} is the equilibrium adsorption capacity in mg/g, t is the time elapsed in adsorption in hours

(h), k_1 is the PFO adsorption rate constant in h^{-1} , k_2 is the PSO adsorption rate constant ($g/mg \cdot h$), α is the Elovich initial rate of adsorption ($mg/kg \cdot h$) and β (kg/mg) is the desorption rate constant for the Elovich equation [33].

4.2.4.5 Thermodynamic parameters and effect of temperature

The Gibb's free energy (ΔG) of a process can provide useful insights on the spontaneity of a process under given conditions, and in turn can be related to the enthalpy change (ΔH) and entropy change (ΔS) of the process, which indicate whether the process is endothermic or exothermic. For adsorption processes, thermodynamic properties can be estimated by analyzing the effects of temperature on the process, which is then related to Gibb's free energy, a measure of the spontaneity of a given process, by the following equations [35].

$$K_d = \frac{q_e}{C_e} \quad (4 - 9)$$

$$\Delta G = -RT \ln(K_d) \quad (4 - 10)$$

$$\Delta G = \Delta H - T \Delta S \quad (4 - 11)$$

Where ΔG is Gibb's energy change in kJ/mol , R is the ideal gas constant ($8.314 J/mol \cdot K$), T is the temperature in kelvin, K_d is the reaction's dissociation constant in L/g , q_e is the adsorption capacity at the given temperature in mg/g , C_e is the equilibrium concentration of the solute at the given temperature in mg/L , and ΔH and ΔS are the enthalpy change and entropy change of the process, in units of kJ/mol and $kJ/mol \cdot K$,

respectively. It should be noted these are not true thermodynamic properties as K_D is not dimensionless but does provide information on the spontaneity of the process.

Adsorption experiments of 24 hours in duration were performed at different temperatures to determine the impact of temperature. Based on prior experiments, a Cu^{2+} concentration of 700mg/L was used. The studied temperatures were 5 °C, 10 °C, and 30 °C, with lower temperatures (5 °C and 10 °C) maintained using a New Brunswick Scientific Innova 4230 Refrigerated Incubator Shaker, while the experiment at 30 °C was maintained using a VWR® Incubating shaker.

4.3 Results and discussion

4.3.1 Effect of Dosage

The results of dosage experiments for Cu^{2+} indicated that the CSB had a very high percent removal of the metal, as shown through Figure 4-1.

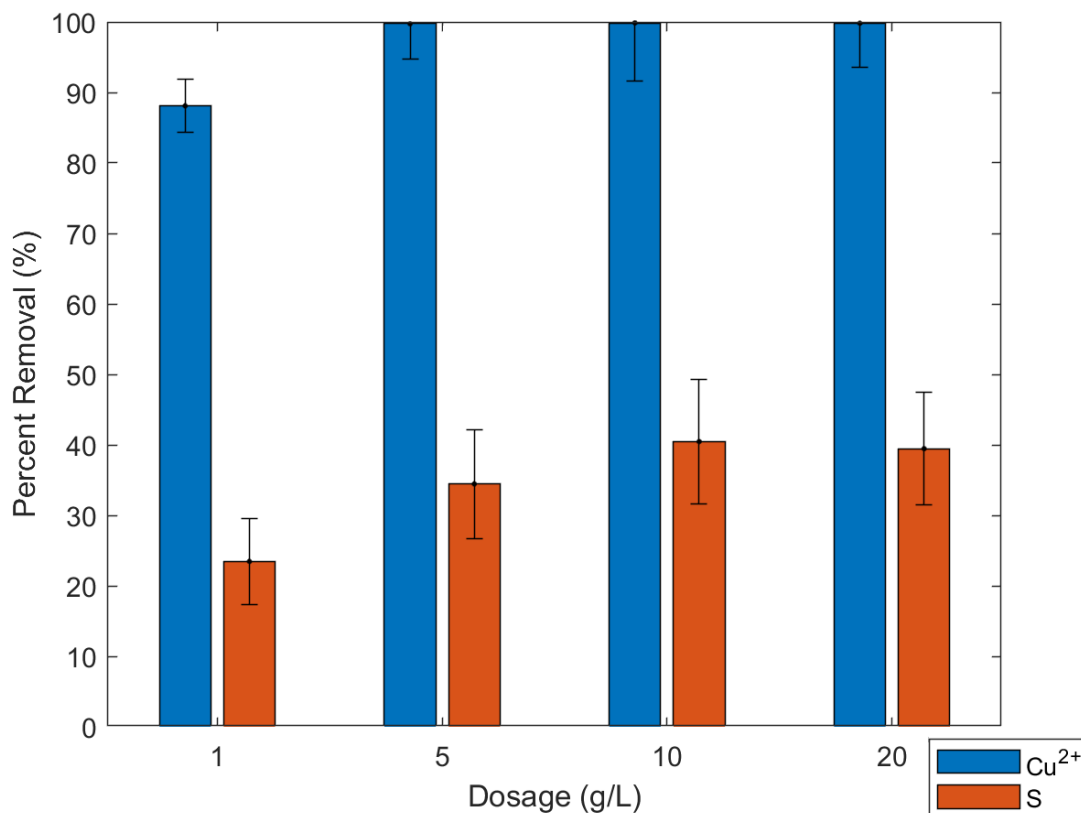
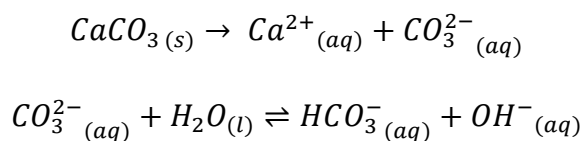


Figure 4-1: Percent Removal of Cu²⁺ and S from solution as a function of CSB dosage

At the lowest dosage of 1 g/L, the percent removal of the metal was 88.10±3.74%, which increased to over 99% for all higher dosages. This high percent removal at low dosage contrasts with biochar of other sources, with Chen et al. observing that removal of Cu²⁺ by their corn stover biochar only reached a comparable extent at a dosage of 10 g/L, while their hardwood biochar was only able to remove 56.7% of Cu²⁺ at a lower concentration of 1.0 mM (63.546 mg/L) [5]. Pelleria et al. also found that their rice husk biochar required 10 g/L at least to achieve near-complete removal of Cu²⁺ from a 20 mg/L solution, while their orange peel and olive pomace biochar required over 20 g/L to achieve that percent removal [36].

Simultaneously, the final pH of the solution at the 1g/L dosage was noted as the lowest of the three dosages at a value of 6.20, while the other dosages produced final pH values between 10 and 11, which rose with increasing dosage. This could be due to the leaching of CaCO_3 in the initial solution, which produces hydroxide ions by the following reactions:



Ions exchange occurred here as well, as observed through the presence of Ca^{2+} and Mg^{2+} in the final solution. Concentrations of Ca^{2+} in solution decreased with increasing dosage, while concentrations of Mg^{2+} increased with increasing dosage, as demonstrated in Table 4-1. This may be because MgCO_3 is more soluble in water (139 mg/L) than CaCO_3 (14 mg/L) [37]. CaCO_3 , in turn, remains more tightly bound in its solid form and as dosage increases, the pH of the solution increases further decreasing the solubility of CaCO_3 .

Table 4-1: Final concentrations of Ca^{2+} and Mg^{2+} in solution as a function of adsorbent dosage

Dosage (g/L)	[Ca^{2+}] (mg/L)	[Mg^{2+}] (mg/L)
1	26.9±0.6	6.65±0.16
5	12.4±0.4	31.6±0.7
10	6.4±0.2	47.8±1.0
20	6.8±0.2	60.7±1.2

Sulfate, on the other hand, did not adsorb well onto the CSB. This result may be due in part to the negative zeta potential of the crab char biochar as outlined in Chapter 3 of this

thesis, which could lead to electrostatic repulsion effects upon adsorption. Additionally, sulfates of Ca^{2+} are relatively soluble in water, much more so than its carbonates [38], and therefore removal of sulfates via coprecipitation with Ca^{2+} is unlikely. S removal was observed concomitantly with Cu^{2+} removal and is also plotted Figure 4-1. The percent removal of S from solution reaches a maximum of $40.46 \pm 8.86\%$ by mass at a dosage of 10 g/L, remaining near the same value upon moving to 20 g/L. This result indicates that a very slight amount of sulfate might be removed through a reaction with Cu^{2+} in solution, perhaps via a mechanism such as coprecipitation [16]. This will be expanded on later where results of surface analysis of the biochar after adsorption are presented. From these results, a dosage of 5 g/L is sufficient for the removal of Cu^{2+} and S from solution and was utilized for subsequent experiments.

4.3.2 Effect of initial pH

The pH of a solution has important effects on the speciation of solutes, and surface charge of materials in solution. Consequently, the adsorption capacity of an adsorbent is often a function of pH [39]. Results for Cu^{2+} adsorption from water as a function of initial pH are shown in Figure 4-2. These results demonstrate that the initial solution pH has little influence on the adsorption capacity of the CSB at this Cu^{2+} concentration and biochar dosage, with very little fluctuation being present in the graph. While this does contrast heavily with results from other biochars demonstrated in literature [5], [40], it is important to realize that the composition of the CSB is very different from more commonly studied lignocellulosic biochars, which are still rich in carbon, while the CSB

is in turn primarily composed of minerals, such as CaCO_3 , which was shown previously to have strong alkalinity. This property gives the CSB a neutralizing capability in acidic solutions and is likely the cause for the lack of change in percent removal of Cu^{2+} as a function of initial pH, as the pH normally reverts to alkaline levels throughout the adsorption process. This property may make the biochar very useful in treatment of the acidity of AMD, with similar sources of biogenic CaCO_3 having been used to treat AMD in past studies [26], [41].

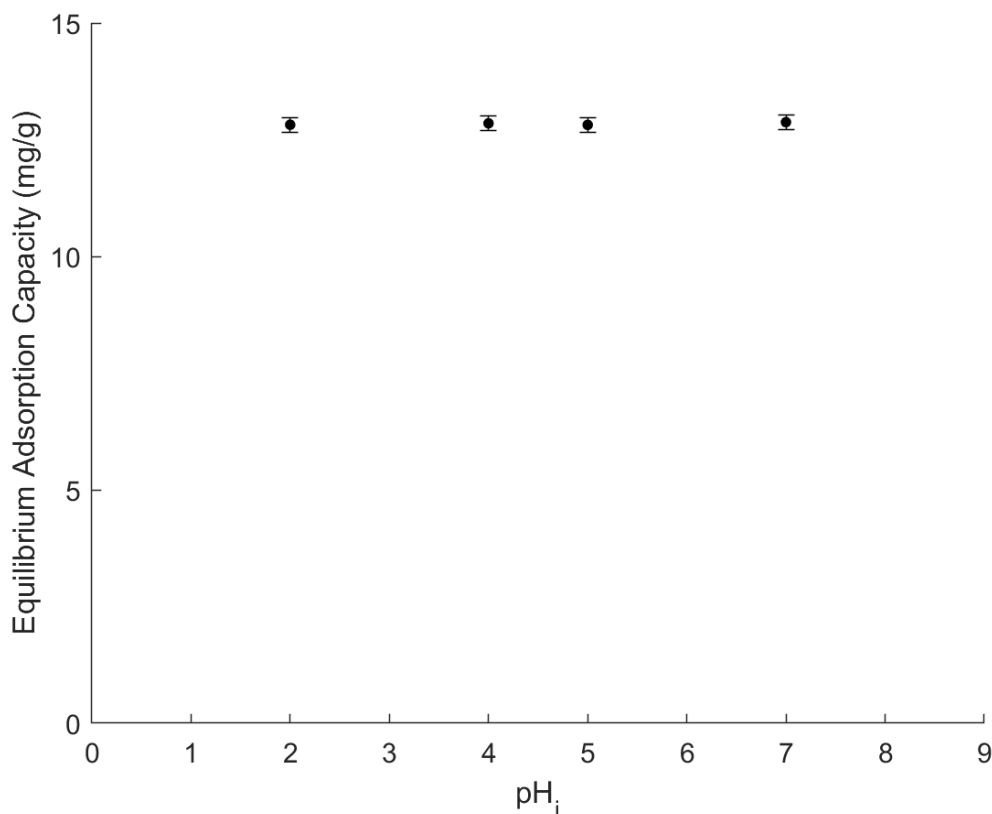


Figure 4-2: Effect of initial pH on adsorption of Cu^{2+} from solution

Removal of sulfur was not observed to occur through experiments with Na_2SO_4 , nor in CuSO_4 solution, despite the latter having occurred in the preceding section on dosage.

This may have been due to the use of HCl as an acid, which would have added chloride

ions to solution which could potentially compete with sulfate ions during co-precipitation reactions. Further analysis of this phenomenon is provided in the discussion section of this chapter.

4.3.3 Adsorption Isotherms

Adsorption isotherms for the adsorption process are shown in Figure 4-3 and Figure 4-4 for Cu^{2+} with statistical data regarding their fit to the Langmuir and Freundlich isotherms shown in Table 4-2. S removal is not studied here due to low rates of removal, as well as high uncertainty in its removal owing to inherent limitations of ICP-OES measurements for this element.

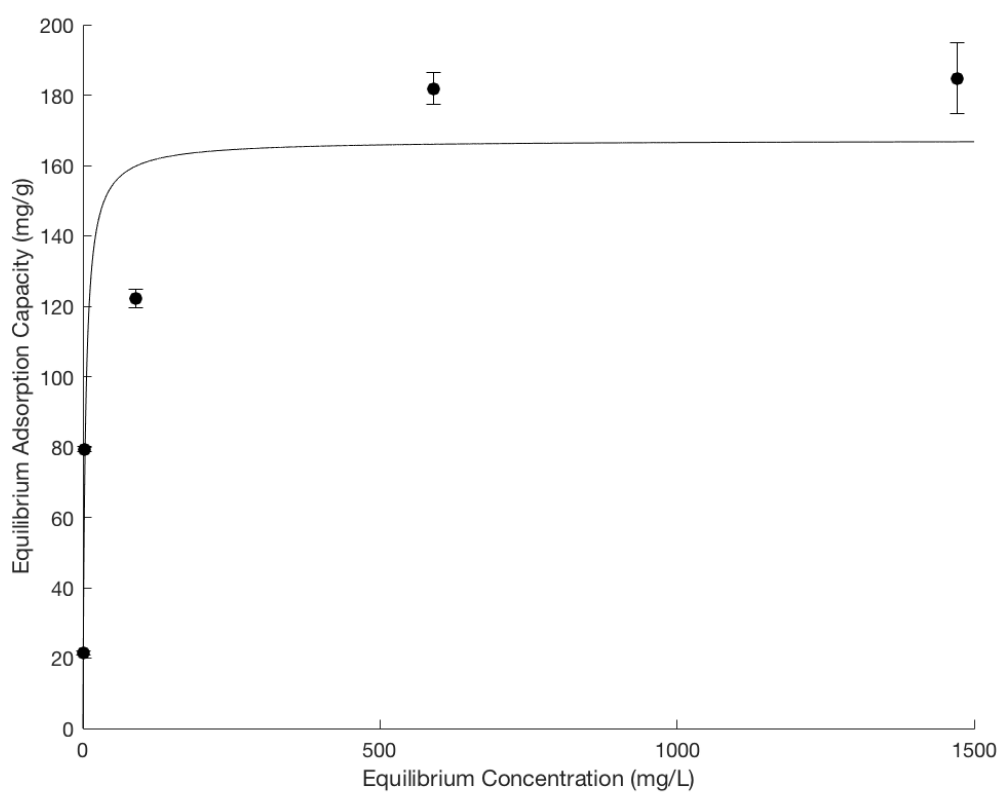


Figure 4-3: Langmuir isotherm fit to adsorption data for Cu^{2+}

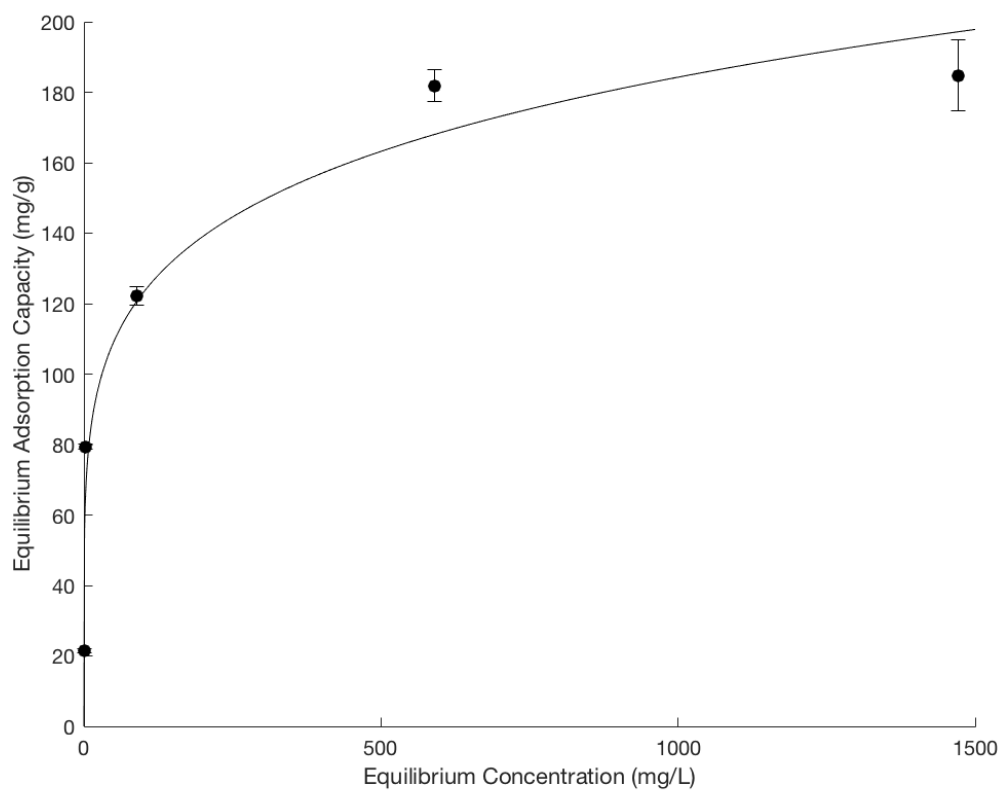


Figure 4-4: Freundlich isotherm fit to adsorption data for Cu^{2+}

Table 4-2: Adsorption isotherm fit statistics

		Cu^{2+}
Langmuir Isotherm	R^2	0.8862
	RMSE	27.09
	q_{\max} (mg/g)	167.2
	K_L (L/mg)	0.2428
Freundlich Isotherm	R^2	0.9561
	RMSE	16.83
	K_F (mg/g)	55
	n	0.175

It is observed here that the Freundlich equation displays a better fit to this data, both in terms of its higher R^2 value, and lower Root Mean Square Error (RMSE). The Freundlich isotherm for this data presents an n value less than 1, representing strong,

favorable adsorption [31]. When studying aqueous systems, the Freundlich isotherm implies that adsorption sites are heterogeneous, which provides an account of the mechanisms in which adsorption may be taking place [42].

Experimentally, this analysis places the maximum adsorption capacity at a value of 184.8 ± 10.2 mg/g for Cu^{2+} . This value is very high in comparison with the Cu^{2+} removal capacity of other adsorbents, with Chen et al. reporting values of 12.52 mg/g and 6.79 mg/g for their corn stover biochar and hardwood biochar, respectively [5], Mahdi, Yu, & El Hanandeh reporting 26.75 mg/g for their date seed biochar [30], and Z. Liu et al. (2010) reporting 2.75 mg/g for their pinewood biochar [43]. This value is also high in comparison with commercial adsorbents, exceeding the values found by Wilson et al. for DARCO 12 x 40, NORIT C GRAN, and MINOTAUR activated carbons, which had values of 26.1 mg/g, 47.8 mg/g, and 61.3 mg/g, respectively [44].

4.3.4 Adsorption Kinetics

Adsorption kinetic experiments demonstrate that the CSB displays fast initial adsorption of Cu^{2+} from solution, achieving over 85% of the total removal in 2 hours. Fitting of this data to experimental models demonstrates further details on the rate of removal for the adsorption process, with fit statistics and parameters listed in Table 4-3 and a plot of the models fit to experimental data in Figure 4-5.

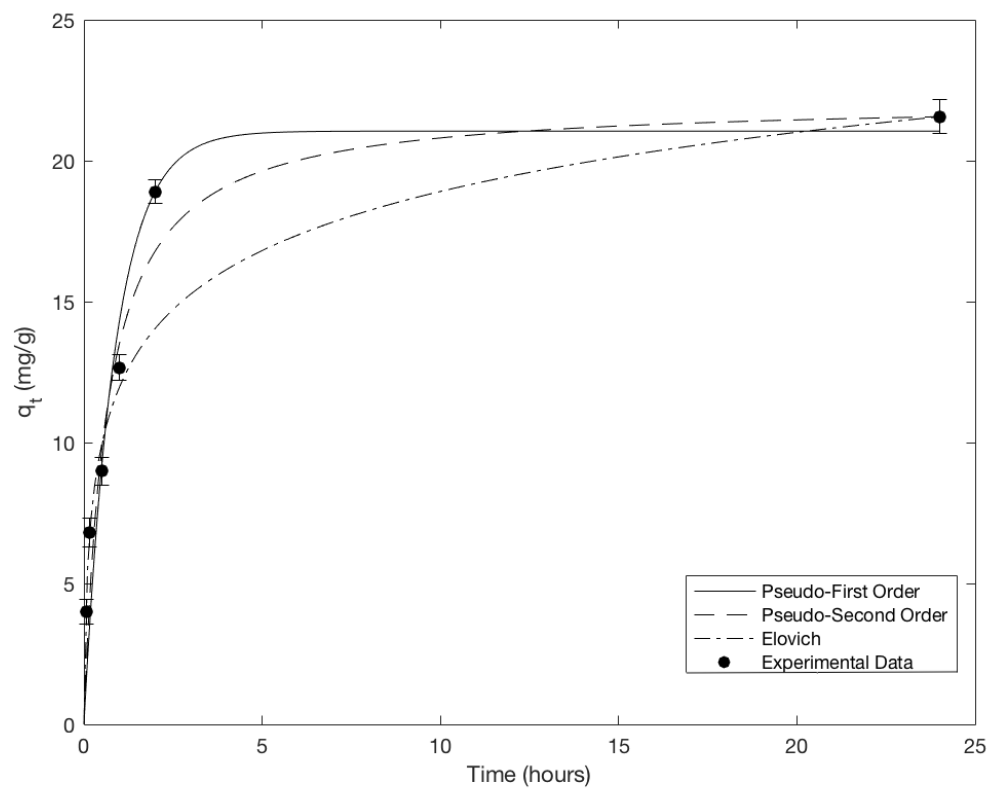


Figure 4-5: Fit of Experimental data to the PFO, PSO, and Elovich models for Cu^{2+} removal

Table 4-3: Adsorption kinetic model statistics for Cu^{2+}

Pseudo First- Order Model	R^2	0.9268
	RMSE	2.092
	q_{\max}	21.05
	k_1	1.144
Pseudo Second- Order Model	R^2	0.9467
	RMSE	1.786
	q_{\max}	22.13
	k_2	0.0711
Elovich Model	R^2	0.8916
	RMSE	2.546
	α	154.1
	β	0.323

Of the kinetic models used, the PSO model displayed the best fit to the experimental data for Cu^{2+} , with the highest R^2 data and lowest RMSE of all models. The PSO model assumes chemically controlled adsorption [45], though this mechanistic implication must also be tested through proper mechanistic analysis. In addition, the predicted q_e at this concentration was 22.13 mg/g, which is in good agreement with the experimental result of 21.56 ± 0.61 mg/g. A strong fit to the PSO model was also observed by Chen et al. in their study on both corn stover and hardwood biochar [5], as well as by Bozbaş and Boz with their *A. Inaequivalvis* shell for both Pb^{2+} and Cu^{2+} [46].

This rapid rate of removal of transition metals has been reported in past for marine-shell-based adsorbents, as Zhou et al. reported removal of Pb^{2+} and Zn^{2+} to occur primarily within 2 hours as well when using raw crab shell as an adsorbent [13], as well as in the removal of Pb^{2+} and Cu^{2+} using *A. Inaequivalvis* shell by Bozbaş and Boz [46]. On the

contrary, results from a crayfish shell biochar for Pb^{2+} adsorption demonstrated much slower kinetics taking 12 hours to complete, implying that the results observed here may be very dependent on the metal studied [47].

4.3.5 Thermodynamic Parameters

Thermodynamic parameters obtained through the study of the effect of temperature on adsorption are presented in Table 4-4 for removal of Cu^{2+} from solution. As demonstrated here, removal of Cu^{2+} with positive ΔG values except for the removal of Cu^{2+} at 30 °C. Removal is still observed in all cases, however, as it can be noted that this analysis does not provide exact thermodynamic parameter estimations, but more so provides trends of adsorptive behaviour as a function of temperature.

Table 4-4: Thermodynamic parameters for the removal of Cu^{2+} from solution

Solute	T (K)	K_d	ΔG (kJ/mol)	ΔH (kJ/mol)	ΔS (kJ/mol·K)
Cu^{2+}	278.15	0.113	5.05	62.1	0.206
	283.15	0.208	3.70		
	303.15	1.08	-0.197		

Whereas many AMD treatment processes take place outdoors and are thus subject to influence by the outside temperatures [1], [48], studying adsorption capacity as a function of temperature is an important measurement. Here, it is observed that the adsorption capacity of the CSB decreases as a function of decreasing temperature, undergoing a 57% decrease in adsorption capacity from 122.2 ± 2.0 mg/g at 30 °C, to just 52.2 ± 3.0 mg/g at 5 °C, which is demonstrated in Figure 4-6. This observation is in line with that of Yan et al. (2018) who studied the removal of As(V) by a crayfish shell-based biochar [49], and

by Sdiri et al. who studied the removal of cadmium (Cd^{2+}), Cu^{2+} , and Zn^{2+} by natural limestone over a similar temperature range [50].

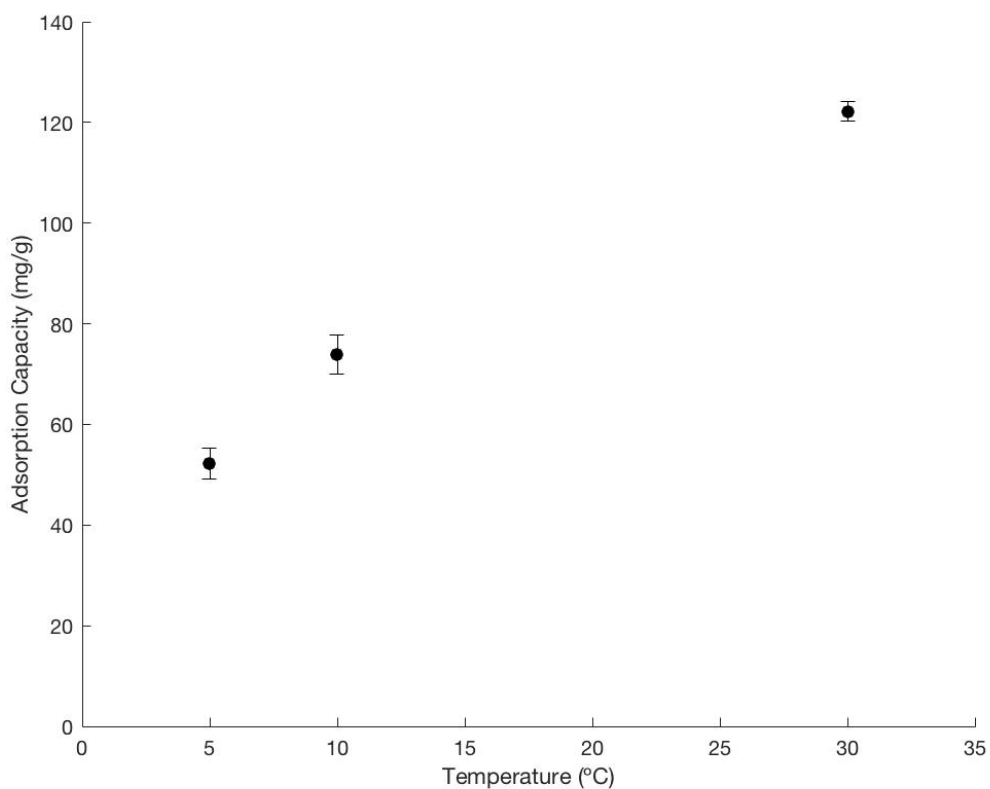


Figure 4-6: Cu^{2+} adsorption capacity of the CSB as a function of temperature

Mechanistically, this may occur due to the decreased dissolution of alkaline minerals from the CSB at lower temperatures, which was observed through decreased concentrations of Ca^{2+} and Mg^{2+} in solution at low temperatures and is presented in Figure 4-7.

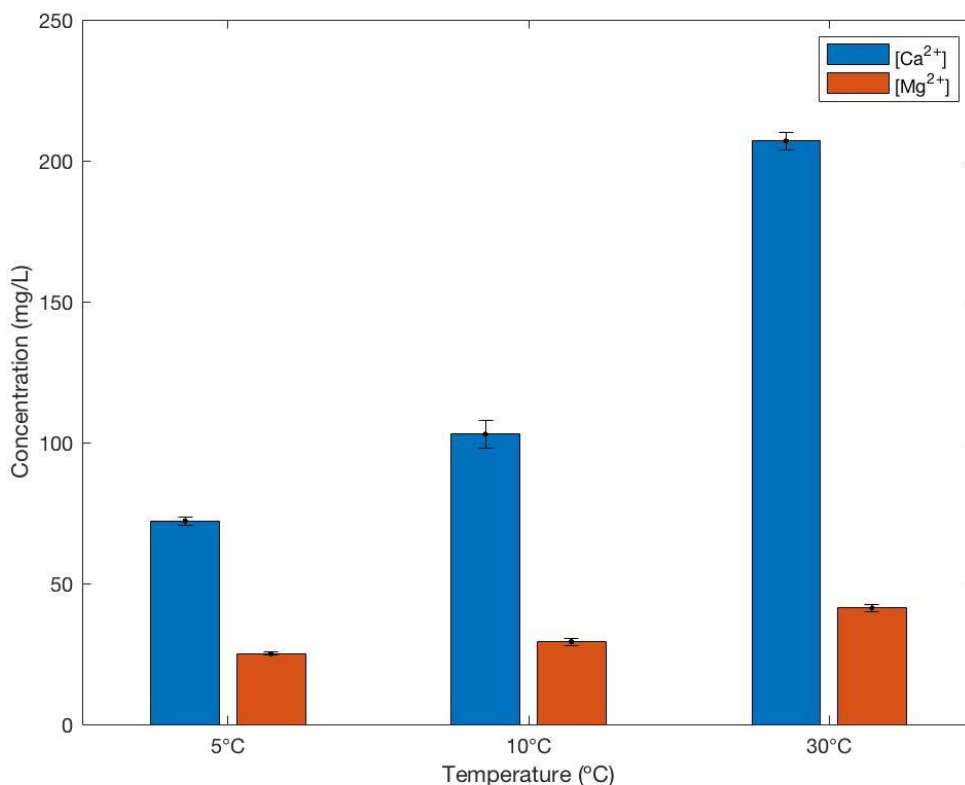


Figure 4-7: Concentrations of Ca^{2+} and Mg^{2+} in solution at equilibrium as a function of temperature

The trend of decreasing Ca^{2+} and Mg^{2+} concentrations with temperature, while Cu^{2+} adsorption capacity increases likely points to the effect of increased leaching of Ca^{2+} and Mg^{2+} carbonates from solution, leading to higher amounts of Cu^{2+} precipitating in the presence of these alkaline compounds, and has been observed in past studies [50], [52]. However, this raises the additional question as to whether the increased loss of Ca^{2+} and Mg^{2+} , via leaching and ion exchange, will lead to decreased performance of the adsorbent if it were to be regenerated and reused in future cycles.

4.3.6 Mechanistic Analysis

Further characterization of the CSB was performed in order to determine the mechanisms in which the Cu^{2+} adsorbed to the biochar surface. XRD analysis of the biochar following adsorption, shown in Figure 4-8, demonstrated new peaks, which were found to correspond with posnjakite ($\text{Cu}_4[(\text{OH})_6\text{SO}_4]\cdot\text{H}_2\text{O}$). Similar descriptions of Cu^{2+} precipitating onto CaCO_3 -based materials have been reported in past, with Wen et al. [17], Zhizaev et al. [52], Zittlau et al. [53], and Hu et al. [16] who reported that formation of this copper mineral was the primary mechanism of Cu^{2+} removal from solution via their CaCO_3 particles. Outside of systems involving CaCO_3 , posnjakite, and its dehydrated form, brochantite, were observed by Marani et al. to form from a copper sulfate solution upon addition of NaOH, further indicating that the formation of this complex is common [54]. In addition to this, some slight evidence of $\text{Cu}(\text{OH})_2$ is shown from XRD analysis, though the extent of this is likely small considering its lower intensity.

The formation of posnjakite confirms that the removal of sulfate is highly dependent on the presence of Cu^{2+} in solution, and owing to the precipitate's stoichiometry, explains the low percent removal of sulfate. Furthermore, it shows that sulfate does not inhibit the adsorption of Cu^{2+} under the experimental conditions, but instead plays a direct role in its removal through formation of this salt.

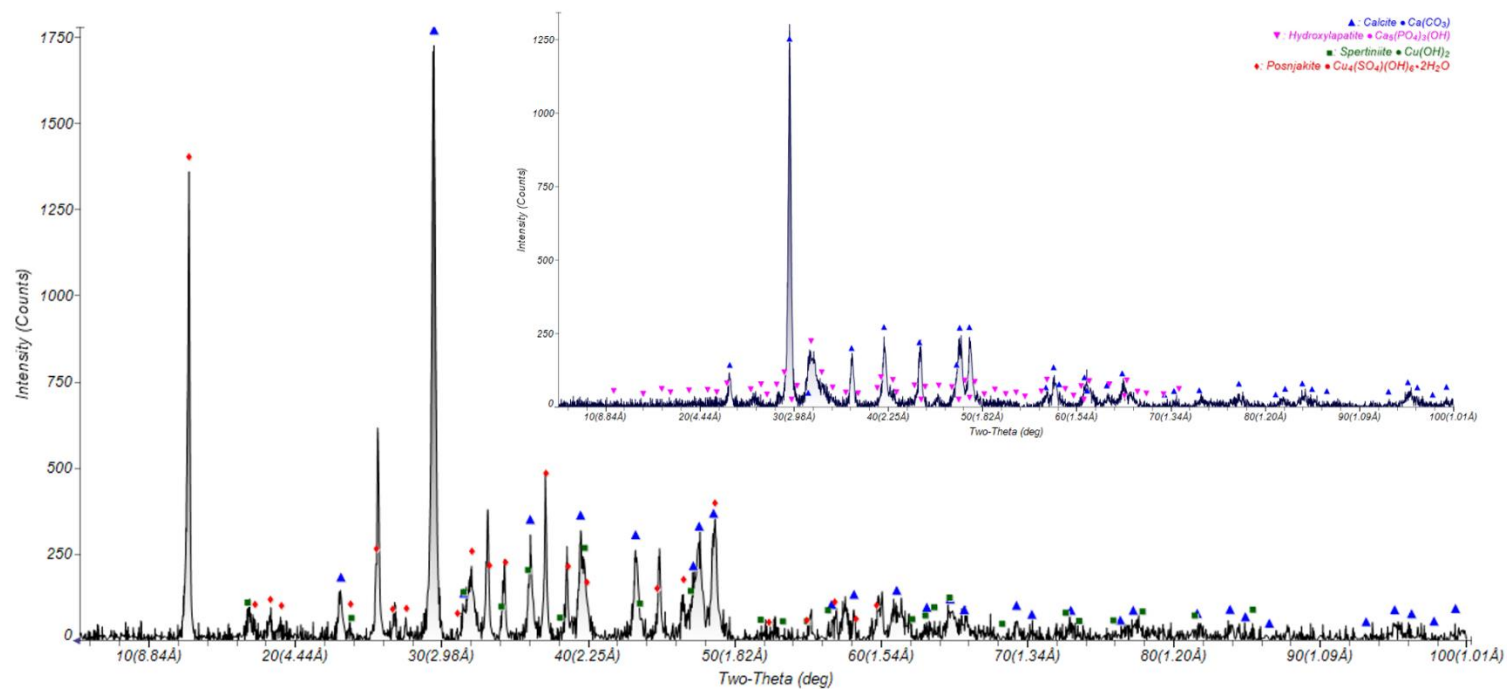


Figure 4-8: XRD spectra of the CSB post-adsorption (pre-adsorption in insert)

XPS analysis of the biochar following adsorption was carried out by analyzing the C1s, O1s, N1s, Ca2p, and Cu2p spectra, with graphs found in Appendix A. Comparing the C1s spectra, the distribution of intensity for each peak varies after adsorption, with increases in the C2, C3, C4, and C5 areas (corresponding to C-O/C-N, C=O, O-C=O, and carbonate, respectively), while the area occupied by C1, representative of saturated C-H groups, decreases. This may be related to interactions of the former functional groups with copper in solution, leading to increased electron density, while the saturated alkanes had no interaction with Cu^{2+} ions and instead decreased in intensity. In the O1s spectra, the O1 peak, corresponding to carbonates, decreases dramatically in relative area, which could be due to its dissolution in solution. The O2 spectra, which had been identified as either being related with C-O or C-O-C groups, increased here, though this may be due to the presence of CuSO_4 bonds which occurs at a similar energy, reported as 532.21 eV by Biesinger [55]. A new peak is observed in the spectra as well at 530.59 eV, with a relative peak area of 15.20% of the spectra. This peak looks to be associated with metal oxides, though it is difficult to ascertain what those oxides could be. Given the low number of counts for this compound, it is also possible that something anomalous has occurred here, as there is little other evidence of metal oxide formation. Regarding the N1s spectra, there is a slight change in the peak areas from the previous spectra, whereas the N1 peak, corresponding to pyridinic nitrogen now takes up slightly more of the spectra than previous which could be due to interaction with Cu^{2+} ions. The Ca2p spectrum has little shifting in terms of peak positions, while the area contributions of each peak vary only slightly. For Cu2p, the auger parameter was investigated, with its value of 1850.57 eV being close to that reported by Biesinger for $\text{Cu}(\text{OH})_2$ at 1850.92 eV [55].

Peak changes are not observed in the FT-IR spectra of the CSB following adsorption, though this may be due to the overwhelming presence of CaCO_3 in the biochar both before and after adsorption, which obfuscates the presence of organic functional groups that have vibrations at similar wavenumbers to those of CaCO_3 .

SEM analysis of the biochar confirms the formation of a precipitate on the surface of the CSB, which can be shown in Figure 4-11, Figure 4-12, and Figure 4-13, with reference images of the CSB prior to pyrolysis shown in Figure 4-9 and Figure 4-10. Here, small, flaky, florette-shaped crystals, like those studied by Zittlau et al. [53] are indicative of the precipitation of Cu^{2+} , with EDX spectra confirming the presence of Cu and S in the crystalline phases. Precipitation is widespread amongst biochar particles and illustrates a large extent of metal adsorption on the biochar surface.

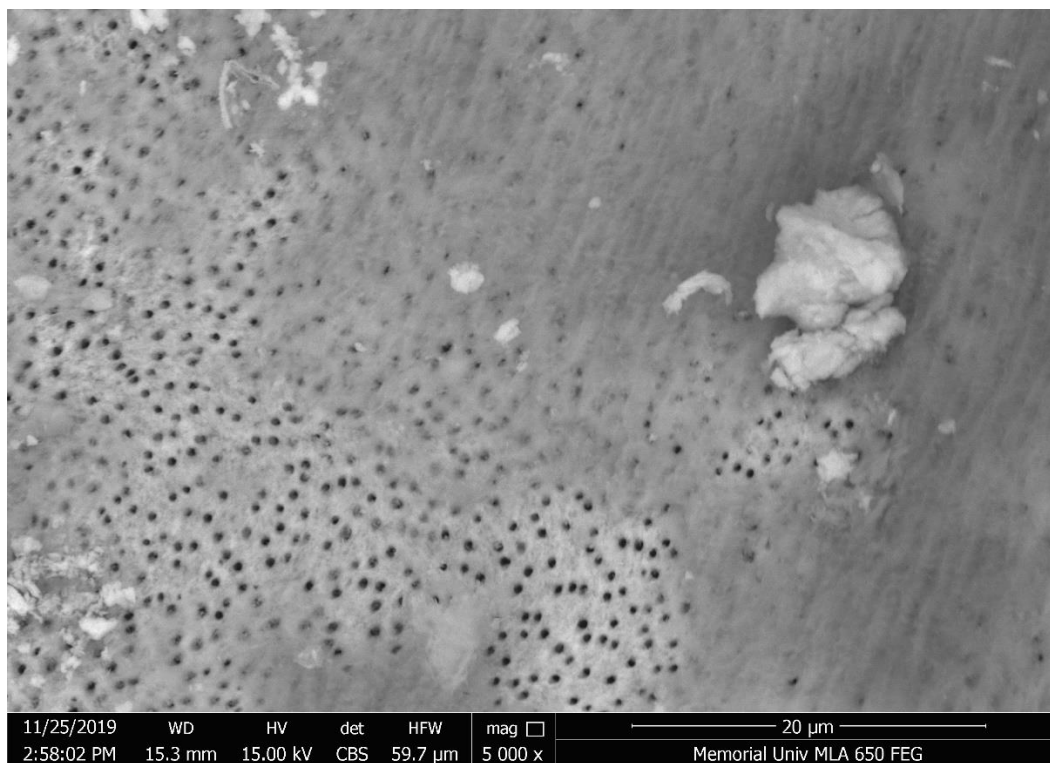


Figure 4-9: Image of the CSB prior to adsorption, showing porous structure.

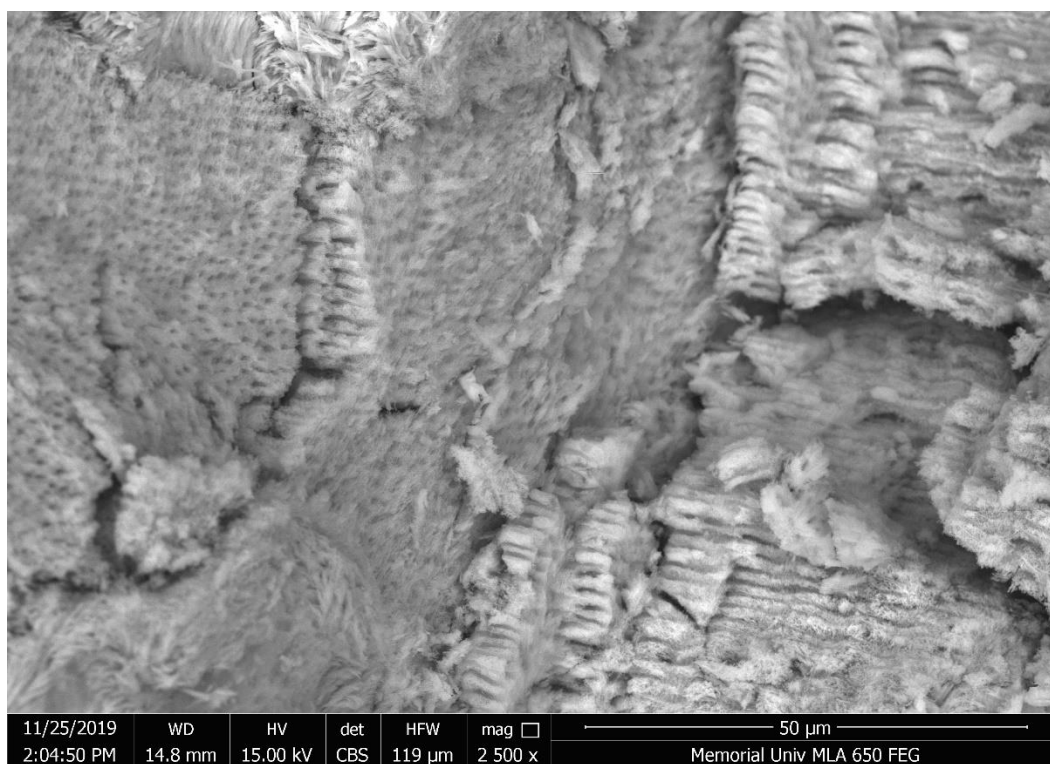


Figure 4-10: SEM image of the CSB prior to pyrolysis

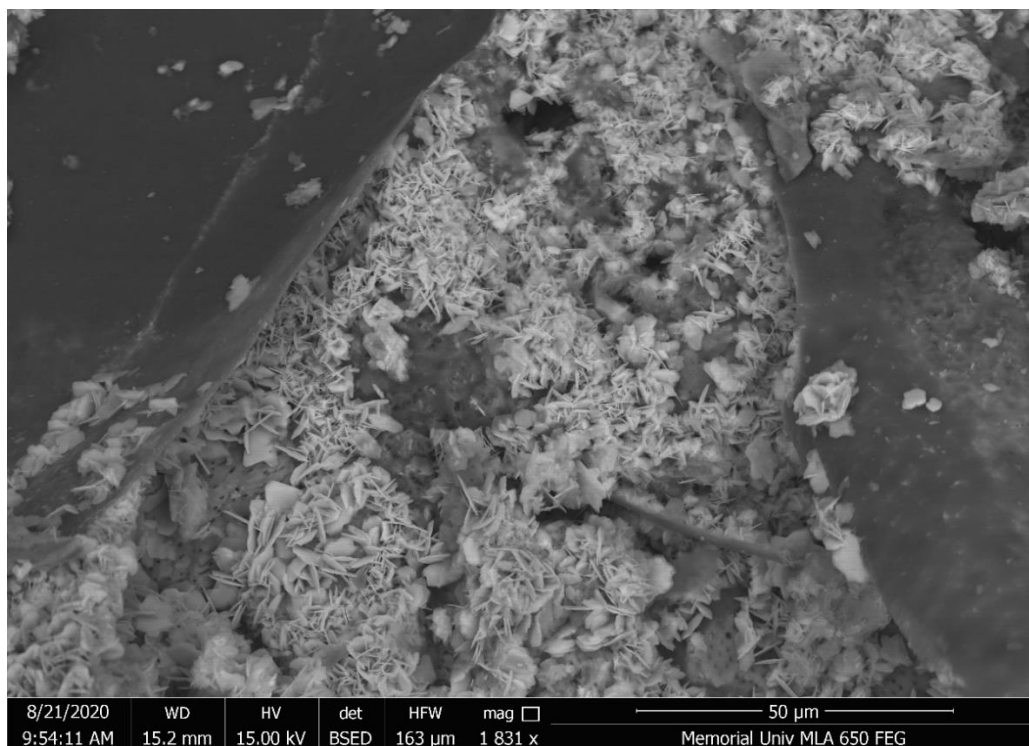


Figure 4-11: SEM Image of CSB post-adsorption illustrating widespread precipitation of Cu-based minerals across the biochar

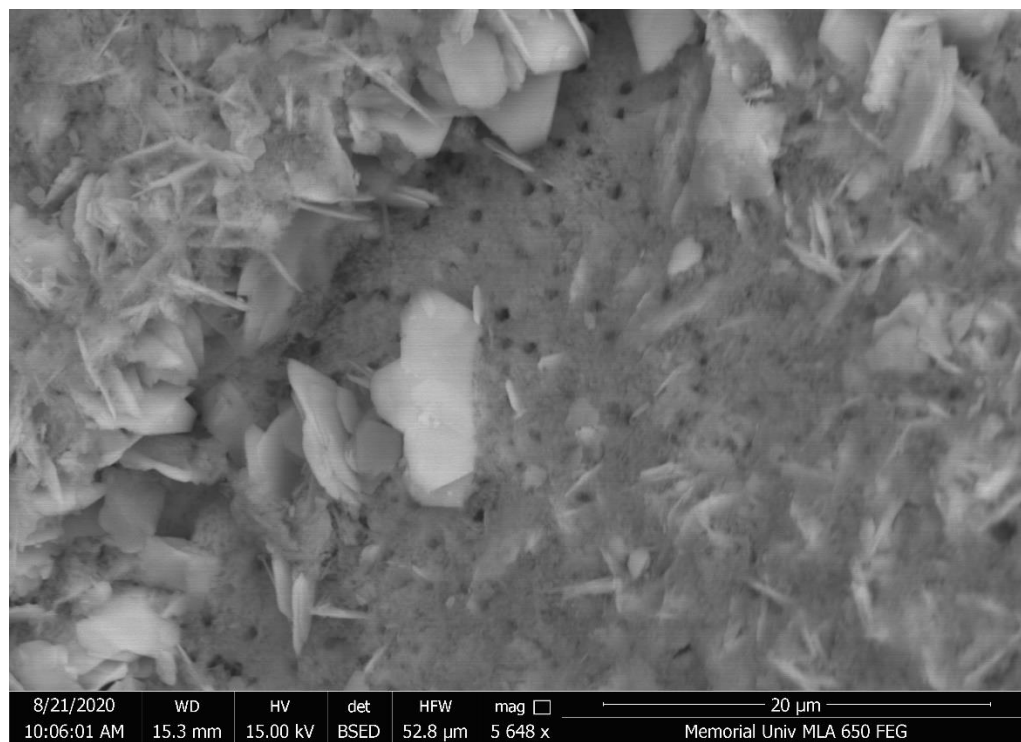


Figure 4-12: SEM Image of CSB post-adsorption showing a close-up view of the Cu²⁺ precipitate, with some biochar pores still visible.

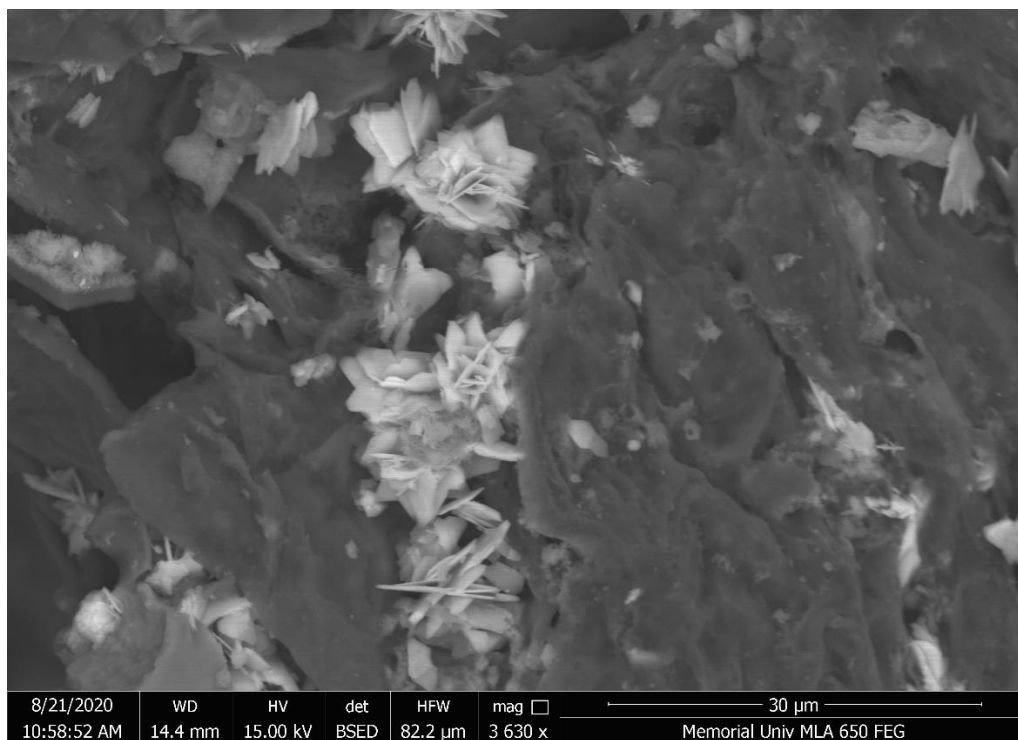


Figure 4-13: Cu^{2+} precipitates, likely in the form of posnjakite, forming flaky, tightly packed crystals on the CSB surface.

Copper basic salts may also precipitate in different forms based on the type of anions present in solution. Under alkaline conditions and when chloride (Cl^-) is present in solution, copper can co-precipitate in the form of the alkaline salt paratacamite ($\text{Cu}_2(\text{OH})_3\text{Cl}$) [17], [56], [57]. This precipitate can also exist in equilibrium with the dehydrated form of posnjakite, brochantite, with brochantite only being stable when the concentration of sulfate in solution is significantly higher than that of chloride [58], [59]. This may describe why S was not removed when the effect of pH was tested, as the addition of HCl may have led to increased Cl^- concentrations which then pushed the posnjakite/paratacamite equilibria in favor of the latter, or at least inhibited the formation of posnjakite crystals.

Table 4-5: Cu^{2+} adsorption capacities from past studies

Adsorbent	Species Adsorbed	Adsorption Capacity (mg/g)	Reference
Crab Shell	Cu^{2+}	79.4	[60]
A. Inaequalvis Shell	Cu^{2+}	330.2	[46]
CaCO_3 Nanoparticles	Cu^{2+}	393.52	[61]
Hardwood Biochar	Cu^{2+}	12.52	[5]
Rice Straw Biochar	Cu^{2+}	56.5	[8]
Commercial Activated Carbon (from coal)	Cu^{2+}	3.6	[62]
Crab Shell Biochar	Cu^{2+}	184.8	<i>This Study</i>

Comparing these results in Table 4-5, the biochar produced in this study has a higher adsorption capacity for Cu^{2+} than raw crab shell or hardwood biochar, while having a lower adsorption capacity in comparison to synthetic CaCO_3 particles and the A Inaequalvis clamshell. The CSB also significantly outperforms the commercial activated carbon studied by Periasamy and Namasivayam (1996), and Wilson et al. (2006). Mechanisms, however, are not discussed at length in either of these studies, and so it is difficult to compare differences [44], [62].

4.4 Conclusion

Crab shell, a major waste product in coastal regions, has great promise to be valorized through pyrolysis, despite limited research. This paper has investigated the potential to use biochar made from crab shell as an adsorbent for copper from solution and increase pH, which are both problematic contaminants in water that often arise in AMD. The analyses performed herein demonstrate that copper could be readily removed at a dosage

rate of 5 g/L, while simultaneously increasing the pH of the CuSO_4 solution. Cu^{2+} removal was found to be unchanged by changes in initial pH, while the removal of S was heavily impacted and did not occur, likely due to competition with Cl^- ions. Adsorption kinetics were shown to be rapid, with equilibrium reached in approximately 2 hours, while adsorption isotherm analysis demonstrated adsorption capacities of 184.8 mg/g of Cu^{2+} . Experiments on the effect of temperature on adsorption demonstrated that the removal of Cu^{2+} from solution increased as a function of increasing temperature. Further study is still needed to investigate the adsorption capacity of other metals onto similar biochar, however, as well as the effects of competition under complex solutions containing many metals and anions which could complicate the adsorption mechanisms observed here. Overall, this chapter has illustrated that the CSB is an effective adsorbent for Cu^{2+} , while simultaneously neutralizing acidity. Sulfate which is present in AMD did not interfere with Cu^{2+} adsorption and at high doses of biochar (relative to this study) showed some adsorption through co-precipitation. This material, being relatively simple to synthesize and vastly outperforming many existing methods in AMD and water treatment, holds significant promise to add value to the fisheries industry.

Bibliography

- [1] H. E. Ben Ali, C. M. Neculita, J. W. Molson, A. Maqsoud, and G. J. Zagury, "Performance of passive systems for mine drainage treatment at low temperature and high salinity: A review," *Miner. Eng.*, vol. 134, pp. 325–344, 2019, doi: <https://doi.org/10.1016/j.mineng.2019.02.010>.
- [2] K. K. Kefeni, T. A. M. Msagati, and B. B. Mamba, "Acid mine drainage: Prevention, treatment options, and resource recovery: A review," *J. Clean. Prod.*, vol. 151, pp. 475–493, May 2017, doi: [10.1016/J.JCLEPRO.2017.03.082](https://doi.org/10.1016/J.JCLEPRO.2017.03.082).
- [3] M. A. Renu and K. Singh, "Heavy metal removal from wastewater using various adsorbents: a review," *J. Water Reuse Desalin.*, vol. 7, no. 4, pp. 387–419, 2017, doi: [10.2166/wrd.2016.104](https://doi.org/10.2166/wrd.2016.104).
- [4] Z. Shen, F. Jin, F. Wang, O. McMillan, and A. Al-Tabbaa, "Sorption of lead by Salisbury biochar produced from British broadleaf hardwood," *Bioresour. Technol.*, vol. 193, pp. 553–556, Oct. 2015, doi: [10.1016/J.BIORTECH.2015.06.111](https://doi.org/10.1016/J.BIORTECH.2015.06.111).
- [5] X. Chen *et al.*, "Adsorption of copper and zinc by biochars produced from pyrolysis of hardwood and corn straw in aqueous solution," *Bioresour. Technol.*, 2011, doi: [10.1016/j.biortech.2011.06.078](https://doi.org/10.1016/j.biortech.2011.06.078).
- [6] D. C. Cruz Ceballos, K. Hawboldt, and R. Hellleur, "Effect of production conditions on self-heating propensity of torrefied sawmill residues," *Fuel*, vol. 160, pp. 227–237, 2015, doi: [10.1016/j.fuel.2015.07.097](https://doi.org/10.1016/j.fuel.2015.07.097).
- [7] M. E. González *et al.*, "Effects of pyrolysis conditions on physicochemical properties of oat hull derived biochar," *BioResources*, vol. 12, no. 1, pp. 2040–2057, 2017, doi: [10.15376/biores.12.1.2040-2057](https://doi.org/10.15376/biores.12.1.2040-2057).
- [8] J. H. Park *et al.*, "Recycling of rice straw through pyrolysis and its adsorption behaviors for Cu and Zn ions in aqueous solution," *Colloids Surfaces A Physicochem. Eng. Asp.*, 2017, doi: [10.1016/j.colsurfa.2017.08.041](https://doi.org/10.1016/j.colsurfa.2017.08.041).
- [9] X. Tong, J. Li, J. Yuan, and R. Xu, "Adsorption of Cu(II) by biochars generated from three crop straws," *Chem. Eng. J.*, vol. 172, no. 2–3, pp. 828–834, Aug. 2011, doi: [10.1016/J.CEJ.2011.06.069](https://doi.org/10.1016/J.CEJ.2011.06.069).
- [10] L. Beaulieu, J. Thibodeau, P. Bryl, and M. É. Carbonneau, "Characterization of enzymatic hydrolyzed snow crab (*Chionoecetes opilio*) by-product fractions: A source of high-valued biomolecules," *Bioresour. Technol.*, vol. 100, no. 13, pp. 3332–3342, 2009, doi: [10.1016/j.biortech.2009.01.073](https://doi.org/10.1016/j.biortech.2009.01.073).
- [11] C. Londono-Zuluaga, H. Jameel, R. W. Gonzalez, and L. Lucia, "Crustacean shell-

- based biosorption water remediation platforms: Status and perspectives,” *J. Environ. Manage.*, vol. 231, pp. 757–762, Feb. 2019, doi: 10.1016/J.JENVMAN.2018.10.096.
- [12] S. Richards, J. Dawson, and M. Stutter, “The potential use of natural vs commercial biosorbent material to remediate stream waters by removing heavy metal contaminants,” *J. Environ. Manage.*, vol. 231, no. June 2018, pp. 275–281, 2019, doi: 10.1016/j.jenvman.2018.10.019.
- [13] C. Zhou, X. Gong, J. Han, and R. Guo, “Removal of Pb(II) and Zn(II) from Aqueous Solutions by Raw Crab Shell: A Comparative Study,” *Water Environ. Res.*, vol. 88, no. 4, pp. 374–383, 2016, doi: 10.2175/106143016X14504669768174.
- [14] R. Zhang, J. J. Richardson, A. F. Masters, G. Yun, K. Liang, and T. Maschmeyer, “Effective Removal of Toxic Heavy Metal Ions from Aqueous Solution by CaCO₃ Microparticles,” *Water, Air, Soil Pollut.*, vol. 229, no. 4, p. 136, Apr. 2018, doi: 10.1007/s11270-018-3787-0.
- [15] J. Zhang *et al.*, “Template-free synthesis of hierarchical porous calcium carbonate microspheres for efficient water treatment,” *RSC Adv.*, vol. 6, no. 1, pp. 472–480, 2015, doi: 10.1039/c5ra18366a.
- [16] H. Hu, X. Li, P. Huang, Q. Zhang, and W. Yuan, “Efficient removal of copper from wastewater by using mechanically activated calcium carbonate,” *J. Environ. Manage.*, vol. 203, pp. 1–7, 2017, doi: 10.1016/j.jenvman.2017.07.066.
- [17] T. Wen *et al.*, “Effect of anions species on copper removal from wastewater by using mechanically activated calcium carbonate,” *Chemosphere*, vol. 230, pp. 127–135, 2019, doi: 10.1016/j.chemosphere.2019.04.213.
- [18] T. Wen *et al.*, “Selective recovery of heavy metals from wastewater by mechanically activated calcium carbonate: Inspiration from nature,” *Chemosphere*, vol. 246, p. 125842, 2020, doi: 10.1016/j.chemosphere.2020.125842.
- [19] H. Hu, Q. Zhang, W. Yuan, Z. Li, Y. Zhao, and W. Gu, “Efficient Pb removal through the formations of (basic) carbonate precipitates from different sources during wet stirred ball milling with CaCO₃,” *Sci. Total Environ.*, vol. 664, pp. 53–59, 2019, doi: 10.1016/j.scitotenv.2019.01.424.
- [20] A. M. Silva, R. M. F. Lima, and V. A. Leão, “Mine water treatment with limestone for sulfate removal,” *J. Hazard. Mater.*, vol. 221–222, pp. 45–55, 2012, doi: 10.1016/j.jhazmat.2012.03.066.
- [21] L. Cai *et al.*, “Effective adsorption of diesel oil by crab-shell-derived biochar nanomaterials,” *Materials (Basel)*, vol. 12, no. 2, 2019, doi:

10.3390/ma12020236.

- [22] Q. Xu, Q. Zhou, M. Pan, and L. Dai, "Interaction between chlortetracycline and calcium-rich biochar: Enhanced removal by adsorption coupled with flocculation," *Chem. Eng. J.*, vol. 382, p. 122705, 2020, doi: <https://doi.org/10.1016/j.cej.2019.122705>.
- [23] L. Dai *et al.*, "Calcium-rich biochar from the pyrolysis of crab shell for phosphorus removal," *J. Environ. Manage.*, 2017, doi: [10.1016/j.jenvman.2017.04.057](https://doi.org/10.1016/j.jenvman.2017.04.057).
- [24] L. Dai *et al.*, "Calcium-rich biochar from crab shell: An unexpected super adsorbent for dye removal," *Bioresour. Technol.*, vol. 267, no. July, pp. 510–516, 2018, doi: [10.1016/j.biortech.2018.07.090](https://doi.org/10.1016/j.biortech.2018.07.090).
- [25] Y. Xiao, Y. Xue, F. Gao, and A. Mosa, "Sorption of heavy metal ions onto crayfish shell biochar: Effect of pyrolysis temperature, pH and ionic strength," *J. Taiwan Inst. Chem. Eng.*, vol. 80, pp. 114–121, Nov. 2017, doi: [10.1016/J.JTICE.2017.08.035](https://doi.org/10.1016/J.JTICE.2017.08.035).
- [26] Z. A. DiLoreto, P. A. Weber, and C. G. Weisener, "Solid phase characterization and metal deportment in a mussel shell bioreactor for the treatment of AMD, Stockton Coal Mine, New Zealand," *Appl. Geochemistry*, vol. 67, pp. 133–143, 2016, doi: [10.1016/j.apgeochem.2016.02.011](https://doi.org/10.1016/j.apgeochem.2016.02.011).
- [27] T. Kraiem, A. Ben Hassen-Trabelsi, S. Naoui, and H. Belayouni, "Characterization of syngas and bio-char: Co-products from pyrolysis of waste fish fats," 2014, doi: [10.1109/IREC.2014.6826976](https://doi.org/10.1109/IREC.2014.6826976).
- [28] S. Chowdhury, M. A. J. Mazumder, O. Al-Attas, and T. Husain, "Heavy metals in drinking water: Occurrences, implications, and future needs in developing countries," *Sci. Total Environ.*, vol. 569–570, pp. 476–488, Nov. 2016, doi: [10.1016/J.SCITOTENV.2016.06.166](https://doi.org/10.1016/J.SCITOTENV.2016.06.166).
- [29] B. M. K. Range and K. A. Hawboldt, "Adsorption of thiosulphate, trithionate, tetrathionate using biomass ash/char," *J. Environ. Chem. Eng.*, vol. 6, no. 4, pp. 5401–5408, Aug. 2018, doi: [10.1016/j.jece.2018.08.006](https://doi.org/10.1016/j.jece.2018.08.006).
- [30] Z. Mahdi, Q. J. Yu, and A. El Hanandeh, "Investigation of the kinetics and mechanisms of nickel and copper ions adsorption from aqueous solutions by date seed derived biochar," *J. Environ. Chem. Eng.*, vol. 6, no. 1, pp. 1171–1181, Feb. 2018, doi: [10.1016/J.JECE.2018.01.021](https://doi.org/10.1016/J.JECE.2018.01.021).
- [31] H. N. Tran, S. J. You, A. Hosseini-Bandegharai, and H. P. Chao, "Mistakes and inconsistencies regarding adsorption of contaminants from aqueous solutions: A critical review," *Water Res.*, vol. 120, pp. 88–116, 2017, doi: [10.1016/j.watres.2017.04.014](https://doi.org/10.1016/j.watres.2017.04.014).

- [32] H. Freundlich, "Über die Adsorption in Lösungen," *Zeitschrift für Phys. Chemie*, vol. 57U, no. 1, pp. 385–470, 1907.
- [33] M. I. Inyang *et al.*, "A review of biochar as a low-cost adsorbent for aqueous heavy metal removal," *Crit. Rev. Environ. Sci. Technol.*, vol. 46, no. 4, pp. 406–433, Feb. 2016, doi: 10.1080/10643389.2015.1096880.
- [34] G. Blanchard, M. Maunaye, and G. Martin, "Removal of heavy metals from waters by means of natural zeolites," *Water Res.*, vol. 18, no. 12, pp. 1501–1507, 1984, doi: [https://doi.org/10.1016/0043-1354\(84\)90124-6](https://doi.org/10.1016/0043-1354(84)90124-6).
- [35] Y. Liu, "Is the free energy change of adsorption correctly calculated?," *J. Chem. Eng. Data*, vol. 54, no. 7, pp. 1981–1985, 2009, doi: 10.1021/je800661q.
- [36] F. M. Pelleria *et al.*, "Adsorption of Cu(II) ions from aqueous solutions on biochars prepared from agricultural by-products," *J. Environ. Manage.*, vol. 96, no. 1, pp. 35–42, 2012, doi: 10.1016/j.jenvman.2011.10.010.
- [37] M. L. Davis, *Water and Wastewater Engineering: Design Principles and Practice*, 1st ed. New York: McGraw-Hill, 2010.
- [38] T. H. Chong and R. Sheikholeslami, "Thermodynamics and kinetics for mixed calcium carbonate and calcium sulfate precipitation," *Chem. Eng. Sci.*, vol. 56, no. 18, pp. 5391–5400, 2001, doi: [https://doi.org/10.1016/S0009-2509\(01\)00237-8](https://doi.org/10.1016/S0009-2509(01)00237-8).
- [39] J. Rivera-Utrilla, M. Sánchez-Polo, V. Gómez-Serrano, P. M. Álvarez, M. C. M. Alvim-Ferraz, and J. M. Dias, "Activated carbon modifications to enhance its water treatment applications. An overview," *J. Hazard. Mater.*, vol. 187, no. 1–3, pp. 1–23, 2011, doi: 10.1016/j.jhazmat.2011.01.033.
- [40] S. Mireles, J. Parsons, T. Trad, C. L. Cheng, and J. Kang, "Lead removal from aqueous solutions using biochars derived from corn stover, orange peel, and pistachio shell," *Int. J. Environ. Sci. Technol.*, vol. 16, no. 10, pp. 5817–5826, 2019, doi: 10.1007/s13762-018-02191-5.
- [41] M. Masukume, M. S. Onyango, and J. P. Maree, "Sea shell derived adsorbent and its potential for treating acid mine drainage," *Int. J. Miner. Process.*, vol. 133, pp. 52–59, 2014, doi: 10.1016/j.minpro.2014.09.005.
- [42] C. D. Hatch, J. S. Wiese, C. C. Crane, K. J. Harris, H. G. Kloss, and J. Baltrusaitis, "Water adsorption on clay minerals as a function of relative humidity: Application of BET and Freundlich adsorption models," *Langmuir*, vol. 28, no. 3, pp. 1790–1803, 2012, doi: 10.1021/la2042873.
- [43] Z. Liu, F. S. Zhang, and J. Wu, "Characterization and application of chars produced from pinewood pyrolysis and hydrothermal treatment," *Fuel*, vol. 89, no.

- 2, pp. 510–514, Feb. 2010, doi: 10.1016/j.fuel.2009.08.042.
- [44] K. Wilson, H. Yang, C. W. Seo, and W. E. Marshall, “Select metal adsorption by activated carbon made from peanut shells,” *Bioresour. Technol.*, vol. 97, no. 18, pp. 2266–2270, Dec. 2006, doi: 10.1016/J.BIORTECH.2005.10.043.
- [45] Y. Xiao, J. Azaiez, and J. M. Hill, “Erroneous Application of Pseudo-Second-Order Adsorption Kinetics Model: Ignored Assumptions and Spurious Correlations,” *Ind. Eng. Chem. Res.*, vol. 57, no. 7, pp. 2705–2709, 2018, doi: 10.1021/acs.iecr.7b04724.
- [46] S. K. Bozbaş and Y. Boz, “Low-cost biosorbent: Anadara inaequalis shells for removal of Pb(II) and Cu(II) from aqueous solution,” *Process Saf. Environ. Prot.*, vol. 103, pp. 144–152, 2016, doi: 10.1016/j.psep.2016.07.007.
- [47] T. Sun, Y. Xu, Y. Sun, L. Wang, X. Liang, and H. Jia, “Crayfish Shell Biochar for the Mitigation of Pb Contaminated Water and Soil: Characteristics, Mechanisms, and Applications,” *Environ. Pollut.*, 2020, doi: 10.1016/j.envpol.2020.116308.
- [48] P. Champagne, P. Van Geel, and W. Parker, “Impact of temperature and loading on the mitigation of AMD in peat biofilter columns,” *Mine Water Environ.*, vol. 27, no. 4, pp. 225–240, 2008, doi: 10.1007/s10230-008-0053-5.
- [49] J. Yan, Y. Xue, L. Long, Y. Zeng, and X. Hu, “Adsorptive removal of As(V) by crawfish shell biochar: batch and column tests,” *Environ. Sci. Pollut. Res.*, vol. 25, no. 34, pp. 34674–34683, 2018, doi: 10.1007/s11356-018-3384-1.
- [50] A. Sdiri, T. Higashi, F. Jamoussi, and S. Bouaziz, “Effects of impurities on the removal of heavy metals by natural limestones in aqueous systems,” *J. Environ. Manage.*, vol. 93, no. 1, pp. 245–253, 2012, doi: <https://doi.org/10.1016/j.jenvman.2011.08.002>.
- [51] H. T. Van *et al.*, “Characteristics and mechanisms of cadmium adsorption onto biogenic aragonite shells-derived biosorbent: Batch and column studies,” *J. Environ. Manage.*, vol. 241, no. September 2018, pp. 535–548, 2019, doi: 10.1016/j.jenvman.2018.09.079.
- [52] A. M. Zhizhaev and E. N. Merkulova, “Interaction of copper(II) and zinc(II) in coprecipitation from sulfate solutions with natural calcium carbonate,” *Russ. J. Appl. Chem.*, vol. 87, no. 1, pp. 16–22, 2014, doi: 10.1134/S1070427214010029.
- [53] A. H. Zittlau, Q. Shi, J. Boerio-Goates, B. F. Woodfield, and J. Majzlan, “Thermodynamics of the basic copper sulfates antlerite, posnjakite, and brochantite,” *Chemie der Erde*, vol. 73, no. 1, pp. 39–50, 2013, doi: 10.1016/j.chemer.2012.12.002.

- [54] D. Marani, J. W. Patterson, and P. R. Anderson, "Alkaline Precipitation And Aging Of Cu(II) in the Presence Of Sulfate," *Water Res.*, vol. 29, no. 5, pp. 1317–1326, 1995, doi: 10.1016/0043-1354(94)00286-G.
- [55] M. C. Biesinger, "Advanced analysis of copper X-ray photoelectron spectra," *Surf. Interface Anal.*, vol. 49, no. 13, pp. 1325–1334, 2017, doi: 10.1002/sia.6239.
- [56] L. Veleva, P. Quintana, R. Ramanauskas, R. Pomes, and L. Maldonado, "Mechanism of copper patina formation in marine environments," *Electrochim. Acta*, vol. 41, no. 10, pp. 1641–1645, 1996, doi: 10.1016/0013-4686(95)00417-3.
- [57] J. B. Sharkey and S. Z. Lewin, "Conditions governing the formation of atacamite and paratacamite," *Am. Mineral.*, vol. 56, no. 1–2, pp. 179–192, 1971.
- [58] A. R. Mendoza, F. Corvo, A. Gómez, and J. Gómez, "Influence of the corrosion products of copper on its atmospheric corrosion kinetics in tropical climate," *Corros. Sci.*, vol. 46, no. 5, pp. 1189–1200, 2004, doi: 10.1016/j.corsci.2003.09.014.
- [59] T. L. Woods and R. M. Garrels, "Phase relations of some cupric hydroxy minerals," *Econ. Geol.*, vol. 81, no. 8, pp. 1989–2007, 1986, doi: 10.2113/gsecongeo.81.8.1989.
- [60] E. L. Cochrane, S. Lu, S. W. Gibb, and I. Villaescusa, "A comparison of low-cost biosorbents and commercial sorbents for the removal of copper from aqueous media," *J. Hazard. Mater.*, vol. 137, no. 1, pp. 198–206, 2006, doi: 10.1016/j.jhazmat.2006.01.054.
- [61] H. Mohammadifard and M. C. Amiri, "Evaluating Cu(II) Removal From Aqueous Solutions with Response Surface Methodology by Using Novel Synthesized CaCO₃ Nanoparticles Prepared in a Colloidal Gas Aphron System," *Chem. Eng. Commun.*, vol. 204, no. 4, pp. 476–484, 2017, doi: 10.1080/00986445.2016.1277522.
- [62] K. Periasamy and C. Namasivayam, "Removal of copper(II) by adsorption onto peanut hull carbon from water and copper plating industry wastewater," *Chemosphere*, vol. 32, no. 4, pp. 769–789, 1996, doi: 10.1016/0045-6535(95)00332-0.

Chapter 5 – Conclusions & Recommendations

Development of green processes to valorize fisheries by-product is critical for the future sustainability of the industry as a whole. Pyrolysis of these by-products to value added products offers a simple process that eliminates concerns associated with bacteria or virus in final product that would occur from use of the raw material in such uses as biosorption. In this thesis, we have investigated the production and characterization of a biochar from crab shell, a major by-product from the fisheries of Atlantic Canada, followed by a study in its use as an adsorbent for copper (Cu^{2+}) from solution and increasing its pH. The literature review shows that crab by-product in general is underutilized and biochar from crab bodies is not well studied. Biochar from these marine sources is primarily mineral rich, consisting largely of calcite (CaCO_3) in the case of crustacean shells, and has been demonstrated to have a high adsorption capacity for many problematic transition metals owing to the alkalinity and exchange capacity of the char, along with some chelation due to residual organics. Adsorption capacity of these shell-based adsorbents is generally higher than those of plant-based, or lignocellulosic biochar, which may be attributed to the higher alkalinity of mineral content of marine shells in comparison with plant-based feedstocks.

The crab shell biochar used in this study was produced at a temperature of 500 °C, with a pyrolysis production yield of 52.7%. The biochar had a BET surface area of 20.71 m^2/g , pH of 11.75, negative zeta potential across all pH values studied, and a high ash content as defined by TGA. FT-IR analysis, along with XRD and XPS analysis identified that the biochar was largely made up of CaCO_3 , as observed with other crustacean shell biochars, along with a few residual organic compounds consisting of some carboxylic acids and pyridinic and pyrrolic nitrogen.

When used as an adsorbent for Cu^{2+} in a sulfate solution, the crab shell biochar demonstrated excellent removal of the metal. The biochar was able to remove $99\pm 5\%$ Cu^{2+} from solution at a dosage of 5 g/L and $34\pm 7\%$ of S. Adsorption of Cu^{2+} was effective across a range of initial solution pH ranging from 2-7, with no observable effect on the percent removal, while sulfate (represented by S) removal was heavily impacted by acidity. This lack of pH effect for Cu^{2+} is likely due to the alkalinity of the biochar, which was observed to have a neutralizing effect, and consistently brought the solution pH above 7 regardless of the amount of acid added. Meanwhile, sulfate ions were likely displaced by chloride from the added HCl in these experiments, which could have impacted its removal. Isotherm studies show the biochar adsorption capacity was 184.8 mg/g for Cu^{2+} , for context biochar from lignocellulosic sources has a capacity ranging from 2.73 mg/g [1] to 56.6 mg/g [2] for Cu^{2+} , with dosages of 2.5 g/L and 2 g/L, respectively. Sulfate adsorption was not measured here or in the following experiments due to the uncertainty in the measurement of S concentrations, which was attributed to inherent limitations in the analytical technique used (ICP-OES). The adsorption kinetics followed the PSO model with maximum removal occurring within 2 hours.

Thermodynamic analysis demonstrated that the adsorption process of Cu^{2+} was not spontaneous using the Van't Hoff method. Adsorption capacity increased with increasing temperature, which has important ramifications on the practical side of adsorbent use in cold climates. The biochar surface was analyzed post adsorption as well, which demonstrated that the Cu^{2+} adsorbed to the biochar primarily through the formation of the basic copper salt posnjakite ($\text{Cu}_4[(\text{OH})_6\text{SO}_4]\cdot\text{H}_2\text{O}$), which forms in a similar manner on other alkaline adsorbents.

This material presents an excellent removal capacity for Cu^{2+} and is unimpeded by the presence of sulfates or acidity in solution, making it a good candidate for the treatment of AMD. Work in this field is still limited, however, and more work is needed to both scale up the production of this material, investigate its interactions with other metals, and research other product streams from this process.

Future Recommendations:

Marine shell biochars are a largely unexplored field in terms of current research, with few studies investigating their characterization and use and further still exploring their use as an adsorbent for heavy metals. With this in mind, additional research is imperative in order to fully understand the properties of marine shell biochars, and how well they can perform in the field as an AMD treatment. Future recommendations for this work are summarized as follows:

- This thesis has analyzed a biochar made at a single production temperature, while pyrolysis temperature, among other factors, are known to have large impacts on the properties of biochar [3]. A study evaluating the dynamics of crab shell biochar properties in line with its ability to adsorb metals from solution would further enable optimization of adsorption capacity through adjustment of temperature.
- The crab shell biochar produced in our studies, as well as in much of the literature, are produced in lab-scale pyrolysis units. Using a large-scale pyrolysis reactor may yield different biochar properties than found on a lab-scale, and so it

is important to research the changes that occur upon scaling up the process to pilot, and eventually, industrial scale.

- This study has focussed on adsorption of one metal, copper, while many other metals and ionic species exist in AMD [4]. Studying the removal capacity of this adsorbent for other metals is an important next step in assessing its overall effectiveness in AMD treatment. Furthermore, whereas certain metals and ionic species can compete for adsorption in solution, multi-metal solutions and solutions containing different anions as found in AMD should also be tested to ensure that the biochar's performance is not impeded in this situation [5].
- Many adsorbents used can be regenerated, reused, or used in other applications (impregnated with adsorbed metals) [6], [7]. The leachability of the spent biochar must be studied to determine the best after use or re-use of the biochar, as some forms of regeneration rely on acid washing which could ultimately dissolve much of the CaCO_3 -based biochar [6].

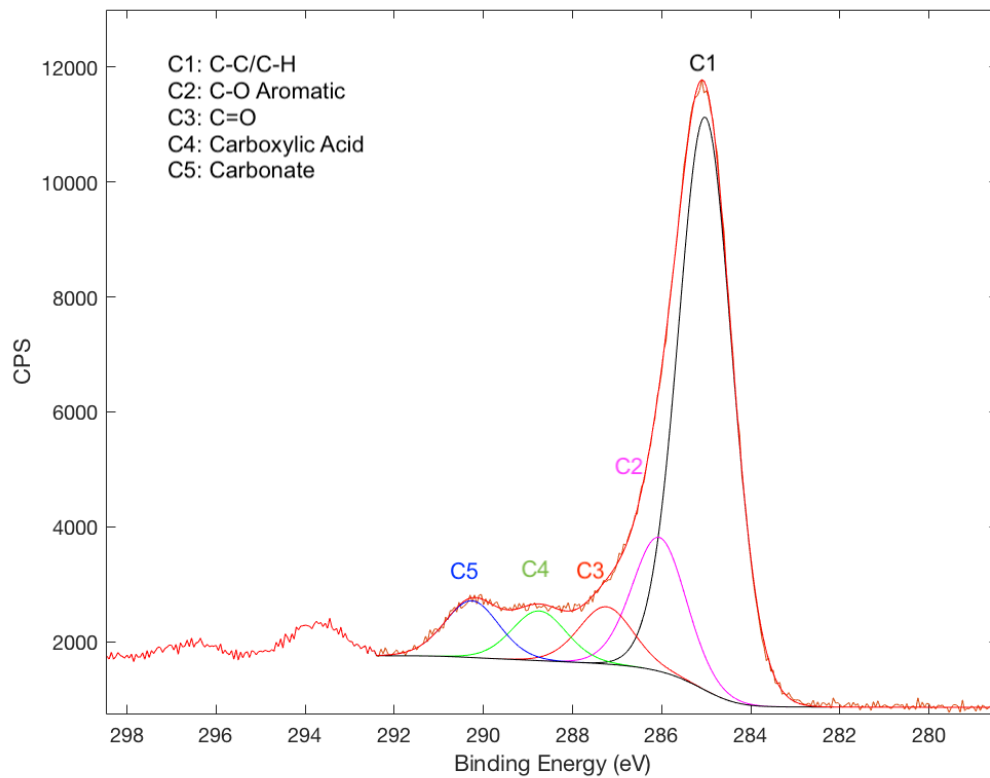
Bibliography:

- [1] Z. Liu, F. S. Zhang, and J. Wu, "Characterization and application of chars produced from pinewood pyrolysis and hydrothermal treatment," *Fuel*, vol. 89, no. 2, pp. 510–514, Feb. 2010.
- [2] J. H. Park *et al.*, "Recycling of rice straw through pyrolysis and its adsorption behaviors for Cu and Zn ions in aqueous solution," *Colloids Surfaces A Physicochem. Eng. Asp.*, 2017.
- [3] M. F. Aller, "Biochar properties: Transport, fate, and impact," *Crit. Rev. Environ. Sci. Technol.*, vol. 46, no. 14–15, pp. 1183–1296, 2016.
- [4] H. E. Ben Ali, C. M. Neculita, J. W. Molson, A. Maqsoud, and G. J. Zagury, "Performance of passive systems for mine drainage treatment at low temperature and high salinity: A review," *Miner. Eng.*, vol. 134, pp. 325–344, 2019.
- [5] H. Hu, Q. Zhang, W. Yuan, Z. Li, Y. Zhao, and W. Gu, "Efficient Pb removal through the formations of (basic) carbonate precipitates from different sources during wet stirred ball milling with CaCO₃," *Sci. Total Environ.*, vol. 664, pp. 53–59, 2019.
- [6] G. A. Maul, Y. Kim, A. Amini, Q. Zhang, and T. H. Boyer, "Efficiency and life cycle environmental impacts of ion-exchange regeneration using sodium, potassium, chloride, and bicarbonate salts," *Chem. Eng. J.*, vol. 254, pp. 198–209, Oct. 2014.
- [7] D. Mohan and C. U. Pittman, "Arsenic removal from water/wastewater using adsorbents—A critical review," *J. Hazard. Mater.*, vol. 142, no. 1–2, pp. 1–53, Apr. 2007.

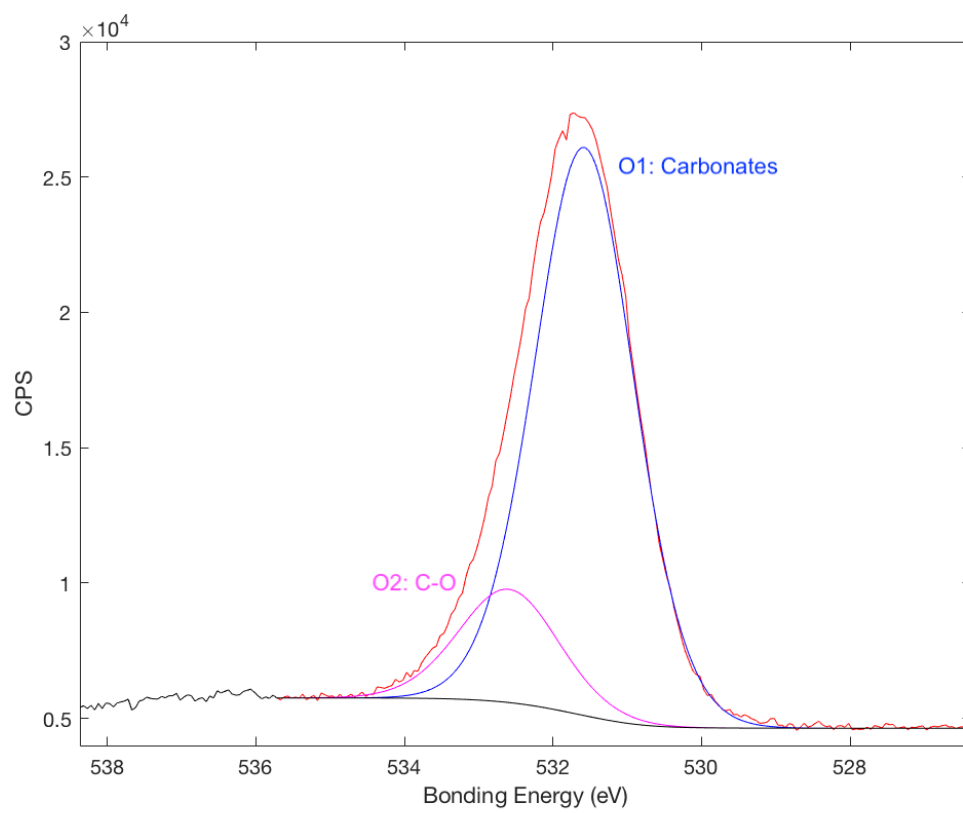
APPENDICES

APPENDIX A: XPS SPECTRA

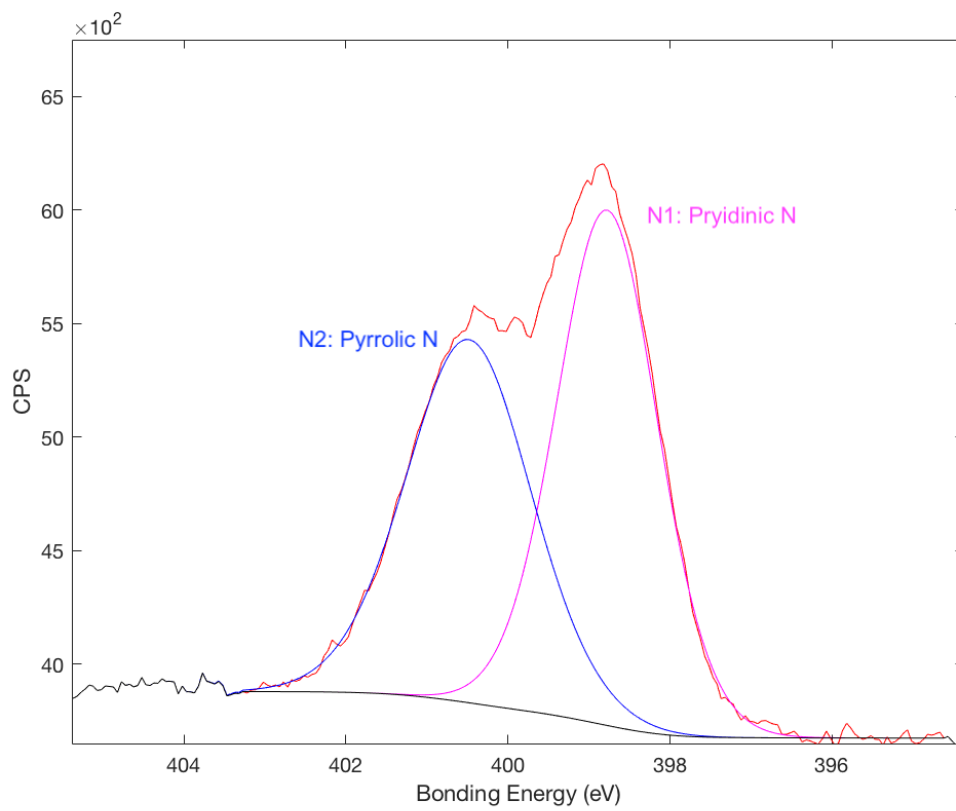
1. C1s spectra of biochar pre-adsorption



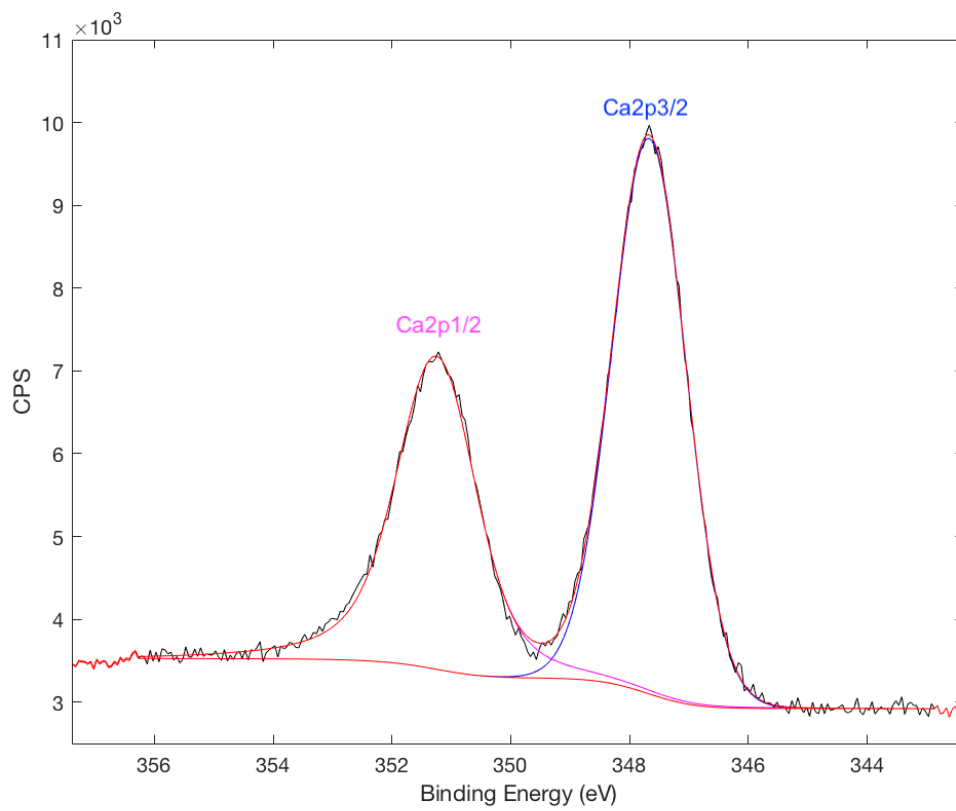
2: O1s spectra of biochar pre-adsorption



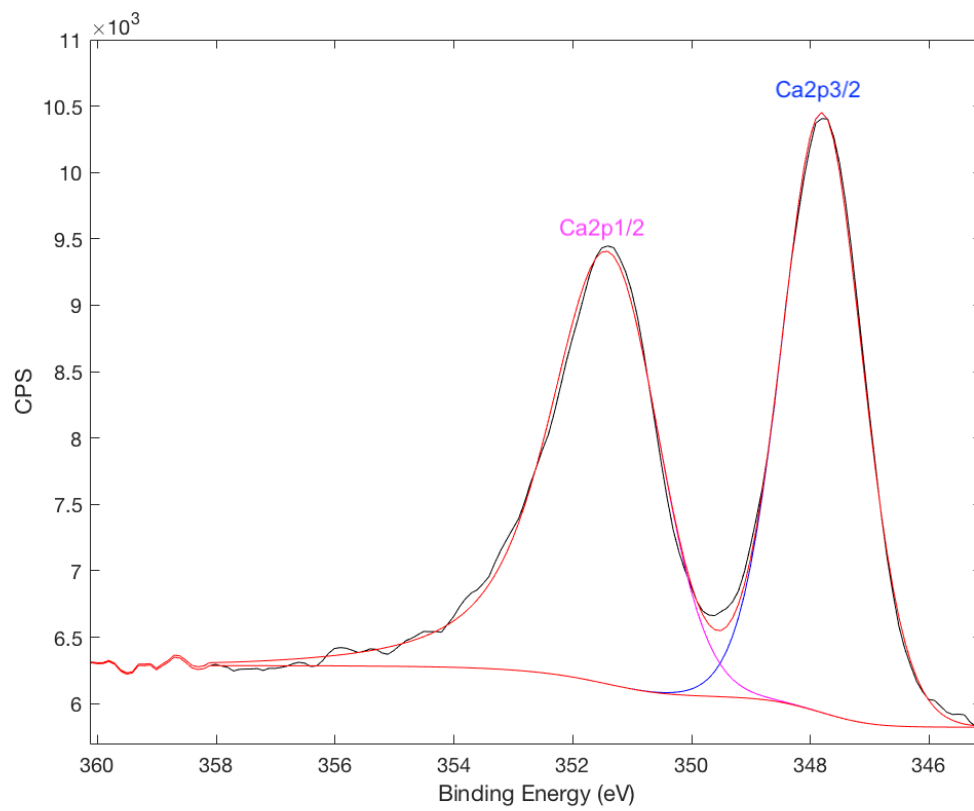
3: N1s spectra of biochar pre-adsorption



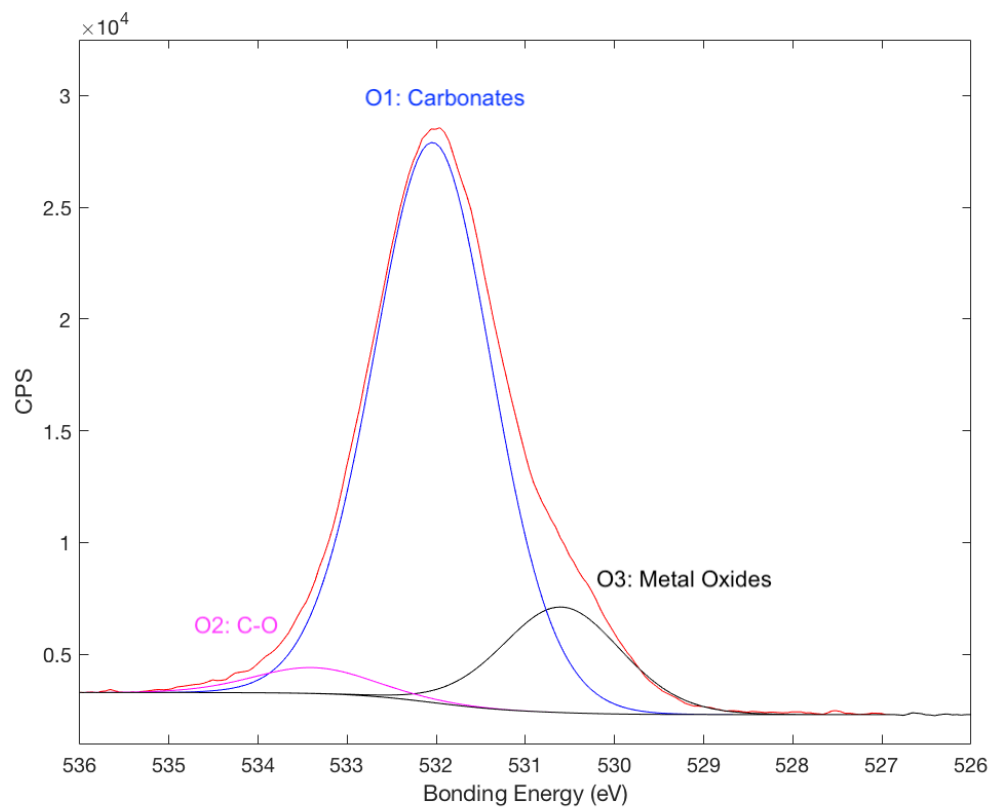
4: Ca2p spectra of biochar pre-adsorption



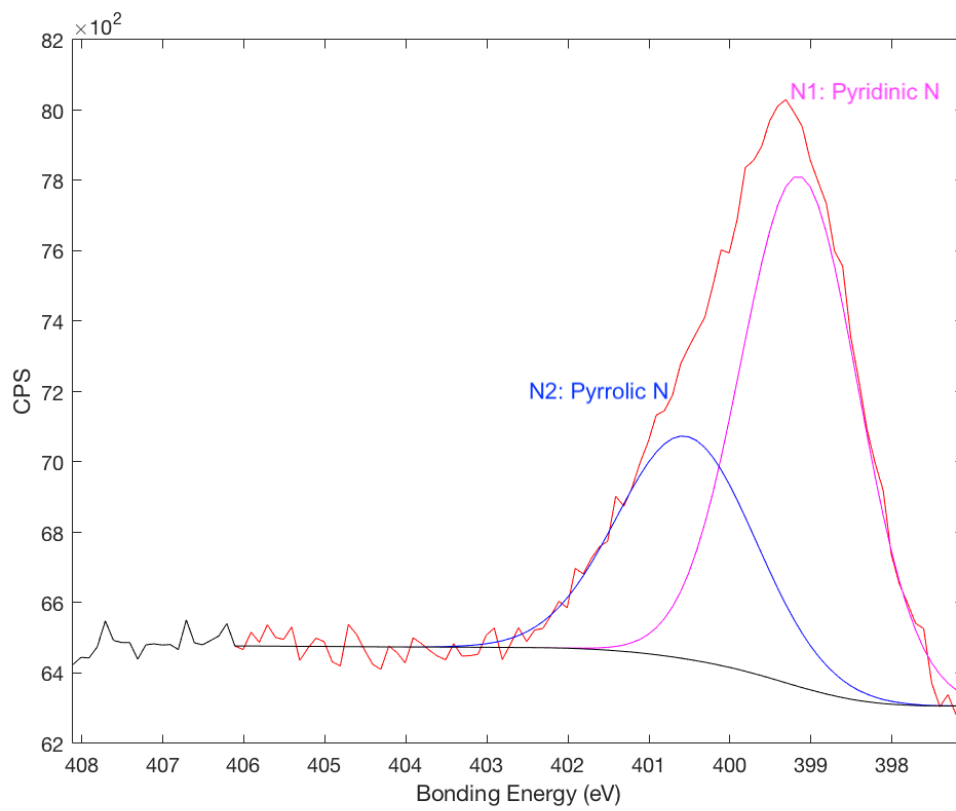
5: C1s spectra of biochar post-adsorption



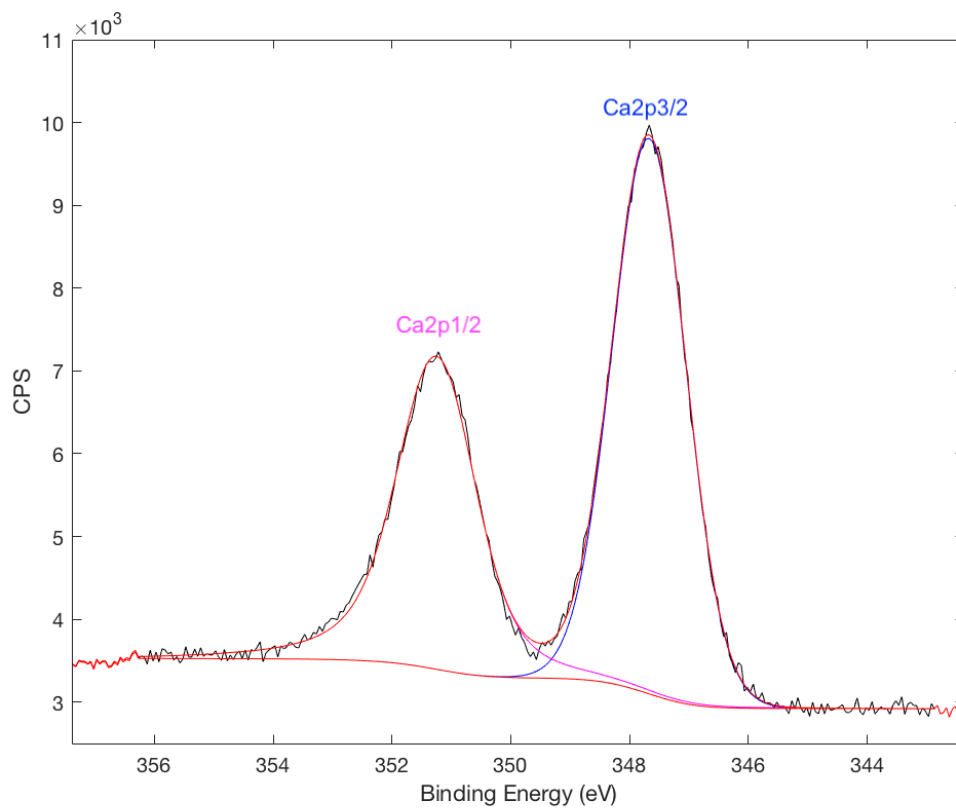
6: O1s spectra of biochar post-adsorption



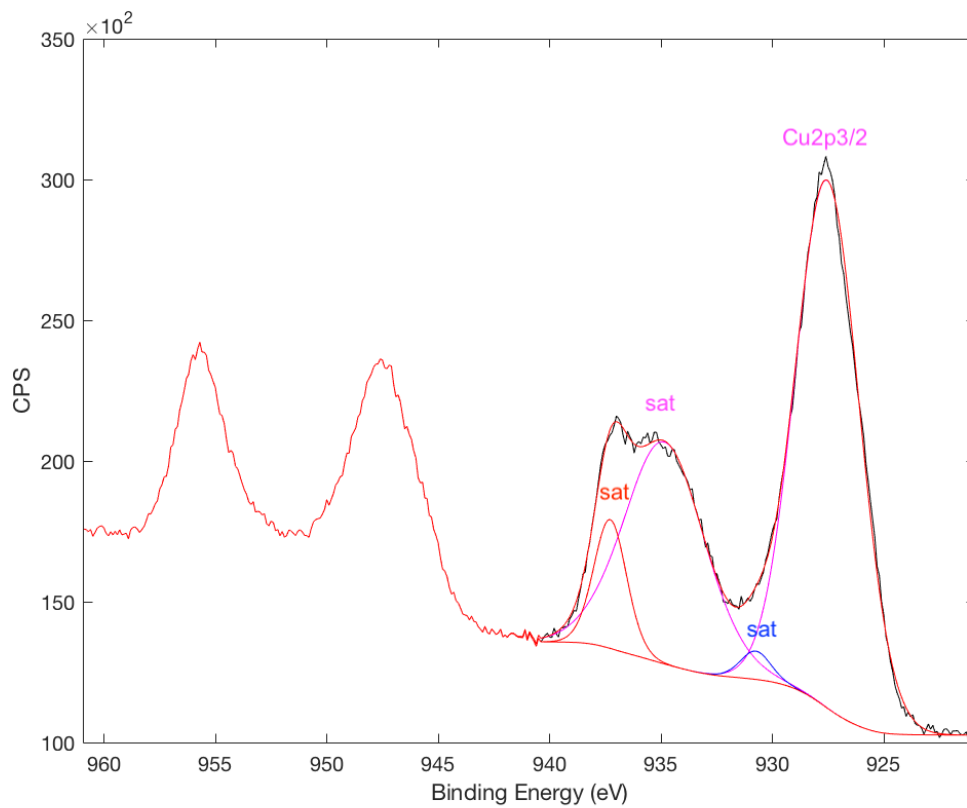
7: N1s spectra of biochar post-adsorption



8: Ca2p spectra of biochar post-adsorption



9: Cu2p spectra of biochar post-adsorption (Binding Energy not corrected as this spectrum was used to calculate auger parameters)



10: Cu2p auger spectra post-adsorption

